

Amalie Ramberg

Analysis of Dropped Objects on Offshore Installations

Master's thesis in Marine Technology

Supervisor: Jørgen Amdahl

Co-supervisor: Torstein Alexander Pettersen

June 2022

NTNU
Norwegian University of Science and Technology
Faculty of Engineering
Department of Marine Technology



Norwegian University of
Science and Technology

Amalie Ramberg

Analysis of Dropped Objects on Offshore Installations

Master's thesis in Marine Technology

Supervisor: Jørgen Amdahl

Co-supervisor: Torstein Alexander Pettersen

June 2022

Norwegian University of Science and Technology

Faculty of Engineering

Department of Marine Technology



Norwegian University of
Science and Technology

MASTER THESIS 2022

for

Stud. techn. **Amalie Ramberg**

Analysis of Dropped Objects on Offshore Installations

Analyse av fallende laster på offshoreinstallasjoner

In the offshore industry there are many situations where heavy objects are lifted to significant heights over installation decks. Such cases are very common when the installation receives supplies from visiting supply ships.

Dropped objects is defined as an accidental event and thus need to be designed for. The design of accidental events are typically determined by risk assessment. The risk assessment is often a “hot topic”, and the focus is placed on avoiding damages to the installation that may escalate and result in catastrophic consequences, such as explosions and fire. Typically, one design scenario is that a dropped object tears through a deck and impact hydrocarbon pipelines or storage tanks in the deck below.

Present guidelines for analysis and design of structures subjected to impacts are relatively limited and based on very simplified assumptions. Interaction between deformations of the dropped object and the impacted structure is for example often disregarded.

The aim of the present work is to gain deeper insight into the subject matter

The project work shall address the following topics:

- 1) Establish a finite element model of a container. Special emphasis shall be placed on the strong members such as the floor beams. The modelling should also be based with due consideration of the impact scenarios that shall be simulated.
- 2) Develop a script so that the geometry of the deck structure can be changed easily. Establish a finite element model of deck structure and perform impact simulations with different impact angles. Include a fracture criterion along with element deletion to predict the degree of penetration of the deck. Determine the damage and energy dissipation in both the container and the deck structure. Compare with the deck damage that would be caused by a rigid container
- 3) Establish relevant deformation mechanisms for the deck structure and the container and check whether the response can be assessed with hand calculation methods based on plastic theory
- 4) Conduct a parametric study where the geometry of the deck structure is varied (for example stiffener and girder size and spacing, plate thickness)
- 5) If time permits perform impact simulations of other dropped objects
- 6) Conclusions and recommendations for further work

Literature studies of specific topics relevant to the thesis work may be included.

The work scope may prove to be larger than initially anticipated. Subject to approval from the supervisor, topics may be deleted from the list above or reduced in extent.

In the thesis the candidate shall present his personal contribution to the resolution of problems within the scope of the thesis work.

Theories and conclusions should be based on mathematical derivations and/or logic reasoning identifying the various steps in the deduction.

The candidate should utilize the existing possibilities for obtaining relevant literature.

The thesis should be organized in a rational manner to give a clear exposition of results, assessments, and conclusions. The text should be brief and to the point, with a clear language. Telegraphic language should be avoided.

The thesis shall contain the following elements: A text defining the scope, preface, list of contents, summary, main body of thesis, conclusions with recommendations for further work, list of symbols and acronyms, references and (optional) appendices. All figures, tables and equations shall be numerated.

The supervisor may require that the candidate, in an early stage of the work, presents a written plan for the completion of the work. The plan should include a budget for the use of computer and laboratory resources which will be charged to the department. Overruns shall be reported to the supervisor.

The original contribution of the candidate and material taken from other sources shall be clearly defined. Work from other sources shall be properly referenced using an acknowledged referencing system.

Supervisor:

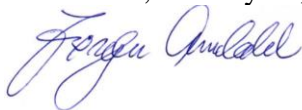
Prof. Jørgen Amdahl

Contact person in Sevan SSP

Torstein Alexander Pettersen

Deadline: June 11 2022

Trondheim, January 10, 2022



Jørgen Amdahl

Preface

This master's thesis was written to finalise a Master's degree in Marine Technology at the Norwegian University of Science and Technology (NTNU). The subject was proposed by Sevan SSP and is therefore written as a cooperation between the Department of Marine Technology at NTNU and Sevan SSP. A project thesis was written the autumn before on the same topic and led to more motivation and curiosity around the topic. The aim of this master's thesis was to gain deeper insight and knowledge into the topic.

Firstly, I would like to say that I found this topic highly interesting. It has been a challenging process and a transition from learning from lectures to learning from yourself. Despite this, I am grateful for the experiences I have accomplished throughout the master's thesis. The aspects involved in the topic are also highly relevant for other impacts like collisions.

I would like to thank my supervisor Jørgen Amdahl for helping me through the thesis, with meaningful discussions, excellent guidance and for giving me motivation on the subject. I would also like to thank Sevan SSP for giving me the opportunity to learn more about the exciting topic. I would like to thank my co-supervisor in Sevan SSP, Torstein Alexander Pettersen for being very helpful throughout the thesis. I am especially grateful for all the help in conjunction with the computer software Abaqus.

I would like to thank Bengt Ullenes and Morten Yttervik in Swire Energy Services AS for giving me drawings of the container. Furthermore, I would like to thank Dave Talloen and Erling Fredriksen in Sevan SSP for helpful information on the subject. I would greatly thank associate professor Zhaolong Yu for helping me with problems in context with understanding and using the supercomputer.

In addition, I would like to thank my fellow students at office C1.080 for meaningful discussions, for making a good working environment and for being motivating in the writing process. Especially, I would like to thank my classmate Stina Bjørgo Fimreite for her helpful discussions throughout the entire writing process. Finally, I would like to thank Tor Erik, friends and family for supporting me when needed.

Trondheim, June 10th 2022



Amalie Ramberg

Abstract

The present master's thesis assesses the structural response of a stiffened panel due to impact from dropped objects, with emphasis on a falling container. The response is carried out using the non-linear finite element software Abaqus/Explicit. A typical container and deck structure are modelled in Abaqus using extruded shells. Different impact scenarios are analysed with emphasis on the energy absorption and damage between the container and the deck. Most of the analyses are performed dynamic with deformable container and deck to obtain a realistic structural response.

An overview of relevant objects which may be lifted above platform decks is presented. This will most often be equipment lifted in containers or lifting frames. A literature study of typical frequencies of the lifted object is given, but is shown to be difficult to obtain. This is since it is either confidential or the statistics are old. Typical kinetic energies involved are calculated based on simplified calculations for different impact mass and drop heights. A 20Te container from a drop height of 24m results in an impact energy of 4.71MJ. For a standard 10 000Te sideways drifting ship collision the impact energy is 28MJ, which indicates that 4.71MJ is a significant high energy and could lead to fatal consequences.

Scenarios for dropped objects are given, among the most critical could be hitting critical equipment below deck. The critical equipment could be tanks, hydrocarbon pipelines etc, and may lead to explosion and fire. Typical deck configurations are also presented. The equipment is in general lifted directly by the shortest and safest way, as low as possible. The deck often consists of several laydown areas and forbidden zones. Objects falling into forbidden zones may result in catastrophic consequences. Critical equipment should be protected by dropped object protection if it is a probability of penetrating the deck in case of a dropped object.

The most important from *DNV-RP-C204*, *DNV-RP-C208* and *DNV-OS-A101* in relation to dropped objects is presented. From *DNV-RP-C204* the calculation of impact energy, force-deformation curves, local buckling and tensile fracture in yield hinges is included. In addition, a review of simplified plastic methods used to assess the resistance of the stiffened panel is given. The importance of strain rate and inertia effects is included with a review of methods that include these effects. The effect of strain rate may be included by the Cowper-Symonds model which is discussed in this report.

In the marine industry many use an informal norm saying that a certain percentage of the energy is absorbed by the container. This assumption can result in non-conservative or conservative results and is very uncertain. The container is often assumed rigid for simplicity, which may result in an unrealistic response of the panel. Results from Abaqus show that around 32-62% of the total plastic dissipation energy is absorbed by the container. This is for the chosen impact scenarios, but will give an indication of the amount of energy the container will be able to absorb. The exact value is dependent on the impact angle and impact location on the panel. It is hence concluded that assuming a rigid container may be very conservative and unrealistic. The results are further compared with the deck damage caused by a rigid container. In addition, the final indentation of deck for the different impact scenarios are found where the worst results in almost 1.4m indentation of the deck.

Further, a parametric study of the deck structure is performed to determine the effect on the structural resistance of the panel. It is desirable to obtain a high energy absorption in the container and the panel should be designed such that this is possible. The parametric study is performed by changing the stiffener size, girder size, plate thickness, stiffener spacing and transverse girder spacing. A script is developed to be able to easily change the geometry of the deck structure instead of remodelling. Each change in stiffener size, girder size, plate thickness, stiffener spacing

and girder spacing is done such that the total weight of the panel is increased the same amount for each change. The background is that the cost of steel is assumed a relevant measure to design the panel efficient for dropped objects. The effect of changing the geometry is found to be dependent on the impact scenario. Changing the stiffener size and girder size is efficient for container falling 45 degrees between two stiffeners with one bottom edge first, while falling with the bottom horizontal beam first shows a negligible increase in the strength of the panel. Changing the plate thickness and stiffener spacing is also efficient for container falling with one edge first. Changing the transverse girder spacing is efficient for container falling 45 degrees with the whole front first, while changing the stiffener spacing results in a decrease in the energy absorption of the container.

Quasi-static analyses are included where the container is forced down with constant velocity. Sensitivity studies of mesh size, boundary condition, friction coefficient, impact mass and impact velocity is included to ensure accurate results. Further, deformation mechanisms from the nonlinear finite element analysis are compared to theory. In addition, the structural response in the panel is assessed with hand calculation using plastic theory with yield hinges and including membrane effects corresponding to theory from *DNV-RP-C204*. Plastic theory using yield hinges results in a significant underestimation of the resistance of the panel, while the results including membrane effects correspond quite well with the results from the finite element analysis.

Sammendrag

Denne masteroppgaven tar for seg den strukturelle responsen av et avstivet panel etter støt fra fallende laster, med hovedvekt på en fallende container. Responsen er funnet ut fra den ikke-lineære elementmetoden med programvaren Abaqus/eksplisitt. En typisk container og dekkstruktur er modellert i Abaqus ved bruk av ekstruderte skall. Forskjellige støtszenarioer er analysert med hovedvekt på energi-absorpsjonen og skaden mellom containeren og dekket. Mesteparten av analysene er utført dynamisk med både deformerbar container og dekk for å oppnå en realistisk respons.

Et overblikk over relevante objekter som vanligvis løftes over plattform dekk er presentert. Dette er ofte utstyr som løftes i containere eller løfterammer. Litteraturstudie av typiske frekvenser for løftede objekter er gitt, men viste seg å være vanskelig. De er enten konfidensielle eller så er statistikken utdatert. Typiske kinetiske energier involvert er regnet ut basert på forenklete beregninger for forskjellige masser og fallhøyder. En 20 tonns container fra en fallhøyde på 24 meter resulterer i en støtenergi på 4.71MJ. For en standard 10 000 tonns sideveis drivende skipskollisjon er støtenergien på 28MJ, noe som gir en indikasjon på at 4.71MJ er en betydelig energi og kan føre til fatale konsekvenser.

Scenarier for fallende laster er gitt, der mest kritisk vil være å treffe kritisk utstyr under dekk. Dette kan blant annet være tanker eller hydrokarbonrør og kan føre til eksplosjon eller brann. Typiske dekk-konfigurasjoner er også presentert. Utstyret er generelt løftet direkte via korteste og tryggeste vei, så lavt som mulig. Dekket består ofte av plasser laget for nedsenking og løfting av utstyr og forbudte soner. Fallende laster i de forbudte sonene vil kunne føre til katastrofale følger. Kritisk utstyr skal være beskyttet mot fallende laster hvis det er en sannsynlighet for gjennomtrenging i dekket.

Den mest relevante teorien for fallende laster fra *DNV-RP-C204*, *DNV-RP-C208* og *DNV-OS-A101* er presentert. Beregning av støtenergien, kraft-deformasjonskurver, lokal knekking og brudd fra *DNV-RP-C204* er inkludert. I tillegg er forenklete plastiske metoder for å finne resistansen av det avstivede panelet presentert. Viktigheten av tøyningshastighet og treghetseffekter er diskutert. Effekten av tøyningshastigheten kan inkluderes med Cowper-Symonds modellen som også er diskutert.

I den marine industrien er det ofte brukt en uskreven regel at en viss prosent av energien er absorbert av containeren. Denne antagelsen kan gi ikke-konservative eller konservative resultater og er veldig usikker å bruke. For enkelthetsskyld er det ofte antatt at containeren ikke kan deformere seg, noe som kan resultere i en urealistisk respons av panelet. Resultater fra Abaqus viser at rundt 32-62% av total plastisk tøyningenergi er absorbert av containeren. Dette er fra de valgte støtszenarioene, men vil gi oss en indikasjon på andelen energi containeren kan absorbere. Den nøyaktige prosenten avhenger av støtvinkel og støtsone på panelet. Det er dermed konkludert at å anta at containeren ikke kan deformere seg kan være veldig konservativt og urealistisk. Resultatene er videre sammenlignet med skaden på panelet fra en analyse der containeren ikke kan deformere seg. I tillegg, er total gjennomtrenging av dekket funnet for de ulike støtszenarioene der den verste resulterer i en gjennomtrenging på nesten 1.4 meter.

Videre er en parametrisert studie av dekkstrukturer utført for å fastslå effekten det har på den strukturelle resistansen til panelet. Det er ønskelig at containeren skal absorbere så mye som mulig av energien og at panelet blir designet slik at dette er mulig. Studien er utført ved å forandre på stiverstørrelsen, bærerstørrelsen, platetykkelsen, stiveravstanden og den tverrgående bæreravstanden. Et skript er utviklet for å raskt kunne endre geometrien i dekket uten å måtte modellere på nytt. Endring i stiverstørrelse, bærerstørrelse, platetykkelse, stiveravstand og bæreravstand er gjort så den totale vekten av panelet øker likt for hver endring. Bakgrunnen er at

kostnaden av stål er antatt et relevant mål for å designe panelet effektivt mot fallende laster. Effekten av å endre geometrien er avhengig av støtscenarioet. Endring av stiver- og bærerstorrelsen er effektiv for container fallende 45 grader mellom to stivere med nederste hjørne først, mens fallende med nederste horisontale bjelke første gir neglisjerbar økning i styrken av panelet. Endring av platetykkelsen og stiveravstanden er også effektivt for container fallende med nederste hjørne først. Endring av den tverrgående bæreravstanden er effektivt for container fallende 45 grader med hele fronten først, mens endring av stiveravstanden resulterer i en lavere andel energi absorbert av containeren.

Kvasi-statiske analyser er inkludert der containeren er tvunget ned med en konstant hastighet. Sensitivitetsanalyser av meshstørrelse, grensebetingelser, friksjonskoeffisient, masse av container og hastighet av container er inkludert. Videre er deformasjonsmekanismer fra den ikke-lineære elementmetoden analysen sammenlignet med teorien. I tillegg er den strukturelle responsen i panelet funnet med håndberegninger ved bruk av plastisk teori med flyteledd og med membraneffekter ved hjelp av teori fra *DNV-RP-C204*. Plastisk teori med flyteledd resulterer i en betydelig undervurdering av resistansen i panelet, mens resultatene der membraneffektene er inkludert korresponderer bra til resultatene fra elementmetoden i Abaqus.

Table of Contents

List of Figures	x
List of Tables	xii
1 Introduction	1
1.1 Motivation	1
1.2 Previous work	2
1.3 Limitations	2
1.4 Challenges	3
2 Background	4
2.1 Offshore containers and lifting frames	4
2.2 Deck configurations and lifting heights	5
2.3 Risk assessment	6
2.4 Petroleum safety authority Norway	7
3 Rules and standards for impact design	8
3.1 DNV Standards	8
3.2 DNV-RP-C204	8
3.2.1 Acceptance criterion	8
3.2.2 Impact energy	8
3.2.3 Force-deformation curves	9
3.2.4 Local buckling	11
3.2.5 Tensile fracture in yield hinges	12
3.3 DNV-RP-C208	13
3.4 DNV-OS-A101	13
3.5 Impact energy	13
3.6 Energy dissipation	14
3.6.1 Eccentric impact	15
4 Simplified plastic methods	16
4.1 Static calculation of plastic resistance	17
4.2 Kinematic calculation of plastic resistance	17

4.3	Combined loading	18
4.4	Plastic capacity of plates	19
5	Bending of stiffeners	21
6	Importance of inertia effects and strain rate	22
6.1	Inertia effects	22
6.2	Strain rate	23
7	Modelling for finite element analysis	25
7.1	Container model	26
7.2	Deck structure	27
7.3	Material properties	28
7.4	Modelling of ductile failure	29
7.4.1	Damage initiation criterion for ductile damage	30
7.4.2	Displacement at failure	31
7.4.3	Alternative fracture criteria	31
7.5	Discretisation and interaction	32
7.5.1	Element type	33
7.5.2	Mesh size	33
7.5.3	Stable time increment	33
7.5.4	contact formulation	34
7.6	Boundary conditions	34
8	Preparation for finite element analyses in Abaqus	35
8.1	Mesh sensitivity study	35
8.1.1	Rigid deck	37
8.1.2	Rigid container	38
8.2	Point masses versus nonstructural mass	39
8.3	Discussion of computational time	40
9	Analysis and Results	42
9.1	Impact scenarios	42
9.1.1	Results	43
9.1.2	Final indentation of deck	48

9.1.3	Deformation mechanisms of panel	49
9.1.4	Note on eccentric impact	52
9.1.5	Note on energy balance	53
9.2	Rigid vs deformable container	54
9.3	Geometry study of the panel	55
9.3.1	Change in stiffener size	55
9.3.2	Change in girder size	56
9.3.3	Change in plate thickness	57
9.3.4	Change in stiffener or girder spacing	58
9.3.5	Comparison	59
9.4	Quasi-static analyses	60
9.4.1	Quasi-static with rigid dekk	60
9.4.2	Force-deformation curves	61
9.4.3	Quasi-static with both deformable	62
9.5	Sensitivity study	64
9.5.1	Boundary condition	64
9.5.2	Friction	64
9.5.3	Mass of container	65
9.5.4	Impact Velocity	66
10	Structural response using hand calculations	68
10.1	Plastic theory using yield hinges	68
10.2	Including membrane effects	69
10.3	Tensile fracture in yield hinges	71
10.4	Comparison with result from nonlinear finite element analysis	72
11	Conclusion	75
12	Further work and improvements	76
	Bibliography	78
	Appendix	82
A	General arrangement 20ft container	83
B	True stress- true strain graphs	85

C	True stress - True strain values	86
D	Final damage of panel shown from stiffener side	91
E	Energies for impact scenario 1-7	92
F	Distribution of plastic dissipation energy for impact scenario 1-7	94
G	Hand calculations	95
G.1	Effective plate width	95
G.2	Plastic neutral axis	95
G.3	Plastic section modulus	95
G.4	Plastic moment capacity	96
G.5	Elastic neutral axis	96
G.6	Moment of inertia	96
G.7	Elastic section modulus	96

List of Figures

2.1	20ft container [59].	5
2.2	Lifting frame [32].	5
2.3	Cranes on a FPSO [48].	5
3.1	Dissipated strain energy [57].	9
3.2	Design principal for impacts [18].	14
3.3	Strain energy dissipation factor versus mass ratios and contact eccentricity [9]. . .	15
4.1	Stress - strain curve.	16
4.2	Linearly elastic perfectly plastic stress - strain curve.	16
4.3	Plastic mechanism for clamped and simply supported beam.	17
4.4	Rooftop mechanism [8].	19
5.1	Stiffened panel [60].	21
5.2	Collapse modes for stiffened plate [5].	21
6.1	Deflections of mid-point of column [7].	22
7.1	Constraint [51].	26
7.2	Material properties [51].	26
7.3	Dimensions of the deck.	27
7.4	Deck structure [51].	28
7.5	Fixed BC for the deck structure [51].	34
8.1	Resulting deformation with fine mesh in impact zone [51].	36
8.2	Internal energy for the analyses with rigid deck [51].	37
8.3	Final deformation for 25mm fine mesh to the left and 50mm fine mesh to the right [51].	37
8.4	Internal energy from quasi-static analyses [51].	38
8.5	Internal energy and displacement for different mesh sizes [51].	38
8.6	Force for different mesh sizes [51].	39
8.7	Distribution of kinetic energy for scenario 4 using point masses [51].	39
8.8	Distribution of kinetic energy for scenario 4 using nonstructural mass [51].	40
9.1	Illustration of the different impact scenarios [51].	44
9.2	Deformed shape of the container at last increment [51].	45
9.3	Deformed shape of the panel from above at last increment [51].	46
9.4	Deformation mechanism plotted from Abaqus [51].	50

9.5	Deformation modes at time: 0.009s, 0.015s, 0.024s and 0.036s without fracture criteria[51].	51
9.6	Deformation at maximum displacement without fracture criteria [51].	51
9.7	Deformation at maximum displacement without fracture criteria [51].	51
9.8	Spatial displacement in y-direction and rotational displacement in y- and z-direction [51].	52
9.9	Deformed shape of the panel from above to the left and from under to the right [51].	54
9.10	Different energies for impact scenario 1 with rigid container [51].	54
9.11	Force-deformation and energy-deformation curve for quasi-static analyses with rigid deck [51].	60
9.12	Deformation of container with rigid deck [51].	61
9.13	Force-deformation curve using rigid container and rigid deck [51].	62
9.14	Distribution of internal energy from quasi-static analysis [51].	63
9.15	ALLPD for fixed and pinned BC for impact scenario 4 to the left and 7 to the right [51].	64
9.16	ALLFD and ALLPD for different friction coefficients [51].	65
9.17	Total plastic dissipation energy for different impact mass [51].	66
9.18	Total plastic dissipation energy for different impact velocities [51].	67
10.1	Deformation point on top of stiffener web [51].	72
10.2	Deformation of stiffener for impact scenario 4[51].	72
10.3	Deformation of stiffener for impact scenario 6 [51].	73
10.4	Deformation to rupture of stiffener from Abaqus[51].	74

List of Tables

2.1	Dimensions, tare weight, payload and MGW for 10ft and 20ft container [31] and lifting frames [22].	4
3.1	Types of cross-sections [55].	12
3.2	Some values for ε_{cr} and H [57].	13
3.3	Impact energy for different masses and drop heights.	14
7.1	Details of the container model in Abaqus.	27
7.2	Detailed dimensions for the deck structure used in Abaqus [12].	28
7.3	Material properties from <i>DNV-RP-C208</i> [58].	29
8.1	Mesh sizes for rigid deck.	36
8.2	Mesh sizes for rigid container.	36
8.3	CPU time for the different analysis [51].	41
9.1	Impact scenarios.	42
9.2	Distribution of plastic dissipation energy [51].	47
9.3	Final indentation of deck [51].	48
9.4	Energies from Abaqus [51].	53
9.5	Impact scenarios for geometry study of the panel.	55
9.6	Values for change in stiffener size.	55
9.7	Plastic dissipation energy with changed stiffener size [51].	56
9.8	Values for change in girder size.	56
9.9	Plastic dissipation energy with changed girder size [51].	57
9.10	Values for change in plate thickness.	57
9.11	Plastic dissipation energy with changed plate thickness [51].	57
9.12	Values for change in stiffener and girder spacing.	58
9.13	Plastic dissipation energy with changed stiffener or girder spacing [51].	58
9.14	Plastic dissipation energy for container for the impact scenario with the highest increase.	59
9.15	Average increase in ALLPD container for the different geometry changes.	59
9.16	Plastic dissipation energies for quasi-static and dynamic analysis - Impact scenario 7 [51].	63
9.17	Plastic dissipation energy for container with changed BC [51].	64
9.18	Energy dissipation due to friction, ALLFD [51].	65
9.19	Values for change in impact mass [51].	65

9.20	Values for change in impact velocity.	66
9.21	Values for change in impact velocity [51].	66
10.1	Cross-sectional values and other parameters used for hand calculations.	68
10.2	Important parameters used for membrane effects.	70
10.3	Total deformation in the middle of the stiffener span.	73
10.4	Total deformations.	74

Abbreviations

ALLAE	Artificial strain energy
ALLCD	Creep dissipation energy
ALLDMD	Damage dissipation energy
ALLFD	Frictional dissipation energy
ALLIE	Internal energy
ALLKE	Kinetic energy
ALLPD	Plastic dissipation energy
ALLSE	Strain energy
ALLVD	Viscous dissipation energy
ALLWK	External work
ALS	Accidental limit state
BC	Boundary condition
CPU time	Computational time
ETOTAL	Total energy of the output set
FPSO	Floating production storage and offloading
MGW	Maximum gross weight
PSV	Platform supply vessel

Symbols

α	Plate aspect parameter/Stress state
β	Energy dissipation correction factor/Factor/Strain state
Δt	Step increment at current time/Stable time increment
ε	Strain
$\dot{\varepsilon}$	Strain rate
ε_{cr}	Critical strain for rupture
ε_{crl}	The maximum principal strain
ε_{crg}	The gross yielding critical strain
ε_{eq}	Fracture strain
$\dot{\varepsilon}_{eq}^p$	Plastic strain rate
ε_{eq}^p	Plastic strain
ε_y	Yield strain
θ	Angle for plastic mechanism
$\bar{\lambda}$	Slenderness ratio
λ	Reduced plate slenderness
ν	Poisson ratio

ρ	Density
σ	Stress
σ^*	Stress triaxiality
σ_I	Principal stress
σ_0	Initial static yield stress
σ_{static}	Static yield stress
σ_y	Yield stress
$\sigma_y^d/\sigma_{dynamic}$	Dynamic yield stress
ω	Cockcroft-Latham failure criterion
a	Plate length
A	Total area of stiffener and plate flange
A_f	Stiffener flange area
A_p	Plate area
A_s	Stiffener area
A_w	Stiffener web area
b	Plate width
b_f	Flange width
b_{f,g}	Girder flange width
b_{f,s}	Stiffener flange width
c	Non-dimensional spring stiffness
c_f	Axial flexibility factor
c_{lp}	Plastic zone length factor
c_w	Displacement factor
C	Material parameter Cowper-Symonds
C_d	Dilational wave speed
C_t	Transition factor
C_{x,s}	Reduction factor due to stresses in longitudinal direction
C_{y,s}	Reduction factor for compression stresses in transverse direction
d_c	Characteristic dimension
D	Diameter
D₁	Model constant Johnson-Cook
D₂	Model constant Johnson-Cook
D₃	Model constant Johnson-Cook
D₄	Model constant Johnson-Cook
D₅	Model constant Johnson-Cook
E	Elastic modulus
E_{kin}	Kinetic energy

E_p	Plastic modulus
E_s	Total dissipated strain energy
$E_{s,i}$	Dissipated strain energy impacted member
$E_{s,o}$	Dissipated strain energy dropped object
E_t	Plastic tangent modulus
f_{cr}	Strength corresponding to ε_{cr}
f_y	Characteristic yield strength
g	Gravity acceleration
h	Drop height
h_w	Web height
$h_{w,g}$	Girder web height
$h_{w,s}$	Stiffener web height
H	Non-dimensional plastic stiffness
i	Radius of gyration
I	Moment of inertia
k	Equivalent elastic, axial stiffness
K_{node}	Axial stiffness of the node with the considered member assumed removed
l_e	Length of the element
l_g	Transverse girder spacing
l_s	Stiffener spacing
L/l	Stiffener span/member length, plate length
L_l	Lode parameter
m	Impact mass
m_{eff}	Effective mass due to eccentric impact
m_i	Mass of impacted member
m_o	Mass of dropped object
M	Cross-sectional moment
M_p	Plastic moment
N	Axial force
N_p	Axial plastic resistance of cross-section
p	Strain
\dot{p}^*	Dimensionless plastic strain rate
p_f	Failure strain
P	Load
P_s	Plastic resistance simply supported
P_c	Plastic resistance clamped
q	Material parameter Cowper-Symonds/ Resistance

q_c	Plastic resistance
r	Resistance
r_c	Plastic resistance in bending for plates with no axial restraint
R	Resistance
R_0	Plastic collapse resistance in bending
R_i	Force impacted member
R_o	Force dropped object
s	Plate width, Stiffener spacing
s_e	Effective width of plate flange
t	Plate thickness/thickness
t_f	Flange thickness
t_w	Web thickness
$t_{f,g}$	Girder flange thickness
$t_{f,s}$	Stiffener flange thickness
$t_{w,g}$	Girder web thickness
$t_{w,s}$	Stiffener web height
T	Stress triaxiality/Temperature
T^*	Homologous temperature
T_0	Reference temperature
T_m	Melting temperature
\bar{u}^{pl}	Equivalent plastic displacement at failure
\dot{u}^{pl}	Equivalent plastic strain rate
v	Impact velocity
v_c	Speed of wave propagation
v_o	Velocity of dropped object
v_i	Velocity of impacted member
w	Deformation, displacement
w_i	Deformation impacted member
w_o	Deformation dropped object
\bar{w}	Non-dimensional displacement parameter
w_c	Characteristic deformation for stiffened plating
W	Elastic section modulus
W_c	Fracture parameter
W_e	External work
$W_{i,c}$	Internal work for clamped
$W_{i,s}$	Internal work for simply supported
W_p	Plastic section modulus

W_{yb}	Elastic section modulus corresponding to y_b
W_{yt}	Elastic section modulus corresponding to y_t
x	Radii of gyration
y_p	Plastic neutral axis from bottom of the stiffener
y_b	Elastic neutral axis from bottom of the stiffener
y_t	Elastic neutral axis from plate top

1 Introduction

In the offshore industry, equipment is often lifted at significant heights over deck and may lead to catastrophic consequences if falling on deck. Dropped objects are hence an important scenario that needs to be taken into account and is therefore categorized as an accidental event. A dropped object will in general result in local damage and therefore minor damage to the structure in total. Despite this, the local damage may lead to catastrophic damage to the plates, stiffeners, girders and most critical may hit equipment below deck leading to fatal consequences [10].

Accidental events are caused by technical faults, human errors or environmental loads. The accidental limit state (ALS) is a check for survival of the structural system which is damaged due to accidental actions or abnormal environmental loads [17]. The main purpose of the ALS check is to ensure that small damages do not result in large fatal consequences. The ALS design check consists first of estimating the damage due to accidental loads at an annual exceedance probability of 10^{-4} . Then checking for the survival of the damaged structure under functional and environmental actions is considered [17].

A dropped object can have different shapes, sizes and weights. This will affect the damage sustained by the impacted member. The impact angle and the location of impact will also have large importance on the damage obtained. This master's thesis will firstly give an overview of the topic by typical accidental scenarios, relevant objects that may be lifted, deck configurations, lifting heights and typical frequencies of the lifted object. Secondly the most important in relation with dropped objects from *DNV-RP-C204*, *DNV-RP-C208* and *DNV-OS-A101* is given. Then some kinetic energies for different weights and drop heights are presented. Further, design principles for impacts, eccentric impact and deformation modes of stiffeners due to bending is discussed. A review of simplified plastic methods for estimating the resistance of stiffened panels is presented, together with a discussion of the importance of inertia effects and strain rate. Next, an explanation of the relevant theory in conjunction with the non-linear finite element method is presented. Then the results from the finite element analyses are discussed with special emphasis on the dissipation of strain energy. Lastly, hand calculations are used to validate the finite element analysis.

In this master's thesis the main focus is the container as dropped object and the deck as the impacted member, which is seen as a critical scenario and will hence give us conservative and realistic results. The deck will consist of stiffeners, girders and plate. Therefore this has been the basis for the modelling in Abaqus. Dynamic analyses have been carried out using Abaqus/Explicit and both the container and the stiffened panel are mostly modelled as deformable. The choice of modelling the container as rigid or deformable is discussed and justified with results from the non-linear finite element analysis. The main focus has been the energy absorption in the container, since it is desirable a low energy absorption in the panel. For the fact that the container is often assumed rigid, it is important to ensure that this isn't too conservative.

1.1 Motivation

The amount of the total strain energy that the container will be able to absorb is a highly relevant issue for the marine industry. For the analytical expressions many use an unwritten rule saying that a certain percentage of the energy can be taken by the container. This is a very uncertain assumption to use and may result in very non-conservative or conservative results. There exist several studies on the impact of deck due to dropped objects, but the dropped object is often modelled as rigid. Depending on the dropped object and what it contains, the dropped object could be able to absorb a significant part of the strain energy. Here is some research presented from a literature review.

The energy dissipation is discussed in the report from the institution of mechanical engineers. It is mentioned that the container often is assumed rigid so all the strain energy must be absorbed by the deck, since this will lead to conservative results as described above. The report only suggests looking at the container as deformable as further work [23].

A report from SINTEF explicitly states that the design philosophy is that all the initial kinetic energy from the container must be absorbed as elastic and plastic work in the deck, without causing structural failure. It is not mentioned that some of the energy could be absorbed by the container [15].

In addition, a master's thesis done for the same topic assumed at first an infinitely rigid container for simplicity, but then the effects of a deformable container were studied by remodelling. This resulted in a decrease of energy absorption in the deck by 93%, meaning most of the energy was actually absorbed by the container [10]. While another master thesis, also written about dropped objects, specifically about dropped object protection assumes a rigid load/container [20]. In other words, the assumption of a deformable container is included to some degree before, but in most cases neglected.

1.2 Previous work

A project thesis was written the autumn before on the same topic to gain insight and motivation on the topic. Only a small part of the bottom of the container was modelled for simplicity and lack of drawings. The container was modelled deformable to obtain the relationship of energy absorption between the deck and the container. The analysis was performed quasi-static by forcing the container down in a constant low velocity to neglect the dynamic effects. Only one impact scenario was analysed. The project work made the foundation for this master's thesis.

1.3 Limitations

The scope of the master's thesis is limited to assessing the structural response of a given stiffened panel due to impact from a falling container. The emphasis is on the energy absorption between the container and the stiffened panel, due to limited research in this field. The analyses are performed dynamic to obtain realistic results. The strain rate is neglected in all the analyses due to many uncertainties.

The main result from the dynamic finite element analysis is the distribution of energy between the container and the panel. The energy-deformation and force-deformation curves are given for quasi-static analyses, hence neglecting dynamic effects and "forcing" the container down with a constant velocity in one direction.

The impact scenarios are limited to seven scenarios with different impact locations and/or impact angles. The emphasis has been to analyse the worst case scenarios. Therefore, falling on the whole bottom/top is neglected. The container is only falling in the middle between two girders, and not on or close to a girder. The geometry study is limited to three of the scenarios assuming the worst and every analysis is done with one test value. Since the container is modelled from confidential drawings, discussion in detail due to the dimensions of the container is limited.

The container is modelled using nonstructural mass distributed equally around the whole container and is fixed during the impact. This simplification is made due to the difficulties in modelling mass inside the container which can move during impact.

The mesh size is limited by the high computational time (CPU time) and the high amount of analyses planned. Further, the container is a combination of S275 and S355 steel, while the panel is S355 steel. The material in the panel has not been changed. In addition, the hand calculations are limited to impact scenarios where the container is falling directly on stiffeners and not on the plate between stiffeners.

1.4 Challenges

Right from the start, it was far more difficult to obtain detailed enough dimensions/drawings of an offshore container than I could ever imagine. This led to around 5 weeks spent waiting to get a drawing, which postponed the plan of modelling.

After some weeks of modelling, I realised the large computational time needed for the analyses. Because of the large number of analyses I had planned, I gained access to a supercomputer. Because of problems with making the analyses run on the supercomputer, I spent time that wasn't planned. Further, it turned out that using the supercomputer led to storage memory issues. The supercomputer uses memory when running and when downloading the files. Since the supercomputer uses another version of Abaqus than I had installed, it also needed storage memory when converting from the two versions. Taking all into account, it was easier to use my own computer. Despite the large time used to learn how to use the supercomputer, I am greatly for what I learned during the process.

2 Background

In the case of dropped objects, different accidental scenarios would cause several consequences for the dropped object and the impacted member. A typical design accidental scenario could be that the dropped object penetrates towards the deck and may hit tanks or hydrocarbon pipelines, which may at worst lead to an explosion or fire. From the hydrocarbon pipelines, some could leak into the sea, but the frequency for this to happen and the volume leaking to the sea is low [47]. The dropped object can also puncture buoyancy tanks and can lead to fatal consequences for the hydrostatic stability of floating installations [57]. Another scenario could be personnel injury by either the object falls or touches a personnel, which at worst may lead to death. The most common scenario offshore is object swinging in the crane and hitting equipment on deck. To protect against this there exist a lot of bumper bars around loading bays. In general, the deck consists of impact protection at places where it is most likely that the object may fall, often where most of the lifting operations take place [47].

In addition to the scenarios mentioned above, a hot topic is the offshore wind turbine industry. Here lifting is a central part, for example lifting of turbine blades for installation of the wind turbine. This is often installed from ships and the blades could fall on deck, which may lead to huge consequences for the shaft and deck [11].

2.1 Offshore containers and lifting frames

For cargo handling between Platform Supply Vessel (PSV) and Floating production storage and offloading (FPSO) almost all cargo comes in containers. There exist a lot of different sizes of containers. Sometimes it may also be lifted some kind of "special equipment" which needs to come with a lifting frame. The inboard lift is somewhat different. Here equipment like pumps, engines and coolers are lifted from the cargo bay to the FPSO. The weight of this can be all from 0.5Te to max crane capacity. The typical weight of a 10ft container being lifted is around 5-6Te. A standard lifting may be considered up to around 10Te, above this is denoted special lifts. This limit will vary from FPSO to FPSO and depending on the crane, weather, supply vessel, deck space etc.[47].

Offshore containers and lifting frames exist in many different sizes depending on the equipment that shall be lifted. The lifting frames are used when the equipment doesn't fit inside a container or it is an easier process to lift with the lifting frame. All the lifting frames are provided with certified slings and shackles [32]. Since the lifting frame is open on one side as seen in Figure 2.2, it could also fall on this side. Depending on the equipment which is lifted this may lead to fatal consequences for the lifted equipment and the impacted member. Below is given a table of typical dimensions, tare weight, payload and maximum gross weight (MGW) for the 10ft and 20ft offshore containers, together with two different lifting frames. The tare weight, payload and MGW typically vary from supplier to supplier.

Table 2.1: Dimensions, tare weight, payload and MGW for 10ft and 20ft container [31] and lifting frames [22].

Measure	10ft container	20ft container	6.8m lifting frame	8m lifting frame
Length [m]	2.991	6.058	6.800	8.010
Width [m]	2.438	2.438	4.500	5.000
Height [m]	2.591	2.591	3.066	3.066
Tare weight [Te]	2.105	3.530	8.800	11.270
Payload [Te]	7.895	16.470	30.000	30.000
MGW [Te]	10.000	20.000	38.800	41.270

Some other types of containers could be a mini container, closed container, food container, half height container, open top containers and IBC Carrier [31]. A typically lifting frame and a 20ft container is shown below in Figure 2.1 and 2.2.



Figure 2.1: 20ft container [59].



Figure 2.2: Lifting frame [32].

2.2 Deck configurations and lifting heights

Containers from PSV to the loading bay are lifted directly by the shortest and safest way, as low as possible. It is also avoided lifting over other equipment, as far as possible. With inboard lifts a risk assessment is carried out for every lift [47]. It is common to have one or several laydown areas, which should be used to lift and lower the object. It is also common to protect the critical equipment, safety-critical systems and hydrocarbon systems which are close to the laydown areas with swinging load protection, as also mentioned above. Especially the ones near the primary or secondary laydown areas. It could also be some forbidden zones, for example where it could result in broken risers or damage of other highly critical equipment [49].

A typical FPSO with cranes is shown below. The FPSO contains of two cranes, where in this case almost all lifts are done by the eastern crane [48].

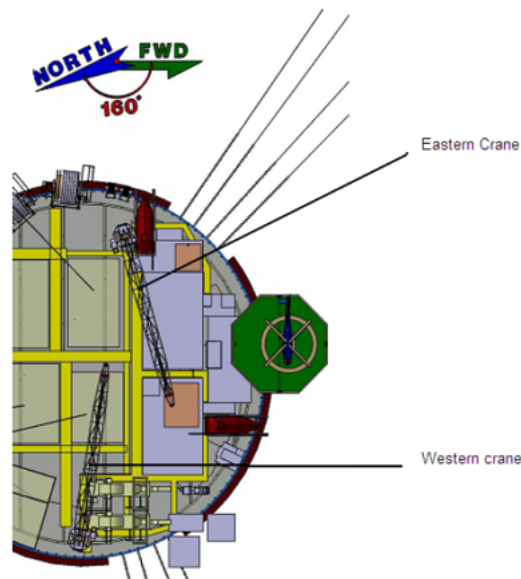


Figure 2.3: Cranes on a FPSO [48].

The typical lifting height is at least 8 meters over the main deck [47]. The impact energies for different lifting heights and weights are considered later in Section 3.5. A more detailed description of typical lifting heights, laydown areas, forbidden zones etc. was preferable. But after a literature study, this was difficult to obtain. It is either from confidential drawings or lack of experience and/or knowledge. The structure in relation to tanks, hydrocarbon pipelines etc was preferable since this would be highly critical to hit.

A typical deck structure consists of stiffeners, girders and plate. Depending on how the dropped object will hit the deck, this will give several consequences. The container could possibly fall straight on a stiffener, straight on a girder, on plate between stiffener and girder, on plate between two stiffeners or over several stiffeners. The most critical will probably be hitting between two stiffeners.

2.3 Risk assessment

The dropped object may hit the impacted member/deck differently, which will affect the energy absorption of the deck. The container may hit the deck with an entire surface, meaning the bottom, top or one of the sides. More critical it could hit with an edge by 45 degrees angle. The last one is most dangerous since the impact force will be distributed in a smaller area of the deck and hence energy absorption distributed in a small area. While for the container hitting with an entire surface the impact force will be distributed over several stiffeners. In addition, the resulting consequence will depend on how much energy the container will be able to absorb in relation to the deck. This will depend on the equipment inside the container, in other words it depends on the stiffness relationship between the two bodies.

The occurrence of dropped objects depends on the lifting activity on the FPSO. Based on statistics for 1980-86, falling pipes have a frequency of about $2.5 \cdot 10^{-5}$ per lift operation in the North Sea. Falling object as cranes and containers has limited statistics, but are much less frequent than falling pipes. For heavy maintenance lifts, the frequency is so low that the risk is considered negligible [17].

For data from 1980 to 2001 for the North Sea (UK and Norwegian sector) it is found that the average activity for a crane is 8000 lifts per crane per year. The dropped object may be divided into three accident types: dropped objects from crane boom, crane boom fall and crane fall. Crane fall has only happened once. Based on the 8000 lifts per crane per year, frequencies have been obtained for the different types of dropped objects. In addition, hit probabilities in relation to where it is most probable to fall are also found. The frequency per crane per year for crane fall is found to be $8.0 \cdot 10^{-5}$ and a 100% probability to fall into the sea. For crane boom fall the frequency per crane year is found to be $1.4 \cdot 10^{-3}$ with a 5% probability of falling into the sea, 30% on vessel and 65% on the topside. For dropped objects from crane boom, the frequency is found to be $2 \cdot 10^{-2}$ and the hit probability is 20% into the sea, 5% on vessel and 75% on topside [48].

In general, data for frequencies of the lifted object is highly difficult to obtain. Either the data is very confidential or too old as the statistics described above. It would have been preferable to have more data and from more recent times.

2.4 Petroleum safety authority Norway

The Petroleum safety authority Norway has responsibility for the petroleum safety, among other things they investigate and follows up on accidents involving dropped objects. Here is presented some of the cases the Petroleum safety authority Norway has followed up on.

At Heidrun September 2015 a lifting operation of a tension rod compensator with riser joints took place. The tension rod compensator bumped into an open deck hatch, which broke loose a deck grate. The deck grate fell 8 meters and hit a person in the shoulder. Luckily it doesn't led to death, but the deck grate could have fell to underlying deck and hit other personnel or hydrocarbon pipelines [27].

At Gullfaks-B March 2017 a 14.4 tons boom on the pipe handling crane fell 10 meters down on the pipe deck after the steel rope collapsed. There was no personnel injury, but it was huge material consequences. The accident also led to stop of the activity on Gullfaks-B [26].

At West Bolsta in October 2020 a riser joint fell from a lifting operation when it was lifted from horizontal to vertical position. The hydraulic riser running tool does not had sufficient grip on it. The accident led to destroyed equipment and the riser joint had to be replaced. Luckily there was no personnel injury. The riser joint was 22.9 meters long and had a weight of 26.5 tons [25].

In addition to some of the cases the Petroleum safety authority Norway has followed up, Stavanger Aftenblad made an article about another critical event. At Statfjord-A September 2012 a 9.9 tons container with nitrogen gas fell from 40 meter on the deck. This happened when the tank was lifted from the platform to the PSV. The wire collapsed and the container fell on the deck, which led to a hole in the tank and the gas leaked out. There was no personnel injury, but it could have led to fatal consequences. The wire collapsed from corrosion, wear and fatigue fracture [30].

3 Rules and standards for impact design

In the following sections are rules and standards for impact design presented and discussed. The most important in relation to dropped objects from the standards are given. Typical impact energies are included and energy dissipation for impacts is presented.

3.1 DNV Standards

There are several DNV standards and recommendations that are relevant to the topic. In this master's thesis the following is mentioned:

- *DNV-RP-C204 Structural design against accidental loads*
- *DNV-RP-C208 Determination of structural capacity by non-linear finite element analysis methods*
- *DNV-OS-A101 Safety principles and arrangements*

3.2 DNV-RP-C204

DNVGL-RP-C204 Structural design against accidental loads is highly relevant for dropped objects, especially chapter 4. In this chapter the most important from this recommended practice is presented and hence used as a reference for the following[57].

3.2.1 Acceptance criterion

Dropped objects may lead to large deformations, partial collapse, inelastic behaviour and fracture. This may be accepted, as well as the load bearing function of the structure is intact after impact. Therefore the dropped object shall not fall through the impacted structure and/or should not hit important inventories or structures underneath. This must be considered with some margin.

3.2.2 Impact energy

The dropped object is characterised by kinetic energy which needs to be dissipated as strain energy in the impacted member and the dropped object. The kinetic energy is given by Equation 1.

$$E_{kin} = \frac{1}{2}mv^2 \quad (1)$$

The velocity can be expressed as below,

$$v = \sqrt{2gh} \quad (2)$$

where h is the drop height. As seen, the energy is proportional with the drop height. *DNV-RP-C204* also addresses objects falling in water, but is not included here since it is not relevant for this master's thesis.

The strain energy dissipation is found from force-deformation relationships for the impacted member and the dropped object, where the area under the force-deformation curve equals the dissipated strain energy. The structural resistance is represented by the force-deformation curve and is a result of the dissipation of elastic and plastic strain energy [10]. This is shown in Figure 3.1, which is taken in context with ship collision, but can directly be used in conjunction with dropped objects. Then the ship is the dropped object and the installation is the impacted member, in our case the deck.

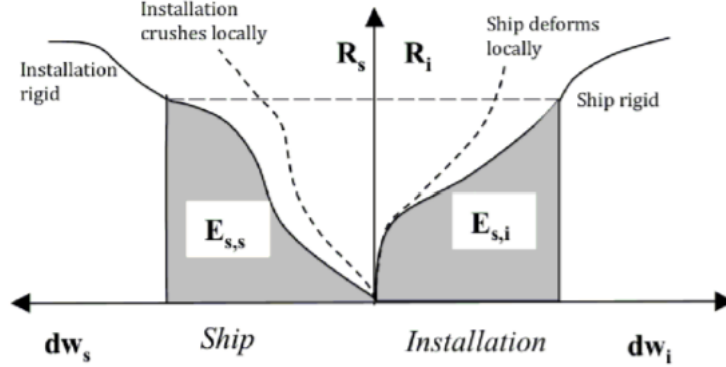


Figure 3.1: Dissipated strain energy [57].

Sometimes the dropped object can be assumed rigid, meaning all the strain energy must be dissipated by the impact member. On the other hand, this is rarely a realistic scenario, since the dropped object will always be able to absorb some of the strain energy, but to varying degrees. How much of the energy the dropped object will be able to absorb depends on how soft and strong the dropped object and impacted member are compared to each other. The stronger one will probably experience less damage than the softer one. Often the load-deformation curve for the impacted member and dropped object is found independently of each other, but this will not account for that the stronger one will probably be less damaged. When the softer structure deforms, the impact force will be distributed over a larger contact area, which may lead to an increase of the resistance of the stronger structure. Therefore an energy dissipation correction factor β is introduced to take into account the energy dissipation. The equation for the dissipated strain energy can now be expressed as Equation 3 below,

$$E_s = E_{s,o} + E_{s,i} = \beta \int_0^{w_{o,max}} R_o dw_o + \int_0^{w_{i,max}} R_i dw_i \quad (3)$$

where the notations o is for dropped object and i for the impacted member.

For more accurate calculations of impact from blunt objects, the recommended practice refers to the chapters that address explosions and fires. Further are some relevant theory and equations from these chapters presented.

3.2.3 Force-deformation curves

As mentioned earlier the force-deformation relationship for the dropped object and the impacted member may be used to find the dissipated strain energy. This will be able to include the effect of membrane effects, which will give better capacity depending on the adjacent structure to restrain the connections at the member ends to inward displacements. The impacted structure should be able to absorb more energy at lower deformation when accounting for membrane effects. The

deformations in the impacted member should meet the stability and ductility requirements. For stiffened plates the plastic force-deformation curve is found by Equation 4 below,

$$\frac{R}{R_0} = \begin{cases} r_1 & \text{if } \bar{w} \leq \bar{w}^* \\ r_2 & \text{if } \bar{w} > \bar{w}^* \end{cases} \quad (4)$$

where

$$r_1 = 1 + \frac{1.8}{a_1} n_1 \cdot \bar{w}$$

$$r_2 = 1 - \frac{1.8}{a_1} \left(\frac{1}{2} a_2 n_2^2 - (n_2 + n^*) \bar{w} \right)$$

$$n_1 = \frac{1}{a_1} \left(\bar{w} - \frac{1 - e^{-a_1 c \bar{w}}}{a_1 c} \right)$$

$$n_2 = \frac{1}{a_2} \left(\bar{w} - \frac{1 - C_t e^{-a_2 c \bar{w}}}{a_2 c} \right)$$

$$C_t = (1 - a_2 \cdot c \cdot \bar{w}^*) e^{a_2 \cdot c \cdot \bar{w}^*}$$

$$\bar{w}^* = \bar{w} \text{ that gives } n_1(\bar{w}) = n^*$$

$$n^* = \frac{A_p - A_s}{A_p + A_s}$$

$$a_1 = \frac{0.9}{a_2} \left(1 + \frac{2A_f}{A_w} \right)$$

$$a_2 = \frac{1}{2} \left(\frac{A_p}{A_s} + 1 \right) \left(\frac{A_f}{A_w} + 1 \right)$$

$$R_0 = \frac{8c_1 f_y W_p}{l}$$

$$\bar{w} = \frac{w}{c_1 w_c}$$

$$w_c = \frac{1.2W_p}{A}$$

$$c = \frac{4c_1 k w_c^2}{f_y A l}$$

where $c_1 = 2$ for clamped beams and $c_1 = 1$ for pinned beams. C_t is the transition factor, W_p is the plastic section modulus and A is the total area of stiffener and plate flange given as $A = A_s + s \cdot t$. $w_c = \frac{D}{2}$ for tubular beams. It is important to note that the requirement $h_w/t_w < 20$ should be satisfied. This is because the plastic interaction relationship is based on compact cross-sectional behaviour through sustained plastic deformations.

The resistance curve for plates subjected to uniform pressure and edges fully restrained against inward displacement can be expressed as Equation 5 below,

$$\frac{r}{r_c} = \begin{cases} 1 + \bar{w}^2 \left(\frac{\alpha + (3-2\alpha)^2}{9-3\alpha} \right) & \text{if } \bar{w} \leq 1 \\ 2\bar{w} \left(1 + \frac{\alpha(2-\alpha)}{3-\alpha} \left(\frac{1}{3\bar{w}^2} - 1 \right) \right) & \text{if } \bar{w} > 1 \end{cases} \quad (5)$$

where

$$r_c = \frac{6c_1 f_y t^2}{l^2 \alpha^2}$$

$$\bar{w} = \frac{2w}{c_1 t}$$

$$\alpha = \frac{s}{l} \left(\sqrt{3 + \left(\frac{s}{l} \right)^2} - \frac{s}{l} \right)$$

The parameters are defined in the same way as described above. α is the plate aspect parameter, l is the plate length, s is the plate width, t is the plate thickness, \bar{w} is the non-dimensional displacement parameter and r_c is the plastic resistance in bending for plates with no axial restraint.

3.2.4 Local buckling

Local buckling on the compressive side or fracture on the tensile side of cross-sections undergoing finite rotation will limit the maximum energy that the impacted member can dissipate. If local buckling takes place on the compression side, the bending capacity will be reduced. If local buckling doesn't take place, fracture is assumed to occur when the tensile strain exceeds a critical value. The tensile strain is due to the combined effect of membrane elongation and rotation. Local buckling does not need to be considered for a beam with axial restraints if Equation 6 below are fulfilled,

$$\beta \leq \left(\frac{14c_f f_y}{c_1} \left(\frac{kl}{d_c} \right)^2 \right)^{\frac{1}{3}} \quad (6)$$

where

$$c_f = \left(\frac{\sqrt{c}}{1 + \sqrt{c}} \right)^2 \quad (7)$$

$$\frac{1}{k} = \frac{1}{K_{node}} + \frac{L}{2EA} \quad (8)$$

$$d_c = 2h_w$$

c , c_1 and w_c is expressed by the same way as in Section 3.2.3. c_f is the axial flexibility factor and kl is the smaller distance from the location of collision load to adjacent joint and is $\leq 0.5L$.

For flanges subjected to compression and type I cross-sections, β is defined as Equation 9:

$$\beta = 2.5 \frac{b_f/t_f}{\sqrt{235/f_y}} \quad (9)$$

and for type II and III cross-sections:

$$\beta = 3 \frac{b_f/t_f}{\sqrt{235/f_y}} \quad (10)$$

For webs subjected to bending and type I cross-sections, β is defined:

$$\beta = 0.7 \frac{h_w/t_w}{\sqrt{235/f_y}} \quad (11)$$

and for type II and III cross-sections:

$$\beta = 0.8 \frac{h_w/t_w}{\sqrt{235/f_y}} \quad (12)$$

If this condition is not met, buckling will occur when the lateral deformation exceeds:

$$\frac{w}{d_c} = \frac{1}{2c_f} \left(1 - \sqrt{1 - \frac{14c_f f_y}{c_1 \beta^3} \left(\frac{kl}{d_c} \right)^2} \right) \quad (13)$$

The different types of cross-sections are directly defined in *DNV-OS-C101* as shown below [55].

Table 3.1: Types of cross-sections [55].

Cross-section type I	Cross-sections that can form a plastic hinge with the rotation capacity required for plastic analysis.
Cross-section type II	Cross-sections that can develop their plastic moment resistance, but have limited rotation capacity.
Cross-section type III	Cross-sections where the calculated stress in the extreme compression fibre of the steel member can reach its yield strength, but local buckling is liable to prevent development.

3.2.5 Tensile fracture in yield hinges

According to tensile fracture in yield hinges, rupture may be assumed to occur when the deformation exceeds a value given by Equation 14 below,

$$\frac{w}{d_c} = \frac{c_1}{2c_f} \left(\sqrt{1 + \frac{4c_w c_f \varepsilon_{cr}}{c_1}} - 1 \right) \quad (14)$$

where the following is defined:

$$c_w = \frac{1}{c_1} \left[c_{lp} \left(1 - \frac{1}{3} c_{lp} \right) + 4 \left(1 - \frac{W}{W_p} \right) \frac{\varepsilon_y}{\varepsilon_{cr}} \right] \left(\frac{kl}{d_c} \right)^2 \quad (15)$$

$$c_{lp} = \frac{\left(\frac{\varepsilon_{cr}}{\varepsilon_y} - 1 \right) \frac{W}{W_p} H}{\left(\frac{\varepsilon_{cr}}{\varepsilon_y} - 1 \right) \frac{W}{W_p} H + 1} \quad (16)$$

$$H = \frac{E_p}{E} = \frac{1}{E} \left(\frac{f_{cr} - f_y}{\varepsilon_{cr} - \varepsilon_y} \right) \quad (17)$$

The factors involved are defined as the same as for local buckling presented in Section 3.2.4. c_w is the displacement factor, c_{lp} is the plastic zone length factor and H is the non-dimensional plastic stiffness. The yield strain ε_y is taken as the yield stress divided by the elastic modulus. The non-dimensional plastic stiffness is given by steel grade and critical strain ε_{cr} . Below are some values given in *DNV-RP-C204*.

Table 3.2: Some values for ε_{cr} and H [57].

Steel grade	ε_{cr}	H
S 235	20%	0.0022
S 355	15%	0.0034
S 460	10%	0.0034

3.3 DNV-RP-C208

DNV-RP-C208 is a recommended practice intended to give guidance on how to establish structural resistance by use of non-linear finite element methods. Among other things, it contains for example requirements to mesh size and other essential choices to obtain a sufficient finite element analysis. When using non-linear finite element analysis to obtain the structural response, the tensile fracture criteria are given in *DNV-RP-C208*. Fracture criteria based on *DNV-RP-C208* is given in Section 7.4.

In general, this recommended practice is meant to supplement structural design standards for offshore steel structures. It is valid for marine structures made from structural steels with maximum yield strength up to 500MPa and meets the requirements to offshore structures. *DNV-RP-C208* only addresses for failure associated extreme loads [58].

3.4 DNV-OS-A101

DNV-OS-A101 provides general safety and arrangement principle for mobile units and offshore installations. The standard addresses requirements for crane and laydown areas. It should be placed such that the risk of dropped object damage to systems and structure is minimized, as described before. The standard specifies that load handling above hazardous inventories, hydrocarbon equipment and important system for safety should be avoided as much as possible. If this isn't possible, impact protection should be used. The same applies for the storage tank and cargo area. The laydown areas should therefore be outside these critical zones and should have heavy-duty barriers [54].

3.5 Impact energy

The kinetic energy involved is calculated by use of Equation 1 and 2 expressed in Section 3.2. Below are some examples of typical masses, drop heights, velocities and resulting impact kinetic energies. The masses for the containers are taken from Table 2.1 as MGW to give conservative results and the drop height is chosen to be informative.

Table 3.3: Impact energy for different masses and drop heights.

Object	Mass [kg]	Drop height [m]	Velocity [m/s]	Energy [kJ]
Container 10ft	10 000	8.0	12.5	781.3
Container 10ft	10 000	16.0	17.7	1566.5
Container 10ft	10 000	24.0	21.7	2354.5
Container 20ft	20 000	8.0	12.5	1562.5
Container 20ft	20 000	16.0	17.7	3132.9
Container 20ft	20 000	24.0	21.7	4708.9

As seen from the table the impact energy is quite high. For a standard 10 000Te sideways drifting ship collision the impact energy is 28MJ. This is based on a standard impact velocity of 2m/s [28]. For the 20ft container with a 24 meter drop height the energy is as high as 4.71MJ. Compared with the ship collision this is a significant high energy which may lead to fatal consequences for both the dropped object and the impacted member. In addition, a 40ft container could also have been compared, which had led to even higher impact energy.

3.6 Energy dissipation

As described in Section 3.2.2 the structural response is found by the force-deformation curve. Depending on how much energy the impacted member and dropped object are able to absorb we can distinguish between ductility design, strength design and shared-energy design. For ductility design, the impacted member will absorb almost all the strain energy. Opposite will the dropped object absorb almost all the strain energy for strength design. For both these cases, the force-deformation curves can be found independently of each other. Despite this, this is rare a realistic scenario. In shared-energy design both the impacted member and the dropped object will be able to absorb some of the strain energy. Then the structural response will be more difficult to obtain [18]. The difference between ductility design, strength design and shared-energy design is presented in Figure 3.2 below. The theory presented is the background for the force-deformation curves in Figure 3.1.

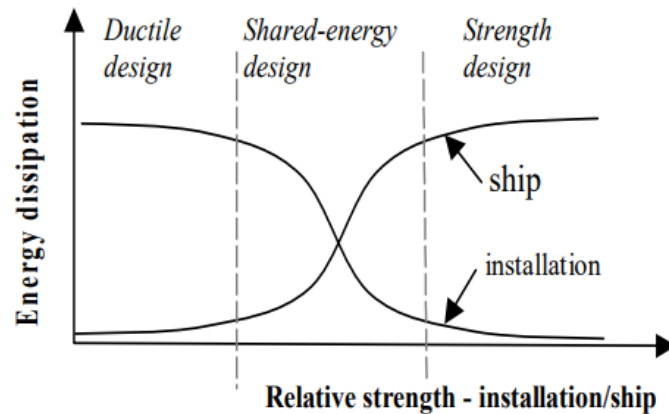


Figure 3.2: Design principal for impacts [18].

3.6.1 Eccentric impact

When two bodies impact, the angle is important for the energies absorbed. Two bodies where the center of mass of the dropped object doesn't go through the line of impact is called eccentric impact. Otherwise is called central impact. In the case of eccentric impact, some of the kinetic energy will be dissipated as energy due to rotation, and the demand for strain energy dissipation is reduced. The energy dissipation may be obtained by Equation 18 below [9],

$$E_s = E_{s,o} + E_{s,i} = \frac{1}{2} m_o v_o^2 \frac{\left(1 - \frac{v_i}{v_o}\right)^2}{1 + \frac{m_o}{m_i}} \quad (18)$$

where i is denotation for the installation, here the deck and o is the denotation for the dropped object. The masses is given by Equation 19 below,

$$\bar{m}_j = \left(\frac{l_j^2}{\bar{m}_{jx}} + \frac{m_j^2}{\bar{m}_{jy}} + \frac{n_j^2}{\bar{m}_{jz}} + \frac{\lambda_j^2}{\bar{I}_{jx}} + \frac{\mu_j^2}{\bar{I}_{jy}} + \frac{\nu_j^2}{\bar{I}_{jz}} \right)^{-1} \quad (19)$$

where $j=o$ (dropped object), $j=i$ (installation). Further, the mass of the deck m_i is assumed infinite and the velocity of the deck is assumed zero. Equation 18 is then simplified as below,

$$E_s = \frac{1}{2} m_o v_o^2$$

where m_o is found from Equation 19 and is the effective mass of the container due to eccentric impact and must be calculated for each impact scenario. The demand for strain energy can also be found with a strain energy dissipation factor given by Figure 3.3, where x is the radii of gyration and z corresponds to different mass relationships between the dropped object and the installation [9]. Figure 3.3 is based on ship collisions and is therefore only valid for the values at the y-axis when the mass ratio is zero. This corresponds to an infinite mass of the deck.

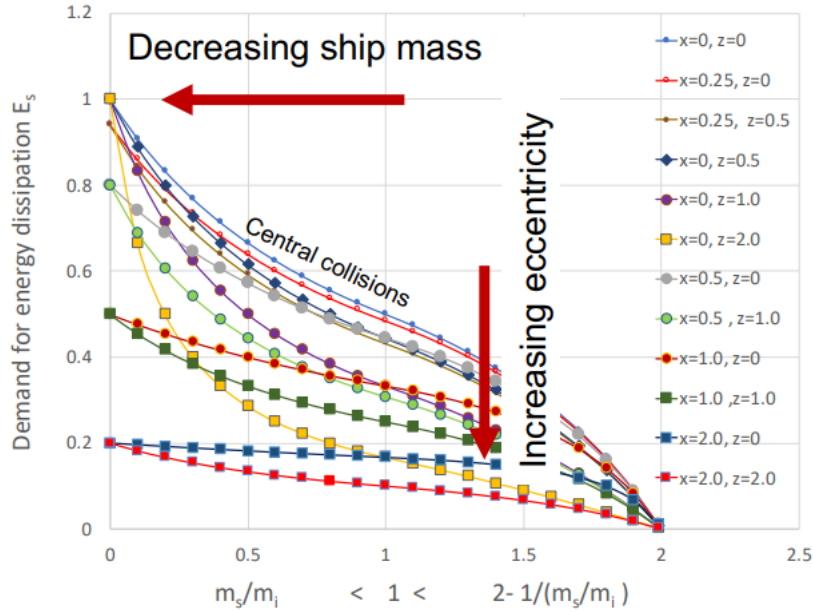


Figure 3.3: Strain energy dissipation factor versus mass ratios and contact eccentricity [9].

4 Simplified plastic methods

The following sections give an overview of simplified plastic methods relevant for dropped objects. The presented simplified plastic methods and the given theory from Chapter 3 and Section 3.2 are based on the same principles.

In the elastic range the stress is expressed as $\sigma = E\varepsilon$ and with deformation the structure will return to the same position without any permanent deformations. When the stress reaches the yield stress, denoted σ_y , the stress is constant for increasing strain. For some value of the yield strain ε_y , often 10-20 times the yield strain, the flow stress increases and results in strain hardening. In other words, yield strength increases by plastic deformation. The yield stress will reach a maximum, starts to neck and results in fracture at a reduced stress level. By assuming only elastic a huge part of the capacity of the structure is neglected. Therefore plastic methods must be used to account for the plastic range. In the plastic range the stress can be expressed as $\sigma = E_t\varepsilon$ where E_t is the plastic tangent modulus [6]. The stress-strain curve is shown in Figure 4.1 below.

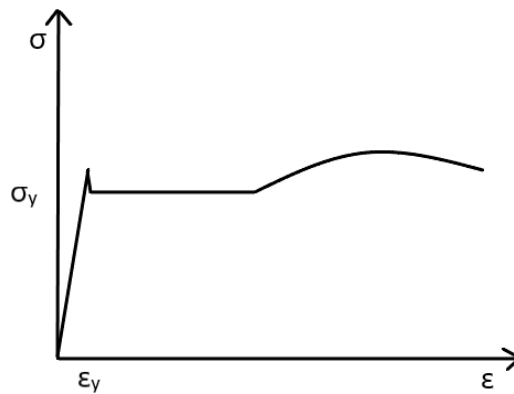


Figure 4.1: Stress - strain curve.

The stress-strain curve can often be idealized as linearly elastic perfectly plastic as shown below, which means that the strain hardening is neglected [6]. This may be reasonable if the moderate strain is accepted.

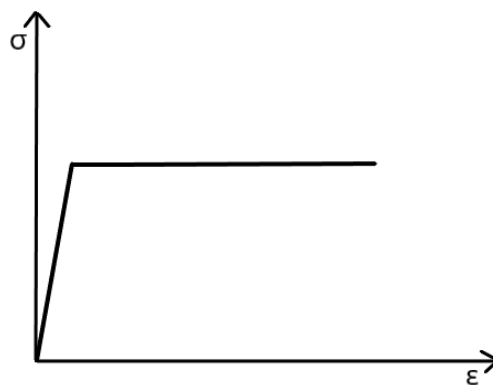


Figure 4.2: Linearly elastic perfectly plastic stress - strain curve.

The bending moment for the elastic and plastic range is calculated differently by use of elastic section modulus and plastic section modulus. The shape factor characterises the ability of the cross-section to carry bending moment beyond first yield moment and is found by dividing the plastic section modulus by the elastic section modulus. The elastic and plastic neutral axis is in

general different from each other. The plastic neutral axis is the axis that divides the cross-section into two equal parts. If we assume that the area of the plate flange is larger than the area of the stiffener web plus the area of the stiffener flange, the plastic neutral axis will be in the plate flange. This is correct for almost all stiffeners offshore.

For elastic-plastic we assume the plastic curvature concentrated in a single point and neglect the elastic deformations. Looking at the plastic response of a beam the deformation field is called a plastic mechanism and the discontinuity is called a plastic hinge [6].

4.1 Static calculation of plastic resistance

By looking at a clamped beam the load could be applied in two steps. For the first step a simple elastic analysis is done and when the moments are longest, yield hinges are formed at the supports. The beam can now be seen as simply supported and the ends are therefore not able to take more bending moment. Then the beam acts as a mechanism and collapses when the beam is loaded such that the bending moment is equal to the plastic moment M_p at the mid section. The plastic resistance is found by equilibrium consideration. Depending on the load and boundary condition (BC) it will be redistribution of forces [6].

4.2 Kinematic calculation of plastic resistance

The same reference as above is also used in this entire Section [6]. Here the principle of virtual work is used to calculate the plastic resistance. The plastic resistance is found by using that the external work equals the internal work. The structure is assumed in static equilibrium and a virtual displacement field that satisfies both BCs and compatibility is assumed. Compatibility means the correspondence between displacement and rotations. The plastic resistance can also be found for structures with unknown hinge position. By plastic mechanism the bending moment is assumed equal to the plastic moment in hinges.

The plastic mechanism for the clamped and simply supported beam is shown below. For the simply supported beam plastic hinge is formed at the mid-span, while for the clamped beam plastic hinges is formed both at the edges and at the mid-span.

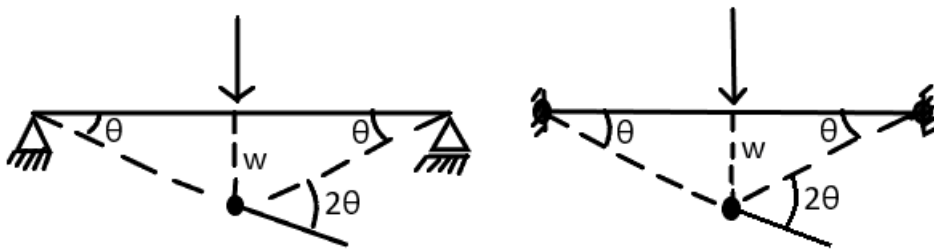


Figure 4.3: Plastic mechanism for clamped and simply supported beam.

The plastic resistance is as mentioned found by using that the external virtual work is equal to the internal virtual work. The load P is represented by the arrow in Figure 4.3 and can be directly used for dropped objects. The external work for both the simply supported beam and the clamped beam can be expressed by Equation 20.

$$\delta W_e = P \cdot \delta w \quad (20)$$

The internal work is related to the plastic moment and will be different for the clamped and simply supported beam. For the simply supported beam, the internal work is given as:

$$\delta W_{i,s} = M_p \cdot 2\delta\theta \quad (21)$$

while for the clamped beam the internal work can be expressed as Equation 22.

$$\delta W_{i,c} = M_p \cdot 4\delta\theta \quad (22)$$

From geometry the deformation can be expressed as shown below.

$$\delta w = \frac{l}{2}\delta\theta \quad (23)$$

By then using that $\delta W_e = \delta W_i$ we get an expression for both beams. For the simply supported beam and the clamped beam this will give the following plastic resistance P_s and P_c , respectively.

$$P_s = \frac{4M_p}{L} \quad (24)$$

$$P_c = \frac{8M_p}{L} \quad (25)$$

For structures with unknown hinge positions a choice of hinge positions must be made. Wrong choice of hinge positions may lead to a bending moment larger than the plastic moment outside the hinge positions. For a mechanism analysis, it is assumed that the bending moment is equal to the plastic moment in the hinges. Therefore by assuming an inaccurate mechanism it is observed that the static and kinematic approaches can give a lower or higher resistance than what is realistic. Therefore the upper bound theorem and the lower bound theorem are introduced, especially useful for more complex systems. Inaccurate mechanism assumed the kinematic approach could give too high resistance and inaccurate mechanism assumed the static approach could give too low resistance.

4.3 Combined loading

The combination of bending moment and axial forces will reduce the plastic moment. A yield contour curve for a rectangular cross-section is found from the relationship below.

$$\frac{M}{M_p} + \left(\frac{N}{N_p}\right)^2 = 1 \quad (26)$$

All the combinations which fall inside the contours are able to be resisted by the cross-section, meaning all points outside the contours are inadmissible. There exist other expressions for the yield contour curves for for example circular cross-section and I-profiles. The expressions for the I-profiles will be different depending on the position of the plastic neutral axis. As discussed, the plastic neutral axis is located in the plate flange for most stiffened panels [6].

DNV-RP-C204 gives the combination of bending and axial forces as:

$$\frac{M}{M_p} + \left(\frac{N}{N_p}\right)^\alpha = 1 \quad (27)$$

where $1 < \alpha < 2$. $\alpha = 1.2$ can be assumed for H or I beams, $\alpha = 1.5$ can be assumed for members with hollow section and $\alpha = 2$ can be assumed for rectangular hollow section. The lastly corresponds to Equation 26.

4.4 Plastic capacity of plates

For the plate subjected to uniform lateral load the collapse model is assumed as the rooftop mechanism as shown in Figure 4.4.

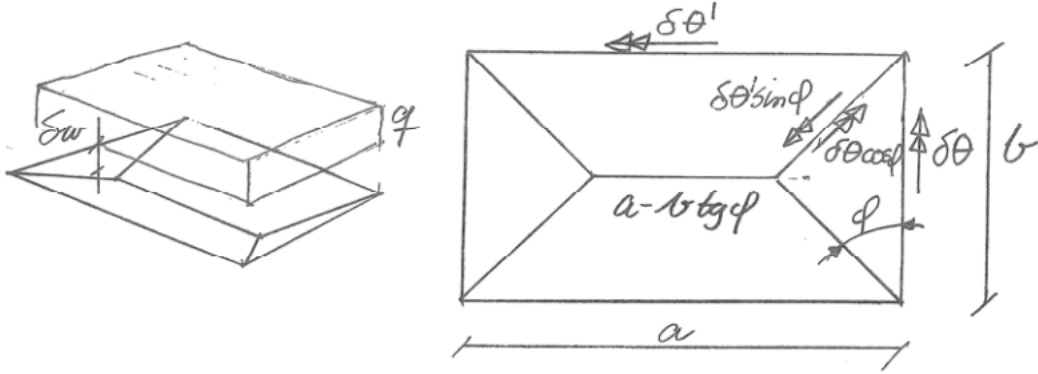


Figure 4.4: Rooftop mechanism [8].

All the plate segments bounded by yield lines rotate as rigid bodies and all energy dissipation takes place in yield lines. The angle θ of the oblique yield lines is unknown. Membrane forces will take place when the deflections at the centre of the plate become finite. The membrane forces will increase the load-carrying capacity [8].

For the analysis it is used a plate strip with a unit width, then the same approaches used for beams with rectangular cross-section can be used for the plate strip. The plate mechanism will hence consist of several plate strips and by integrating the contribution for all the plate strips the closed-form solutions for the load-carrying capacity can be found [4]. Meaning as for beams the collapse load q is found by using that external virtual work equals internal virtual work, where the external virtual work corresponds to the volume of the rooftop. For simply supported edges the collapse is halved compared with fixed edges since the internal virtual work is halved. Then the relationship for plastic capacity of plates is given in Equation 28.

$$\frac{q}{q_c} = \begin{cases} 1 + z^2 \left(\frac{\alpha + (3-2\alpha)^2}{9-3\alpha} \right) & \text{if } z \leq 1 \\ 2z \left(1 + \frac{\alpha(2-\alpha)}{3-\alpha} \left(\frac{1}{3z^2-1} \right) \right) & \text{if } z \geq 1 \end{cases} \quad (28)$$

Where

$$z = 2 \frac{w}{t}$$

$$q_c = \frac{24M_p}{a^2\alpha^2}$$

for pinned ends, and

$$z = \frac{w}{t}$$

$$q_c = \frac{48M_p}{a^2\alpha^2}$$

for clamped ends. The plate aspect parameter α is defined as:

$$\alpha = \frac{b}{a} \left(\sqrt{3 + \left(\frac{b}{a}\right)^2} - \frac{b}{a} \right)$$

M_p is defined as:

$$M_p = \sigma_y \frac{t^2}{4}$$

where t is the plate thickness, a is plate length and b is plate width [4]. It is to be noted that this relationship is equivalent to the force-deformation relationship for plates from *DNV-RP-C204* as presented in Section 3.2.3. When b/a approximates zero, the plate strip relationships can be expressed by the following:

$$\frac{q}{q_c} = \begin{cases} 1 + z^2 & \text{if } z \leq 1 \\ 2z & \text{if } z \geq 1 \end{cases} \quad (29)$$

5 Bending of stiffeners

Stiffened plates are used as structural components in offshore installations. The typical panels contains of longitudinal stiffeners with heavier girders with larger spacing in the transverse direction [5].

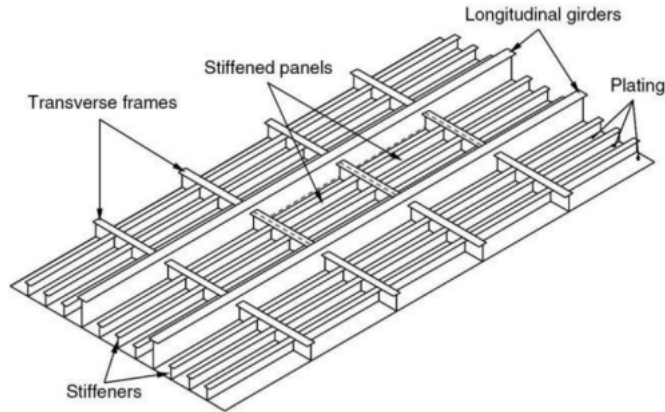


Figure 5.1: Stiffened panel [60].

The main collapse modes of a stiffened plate may be categorized as flexural buckling and tripping sideways of stiffener, where the flexural buckling is either towards the stiffener called plate induced failure or towards the plate called stiffener induced failure. The different collapse modes is shown in Figure 5.2 [5].

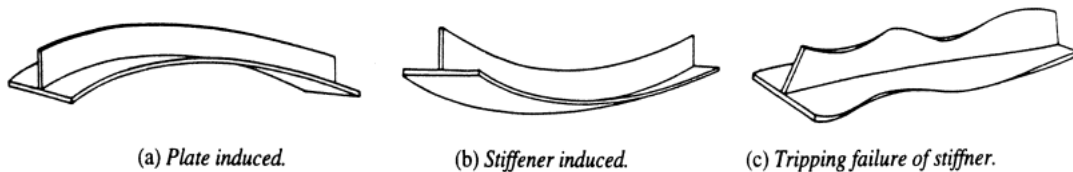


Figure 5.2: Collapse modes for stiffened plate [5].

Most of the methods do not account for tripping of the stiffener since it is a phenomenon which is difficult to analyse analytically. To avoid tripping of the stiffeners, the following equation should be satisfied. This applies for the flat bar stiffeners [5].

$$\frac{h_w}{t_w} \leq C \sqrt{\frac{E}{f_y}} \quad (30)$$

where C is somewhere around 0.35 to 0.37.

6 Importance of inertia effects and strain rate

In the hand calculations the dropped object is introduced as a statically applied load, meaning neglecting the dynamic effects. A dropped object is often referred to as an impact or impulse load due to a dynamic load of short duration. The importance of dynamic effects will depend on the eigenperiod of the structure. The load can be considered static if the load varies slowly compared to the eigenperiod of the structure. On the other hand, if the eigenperiod of the structure is close to or larger than the eigenperiod of the load it could have a huge effect on the motion. It may be important to include the effect of dynamic effects to obtain accurate results. The dynamic amplification factor is often used as a representation for the dynamic effect, which gives us the ratio between the dynamic deflection and the static deflection. [46].

6.1 Inertia effects

For a quasi-static analysis the dropped object is "forced" with a relative velocity which is very low, so the inertia effects can be neglected. This will lead to a relatively static force-deformation curve. Despite this, the real velocity will be much higher. Taken from Table 3.3, a realistic drop height could be 16m which will lead to a velocity of 17.7m/s. The high velocity will cause significant inertia forces. Due to the large mass of the dropped object, the inertia forces will dominate straight after impact. The inertia will increase with the mass [13]. A non-linear finite element analysis in Abaqus/Explicit can be used to model the effect of inertia on the dynamic response. It has been shown that the inertia is dependent on impact velocities and that inertia may result in a significant increase in the flow stress [24].

For the simplified calculations a static equilibrium between internal and external forces is assumed, hence neglecting the inertia forces. On the other hand, inertia forces may be significant for dynamic applied loads. Figure 6.1 show the difference for a static and dynamic solution [7].

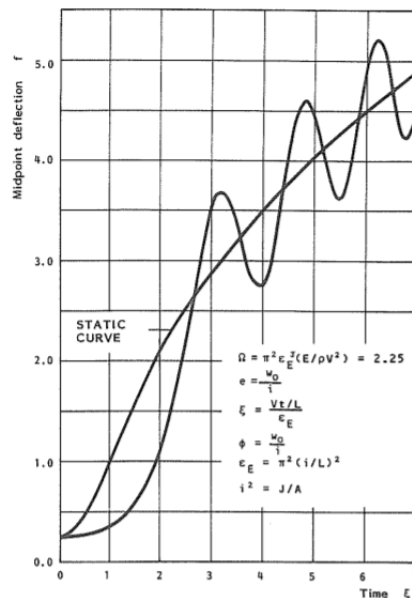


Figure 6.1: Deflections of mid-point of column [7].

The dynamic response is oscillating about the static curve, because of a time lag between the static and dynamic solution. This is due to the inertia forces which increase with the impact velocity. For

impact loads, the effects are considered by stress wave propagation along the member. Buckling will hence occur when it has traversed a length equal to the static instability wave length corresponding to the stress level. It is shown that the following expression for the reduced slenderness may be obtained.

$$\bar{\lambda} = \frac{l}{i} = \pi \sqrt{\frac{v_c}{v}} \quad (31)$$

where l is the length of the member, i is the radius of gyration, v_c is the speed of wave propagation and v is the impact velocity. Hence, the wave length will decrease with increasing velocity. Often the effect is of minor importance and neglected.

Furthermore, the committee of the 20th International Ship and Offshore structures congress meant that inertia effects and effects due to strain rate often is acceptable to neglect. This was based on a ship collision performed with nonlinear finite element analyses. The inertia effects and the effects due to strain rate are locally concentrated near the contact area and the total contribution is assumed small. The committee did not look into dropped objects [28].

6.2 Strain rate

In dynamic problems, such as dropped objects, it is highly important that a constitutive material model can predict the strain rate effects correctly [52]. The effect of strain rate is not included by the simplified plastic methods. One of the most famous models to take into account the effect of strain rate is the Cowper-Symonds model. The model is given as:

$$\sigma_{dynamic} = \sigma_{static} \cdot \left(1 + \frac{\dot{\varepsilon}}{C} \right)^{\frac{1}{q}} \quad (32)$$

where $\dot{\varepsilon}$ is the strain rate and C and q are material parameters. By this, the yield strength is adjusted due to strain rate dependence since the effect of strain rate will increase the yield stress to a certain level in correlation with a change in strain [29]. This may be included for materials that are sensitive to the rate of straining. Cowper-Symonds gives the empirical relationship between the dynamic and static flow stress. For mild steel $C = 40$ and $q = 5$ found from tests, meaning the yield stress is doubled for $\varepsilon = 40s^{-1}$. When contained large plastic deflections and high strain rates, Equation 32 must be used with great care and $C = 4000$ is often proposed. For large strains the influence of strain rate is less pronounced and the model is therefore strictly valid for the initial yield stress [8]. It is found that for strain rates above $0.1s^{-1}$, the yield strength is increased and leads to reduced ductility [58].

Despite this, if the value for the material parameters is used for the entire stress-strain range, it will give a very high ultimate stress. Use of $C = 40$ and $q = 5$ may give a response that is far too stiff and will give less penetration depth. Tørnqvist discussed the uncertainties of adjusting the yield strength due to strain rate dependence. It is difficult to obtain accurate measurements from the tests and the parameters will be average values. The problem is that the strain rate changes over time during loading when conducting a strain rate test. When the test specimen will start to neck, all deformation will take place in the necking area and the material in this region will hence have even larger strain rates compared to the rest of the specimen. This results in an average value for the strain rate [52].

Alternatively, a rate-dependent plasticity option may be used, which will avoid spurious noise in the numerical solution due to the elastic part in the strain rate. It is based on the equivalent

plastic strain rate and the dynamic yield stress is expressed as [52]:

$$\sigma_y^d(\varepsilon_{eq}^p, \dot{\varepsilon}_{eq}^p) = \sigma_y(\varepsilon_{eq}^p) + \sigma_0 \left(\frac{\dot{\varepsilon}_{eq}^p}{C} \right)^{\frac{1}{q}} \quad (33)$$

where

$$\dot{\varepsilon}_{eq}^p = \frac{\varepsilon_{eq}^p}{\Delta t} \quad (34)$$

where σ_0 is the initial static yield stress, $\dot{\varepsilon}_{eq}^p$ is the plastic strain rate and Δt is the step increment at the current time. But for this approach Newton-Raphson must be used to iteratively solve the plastic strain increment, which will increase the CPU time. On the other hand, the results are improved by the use of this method instead of scaling the yield stress directly as by the Cowper-Symonds model. Note that using the same material parameters for the two approaches will not lead to the same stress level [52].

In general, how and when strain rate effects should be included is highly discussed in the industry. Among other uncertainties, is the dynamic behaviour of steel at low temperatures. Marine activities in Arctic are increasing, where the structures are exposed to sub-zero temperatures. Nam, Hopperstad and Amdahl studied the modelling of the ductile-brittle fracture transition in steel structures, where the strain energy density criterion was used to predict the transition between ductile and brittle fracture and the strain rate effects were neglected [19].

7 Modelling for finite element analysis

There exist several methods used to assess structural damage. This is either non-linear finite element methods, experimental methods or simplified analytical methods. The simplified elastic-plastic methods and analytical expressions presented in Section 4 and 3.2 are examples of the last mentioned. In the design state simple analytical methods could give us approximated results that are sufficient enough to be used as an early design check [60]. For risk analysis, it could be useful to establish a basis for optimum strengthening and/or consequence evaluation [21]. In summary, the structural response of the dropped object may be determined by non-linear finite element analysis or by energy considerations combined with simple elastic-plastic methods [57].

The hand calculations will not take into account the effect of redistribution of forces, adjacent members etc, which the non-linear finite element analysis will include. The simplified analytical methods will to some extent take into account the load carrying capacity, but will lead to complicated equations which can be time consuming. On the other hand, the simplified methods will in general give conservative results. [46].

The experimental methods and non-linear finite element methods are often too costly and the CPU time of a finite element analysis is too long for a design check at an early state [60]. The finite element analysis could be established as a dynamic or static analysis. The dynamic effects are neglected for the static analysis [21]. When doing a finite element analysis it is important to do sensitivity studies such as mesh size and understand the consequences of the assumptions used.

Using the non-linear finite element method, two time integration methods are possible. Explicit time integration, often by use of central difference scheme. Or Implicit time integration by for example Newton-Raphson method. The implicit analysis uses values known at the previous step, in addition to the velocities and accelerations from the new time step to find the response at the new time step. For the explicit analysis, the new time step is computed only based on the displacement, velocities and accelerations at the previous step. The implicit method is unconditionally stable, but may require large CPU time and memory. The explicit method is conditionally stable and requires small time steps [10].

Explicit analysis is appropriate for rapid and highly non-linear problems, since the time integration requires small time steps. For explicit finite element simulations there are no increments or iterations. It is therefore important to check the energy balance to ensure that the energy is conserved during the simulation. Strain softening may lead to strong mesh sensitivity. Strain softening is when thermal softening overtakes the strain hardening, resulting in a decrease in yield strength for an increase in temperature [14].

An installation exposed to dropped objects will result in large displacements and a plastic material. Hence a non-linear finite element method needs to be applied where geometrical non-linearity, material non-linearity and non-linearity in relation with BCs are accounted for [18]. Both the container model and the deck structure were modelled as deformable to obtain the most realistic results. Since dropped object scenarios are characterised as a rapid and non-linear problem, an explicit analysis was the most correct choice.

There exist several studies on the impact of deck from a dropped object. According to the report from the institution of mechanical engineers, there are used several non-linear finite element programs like LS-DYNA, Abaqus or USFOS [23]. The background for the non-linear analysis for assessing the structural damage is taken from *DNV-RP-C208*. Abaqus/explicit [51] was chosen to be sufficient for the purpose of this master's thesis and the theory relevant for the finite element analysis is further presented in the subsections below.

7.1 Container model

The container was modelled equal in both ends, where the geometry of the back was also used for the front, due to simplicity. This assumption was assumed to be conservative since the front often is more robust compared to the back end. The container was modelled in Abaqus/Explicit by using extruded shells and the dimensions of the container were given by Swire Energy Services AS. A general arrangement was given from Swire Energy Services AS to give an overview and is attached in Appendix A. The more detailed drawings and dimensions are not included because it was handed out as confidential information.

For the quasi-static analyses, the container was modelled by using coupling constraint in Abaqus, meaning assigning several nodes to behave as the reference point [44]. The reference point was fixed in all degrees except for the y-direction. The container was then forced down with a constant velocity in the reference point together with an initial velocity given by a predefined field. The container was constrained as shown in Figure 7.1.

The rear part will deform from forcing the container with a constant velocity in the reference point, but this was solved by modelling some of the rear part of the container as elastic. This is shown in Figure 7.2 below, where the different colours indicate different material properties.

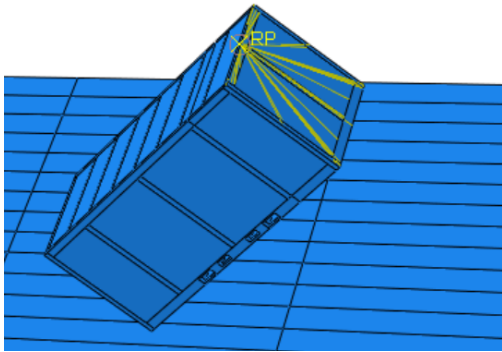


Figure 7.1: Constraint [51].

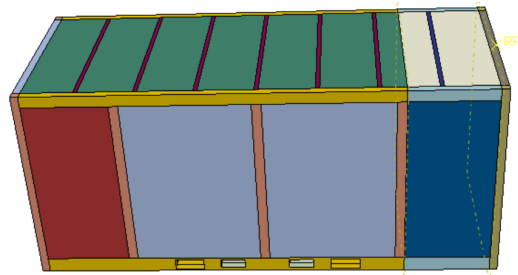


Figure 7.2: Material properties [51].

For the dynamic analyses, only the initial velocity was applied. The container was placed right above the panel and given an initial velocity in all the nodes of the container. Doing a dynamic analysis will result in a probably more realistic response, since the container will now be able to fall and rotate in all degrees of freedom with a realistic initial velocity.

For some of the analyses, the container was modelled rigid to see the effect when neglecting the energy the container will be able to absorb. There exist several methods to make the container rigid. A rigid body constraint was applied for the entire container by using body elements and a reference point on the container. The reference point was adjusted to the center of mass at the start of the analysis. Reference is made to the Abaqus manual for further reading [36].

Some of the external dimensions and parameters of the container are presented in Table 7.1 below.

Table 7.1: Details of the container model in Abaqus.

Part	Value
Length [mm]	6004
Width [mm]	2428
Height [mm]	2620
Tare weight [kg]	4833
Payload [kg]	15168
MGW [kg]	20000

The values are somewhat different from the one presented in Table 2.1, which is due to assumptions made when modelling the container. All the assumptions were assumed to be conservative and modelling the container exactly as the drawing would have been time consuming. The tare weight of the container was higher than given from Table 2.1, but the tare weight of the container from the drawings was around the same as the one modelled in Abaqus. The tare weight from Table 2.1 is just an example and the weight is different from one container to another, dependent on the design. Among other things, the container will have different weights depending on corrugated side walls or not.

7.2 Deck structure

The panel was modelled in Abaqus/Explicit by using extruded shells. The dimensions of the deck structure were given by supervisor Jørgen Amdahl and the structure is demonstrated in Figure 7.3 below [12].

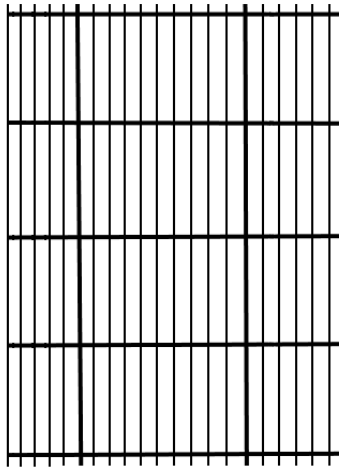


Figure 7.3: Dimensions of the deck.

The thick lines are the longitudinal and transverse girders and the thin lines are the longitudinal stiffeners. The longitudinal and transverse girders have the same dimensions. More detailed dimensions are given in Table 7.2 below.

Table 7.2: Detailed dimensions for the deck structure used in Abaqus [12].

Part	Dimension [mm]
Stiffener spacing	640
Longitudinal girder spacing	6135
Transverse girder spacing	6400
Stiffener web height	300
Stiffener flange width	200
Girder web height	1200
Girder flange width	400
Plate thickness	10
Stiffener web thickness	11
Stiffener flange thickness	17
Girder web thickness	15
Girder flange thickness	20

The deck structure modelled in Abaqus using the dimensions given in Table 7.2 is shown in Figure 7.4 below.

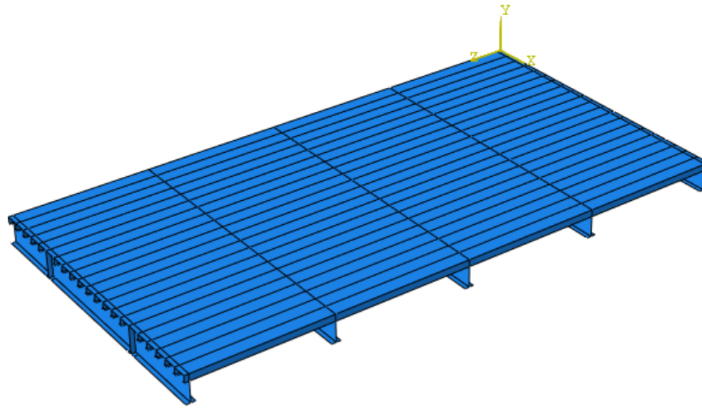


Figure 7.4: Deck structure [51].

For some of the analyses, the deck was modelled rigid. In the part module, the deck was changed from a 3D deformable to a 3D discrete rigid part. A discrete rigid part requires a rigid body reference node which is fixed in all degrees of freedom. In addition, an inertia mass must be attached to the rigid body reference node. Reference is made to the Abaqus manual for further reading [41].

7.3 Material properties

The finite element models were divided into sections which each had different material properties depending on the thickness and the element size. The true stress - true strain curve were calculated based on recommendations from *DNV-RP-C208* [58]. Three different curves were needed, one for material S275 with thickness less than 16mm, one for S355 for thickness less than 16mm and one for S355 for thickness larger than 16mm. Below is the properties taken from *DNV-RP-C208* presented. The resulting true stress- true strain curves and the corresponding exact values is attached in Appendix, respectively Appendix B and Appendix C.

Table 7.3: Material properties from *DNV-RP-C208* [58].

Steel	S275, t < 16mm	S355, t < 16mm	S355, t > 16mm
E [MPa]	210000	210000	210000
$\rho[\frac{kg}{m^3}]$	7850	7850	7850
$\nu[-]$	0.3	0.3	0.3
$\sigma_{prop}[MPa]$	248.0	320.0	311.0
$\sigma_{yield}[MPa]$	276.5	357.0	346.9
$\sigma_{yield2}[MPa]$	283.9	366.1	355.9
$\varepsilon_{p_y1}[-]$	0.004	0.004	0.004
$\varepsilon_{p_y2}[-]$	0.017	0.015	0.015
K [MPa]	620	740	740
n [-]	0.166	0.166	0.166

For the elastic part of the container as described in Section 7.1, the material properties will be the same, except that the true stress-true strain curve is not used for the elastic elements. It is also worth mentioning that *DNV-RP-C208* gives other true stress-true strain curves in cases where low capacity is unfavourable. In the case of dropped objects and assuming energy absorption of both the dropped object and the impacted member, it may be unfavourable for estimating of the structural integrity of the dropped object. On the other hand assuming the simplified case as the values given from Table 7.3 will be conservative for the panel, but not for the container [58]. Due to that the structural integrity in the panel is prioritised, the material properties from Table 7.3 were assumed sufficient for the finite element analyses.

7.4 Modelling of ductile failure

Material fracture is highly important, and background knowledge is principal when material modelling. Real life experiments for test specimens or structures are desirable to compare with numerical analysis, to obtain accurate results. Most metal alloys are ductile and will fail by ductile fracture when the plastic deformations become very high. This is due to void nucleation, growth and coalescence. It is also seen that the ductility decreases with increasing stress triaxiality, meaning the ductile damage depends strongly on the stress triaxiality since it is important for the void growth and the deviatoric stress [14]. The stress triaxiality gives us the relation between the hydrostatic and deviatoric stress [50].

Choosing failure model is important to be able to model the failure as realistic as possible. There exist several different failure criteria, but not all can be used in Abaqus. First a damage initiation criterion was needed to state the onset of damage, which was specified in the material properties in Abaqus. The choice fell on a damage initiation criterion based on the ductile failure strain by using ductile damage in the material properties [2].

Together with the damage initiation criterion a damage evolution was used to define the evolution of damage and was also specified in the material properties. Here the damage evolution was included as a displacement at failure [3]. Once the damage initiation criterion has been reached, the damage evolution law is needed to describe the rate of degradation of the material stiffness [2]. The damage evolution can be specified in Abaqus either by equivalent plastic displacement or fracture energy, which both depend on the characteristic element length. As mentioned above, the choice fell on using the equivalent plastic displacement, which can be inserted in tabular, linear or exponential form in Abaqus [45]. In this master's thesis a linear form was chosen.

7.4.1 Damage initiation criterion for ductile damage

DNV-RP-C208 specifies deformation limits for different materials obtained from tensile tests. The given deformation limits were used to obtain the equivalent plastic strain and the stress triaxiality. Tensile failure is mostly relevant for checking structures against accidental actions. The gross yielding critical strain ε_{crg} will limit the maximum gross yielding strain. ε_{crg} was found by using the deformation limits for the calibration case CC01 given from Table 5-1 in *DNV-RP-C208*. By using *S355*, $\varepsilon_{crg} = 21/450$ and using *S275*, $\varepsilon_{crg} = 24/450$. Local yielding will be a result of out-of-plane bending, strain gradients or a combination of these. For problems dominated by membrane strains, the maximum principal strain should be less than:

$$\varepsilon_{crl} \leq \varepsilon_{crg} \left(1 + \frac{5t}{3l_e} \right) \quad (35)$$

where t is the thickness and l_e is the length of the element. Meaning the model in Abaqus had a fracture model for each thickness and element size.

In Abaqus, the stress triaxiality and fracture strain must be applied. Fracture is dependent on the multi-axial state of stresses and strains. The stress state and strain state is defined as the ratio between the minor and major principal stresses and strains, respectively. The stress and strain states may be expressed as in Equation 36 and 37 below [50].

$$\beta = \frac{\dot{\varepsilon}_2}{\dot{\varepsilon}_1} \quad (36)$$

$$\alpha = \frac{\sigma_2}{\sigma_1} \quad (37)$$

The stress triaxiality, denoted T is the stress state. The stress triaxiality gives us the degree of hydrostatic stress in relation to the deviatoric stress in a given stress state. The hydrostatic stress is due to volume change, while the deviatoric stress is due to the shape change. T may be expressed as below [50].

$$T = \frac{\sigma_1 + \sigma_2 + \sigma_3}{3\sigma_{eq}} \quad (38)$$

For this fracture model plane stress and that fracture will occur at maximum principal stress were assumed. This is since shell elements represents a biaxial stress state. Martin Storheim presented conversion formulas for plane stress in his doctoral thesis, which gives a relation between T , β and α . The resulting formulas for stress triaxiality and fracture strain are shown below and were used as input to Abaqus for different β values [50].

$$T = \frac{1}{\sqrt{3}} \frac{\beta + 1}{\sqrt{1 + \beta + \beta^2}} \quad (39)$$

$$\varepsilon_{eq} = \sqrt{\frac{4}{3} \cdot \varepsilon_{crl}^2 \cdot (1 + \beta + \beta^2)} \quad (40)$$

ε_{crl} is the maximum principal strain in Equation 35 and used as:

$$\varepsilon_{crl} = \varepsilon_{crg} \left(1 + \frac{5t}{3l_e} \right) \quad (41)$$

7.4.2 Displacement at failure

Displacement at failure was also included in the material parameters by a damage evolution law. An equivalent plastic displacement at failure \bar{u}^{pl} was specified and defined with the evolution law below. The evolution law describes the development of plastic deformation after fracture.

$$\dot{\bar{u}}^{pl} = l_e \dot{\bar{\varepsilon}}^{pl} \quad (42)$$

$\dot{\bar{u}}^{pl}$ is the equivalent plastic strain rate and l_e is the element length. Equation 42 is valid once the damage initiation criterion has been reached. Before the damage initiation criterion is reached, $\dot{\bar{u}}^{pl} = 0$ [1].

The displacement at failure was used as $(n - \varepsilon_{crl}) \cdot l_e$ where ε_{crl} is given by Equation 41, l_e is the element length and $n = 0.166$ is the strain hardening exponent taken from Table 7.3. The background for using the strain hardening exponent is explained below.

Diffuse necking starts at the maximum value of the engineering stress-strain curve. Determined from the true stress-true strain curve, the true stress at necking is found as [53]:

$$\sigma_{t,necking} = \left. \frac{d\sigma_t}{d\varepsilon_t} \right|_{\varepsilon_t = \varepsilon_{t,necking}} \quad (43)$$

$\sigma_{t,necking}$ is the true stress at diffuse necking and $\varepsilon_{t,necking}$ is the true strain at diffuse necking. The power law given by the Hollomon model is used to relate σ_t to ε_t and is given in Equation 44.

$$\sigma_t = K \varepsilon_t^n \quad (44)$$

K is the strength coefficient and n is the strain hardening exponent. Combining Equation 43 and 44, the true strain at necking is equal to the strain hardening exponent, $\varepsilon_{t,necking} = n$. Meaning, the diffuse necking occurs at the value of n [53]. Since Abaqus is using the displacement at failure, the displacement is found by $(n - \varepsilon_{crl}) \cdot l_e$.

Together with the damage initiation and the damage evolution, element erosion was used. When the failure criterion is reached in all or a given number of integration points of the element, the element is deleted, meaning the stress in the element is set to zero [14]. The failure criterion is reached when the applied displacement at failure is reached. To exclude the failed elements from the visualisation module, the output variable STATUS was requested in the field output [33].

7.4.3 Alternative fracture criteria

There exist several fracture criteria that may be included in Abaqus. Johnson-Cook failure criterion and Cockcroft-Latham failure criterion are other examples of empirical criterion [52] and is presented to give an overview of some other existing fracture criteria.

For the Johnson-Cook failure criterion the effects of stress triaxiality, here denoted σ^* , strain rate \dot{p} and temperature T are included. The failure strain is expressed by Equation 45 below [14].

$$p_f = p_f(\sigma^*, \dot{p}^*, T^*) = [D_1 + D_2 \exp(D_3 \sigma^*)][1 + D_4 \ln \dot{p}^*][1 + D_5 T^*] \quad (45)$$

D_1, D_2, D_3, D_4 and D_5 are model constants and are often determined by tension tests for different range of strain rate and temperature. Notched tensile specimens are used to vary the stress

triaxiality. D_1 , D_2 and D_5 is positive, D_3 is negative and D_4 is either positive or negative. D_5 is positive since the failure strain increases with increasing temperature. D_3 is negative since failure strain decreases for increasing stress triaxiality. D_4 is either positive or negative since the failure strain may increase or decrease by increasing the strain rate. \dot{p}^* is the dimensionless plastic strain rate and is defined as the plastic strain rate divided by a reference strain rate. T^* is the homologous temperature and divided as shown below [14],

$$T^* = \frac{T - T_0}{T_m - T_0} \quad (46)$$

where T is the temperature, T_m is the melting temperature and T_0 is the reference temperature.

The Cockcroft-Latham failure criterion is defined by [14]:

$$\omega = \frac{1}{W_c} \int_0^p \max(\sigma_I, 0) dp \quad (47)$$

where the fracture parameter W_c is a constant which is easily calibrated from tests and σ_I is the principal stress. This may be further written by the stress triaxiality and the Lode parameter as Equation 48 below [14],

$$\omega = \frac{1}{W_c} \int_0^p \max\left(\sigma^* + \frac{3 - L_l}{3\sqrt{3 + L_l^2}}, 0\right) \sigma_{eq} dp \quad (48)$$

where L_l is the Lode parameter and is defined as [14]:

$$L_l = \frac{2\sigma_{II} - \sigma_I - \sigma_{III}}{\sigma_I - \sigma_{III}} \quad (49)$$

where $\sigma_I \geq \sigma_{II} \geq \sigma_{III}$ are the principal deviatoric stresses. By assuming proportional loading paths, meaning constant stress triaxiality and Lode parameter, and also assuming that the temperature and strain rate is constant, we may find an expression for the fracture strain p_f . Using $f = \sigma_{eq} - \sigma_0$ in the plastic domain for a material obeying von Mises plasticity, the fracture strain may be expressed as [14]:

$$p_f = \left[\max\left(\sigma^* + \frac{3 - L_l}{3\sqrt{3 + L_l^2}}, 0\right) \right]^{-1} \frac{W_c}{\sigma_0} \quad (50)$$

The influence of the Lode parameter is neglected for the Johnson-Cook failure criterion.

The Johnson-Cook and Cockcroft-Latham failure criterion may also be directly specified in the material properties in Abaqus. The fracture criterion based on the equation in *DNV-RP-C204* together with the conversion formulas presented by Martin Storheim was chosen in the finite element analysis due to simplicity. The Johnson-Cook and Cockcroft-Latham are dependent on constants calibrated from tests and Johnson-Cook is temperature dependent, resulting in an advanced fracture criterion for the purpose of this master's thesis.

7.5 Discretisation and interaction

Below are the element type, mesh size, stable time increment, contact formulation and boundary conditions relevant for the finite element analysis presented in more detail. Abaqus gives several choices adapted to different analysis purposes.

7.5.1 Element type

For the finite element analysis mainly explicit S4R was used. This is a four-node general-purpose shell with reduced integration, relaxed stiffness hourglass control and finite membrane strains. S3R was used to a small degree and corresponds to a three-node shell. Element deletion was included to see the elements achieved fracture as described in Section 7.4. For the rigid deck, the element was linear discrete rigid elements. Reference is made to the Abaqus manual for further reading [42].

7.5.2 Mesh size

The mesh size should be done with the requirements given in *DNV-RP-C208*. By using the recommended true stress and true strain values from *DNV-RP-C208*, it sets some requirements for the mesh size. It is recommended to use element length between the value of the thickness and five times the thickness of the element [58]. A mesh sensitivity study for different mesh sizes was performed and described in Section 8.1. The study made the foundation for further analyses. Since the fracture strain is dependent on both the thickness and mesh size, Abaqus needed different material properties for each mesh size. On the other hand, using the same mesh size for the whole model will increase the CPU time, since the mesh size must be finer in the impact zone than over the whole model. This is especially for the panel, due to a large number of elements. The mesh size is important to obtain results with sufficient accuracy. On the other hand, finer mesh requires more memory and has longer CPU time due to lower stable time increment. A mesh sensitivity study for different mesh sizes was performed and described in Section 8.1. The study made the foundation for further analyses.

7.5.3 Stable time increment

An automatic time incrementation with a global stable increment estimator was used. Abaqus has two methods to find the stability limit, either the element by element estimate or the global estimate. The global stable increment estimation method is used when the algorithm finds the accuracy for this method sufficient enough. Using the dilatational wave speed, the maximum frequency of the entire model is estimated. Unlike the element by element method, which determines the dilatational wave speed in each element. The advantage is that the global method may accept larger stable time increments than the element by element method. If the global method is more time consuming, it will automatically switch to the element by element method. In addition, the "improved" stable time increment method was switched on, which is available for 3D continuum shell elements. The method often gives a larger acceptable stable time increment [38].

The stable time increment is found using the formulas presented below,

$$C_d = \sqrt{\frac{E}{\rho}} \quad (51)$$

$$\Delta t = \frac{l_e}{C_d} \quad (52)$$

where C_d is the dilatational wave speed and Δt is the stable time increment [38].

7.5.4 contact formulation

In Abaqus an interaction was created with mechanical general contact (explicit). First a contact property was made and assigned to an interaction. The contact property was chosen as the default in Abaqus, which assumes "hard" contact in the normal direction. In addition, a penalty friction formulation was applied with a friction coefficient of 0.2. By default, the applied friction coefficient was not dependent on slip rate, contact pressure or temperature. Reference is made to the Abaqus manual for further reading [34].

7.6 Boundary conditions

The deck structure was modelled with fixed BC for all rotational and translational degrees by using *ENCASTRE* in Abaqus for all the analyses [35]. The resulting boundary conditions in Abaqus of the deck structure are shown in Figure 7.5 below.

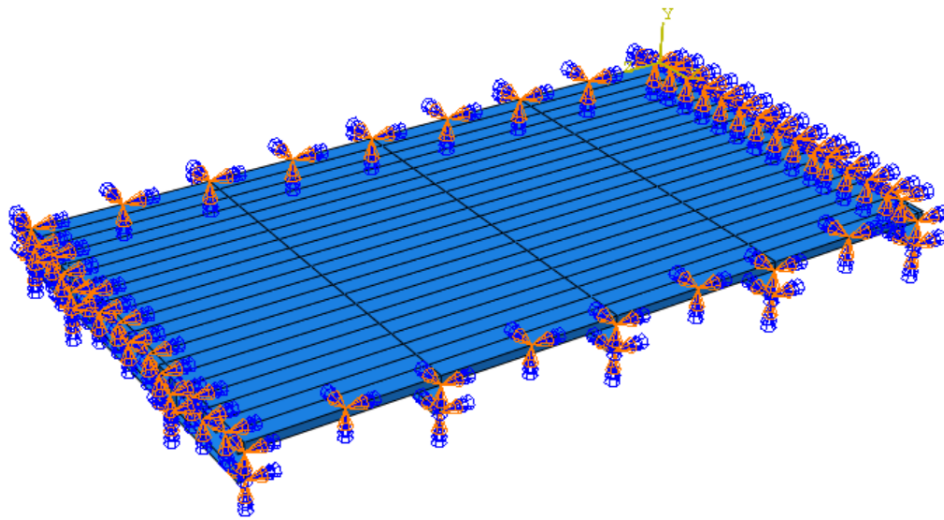


Figure 7.5: Fixed BC for the deck structure [51].

For the explicit analysis, the container was in free fall and therefore not assigned any BCs, meaning allows for rotations and motion in all degrees of motion. The reason was to perform the impact as close to real life as possible. For the quasi-static analyses, the container was forced down with a constant velocity using constraint. The reference point used with the constraint was assigned two BCs. The first one only allowed displacement in the y-direction, meaning motion and rotation in other directions were fixed. The second BC was of velocity/angular velocity type and was used to force the container down in the y-direction with a constant velocity. The velocities and angular velocities in the other directions were fixed.

8 Preparation for finite element analyses in Abaqus

Analyses for mesh refinement were performed to ensure sufficient results. The use of point masses versus nonstructural mass and the corresponding CPU time is discussed.

Some of the analyses were done quasi-static by using a reference point and a constraint and forcing the container down by a constant velocity over a time period. Since the container was forced down, the mass of the container was irrelevant. Later the analysis was done dynamic by only applying an initial velocity using a predefined field in Abaqus. All the quasi-static analyses were performed with 2m/s as constant velocity and the dynamic analyses with 20m/s as initial velocity.

The mass of the container itself was almost 5Te. To begin with four point masses with the same mass were distributed around the bottom of the container so that the total mass of the container was exactly 20Te. Taken from Table 2.1 the MGW of the 20ft container is 20Te and is therefore used in the analyses to obtain the most conservative and critical scenarios. Through some of the first analyses, using the point masses caused odd results. Therefore, a nonstructural mass distributed equally throughout the container was introduced instead of using point masses. The nonstructural mass was also applied such that the total mass of the container was 20Te.

8.1 Mesh sensitivity study

A parametric study of the mesh size has been conducted by changing the mesh size for each analysis and seeing the difference in the results until the result had a neglecting difference. The results have been used to decide the mesh size for all the analyses. The mesh size sensitivity has been investigated by a container impacting with the whole horizontal bottom beam first since that was the impact scenario which was modelled first. The results have been plotted either directly from Abaqus or using MATLAB [16].

As described, the fracture model with stress triaxiality, equivalent plastic strain and displacement at failure was given for each mesh size. The stress triaxiality is independent of the mesh size and thickness of the element, but the plastic strain and displacement at failure will vary for different mesh sizes and thicknesses.

Due to the large CPU time, the panel was modelled using two different mesh sizes. A finer mesh was used in the impact zone to correctly represent the impact. For the other part of the panel a coarser mesh was used with 200mm as element length. The container was first modelled also with two different mesh sizes, but resulted in an unnatural deformation since the container then was divided into two parts. It was divided into two parts so that it could be assessed different fracture materials dependent on the mesh size. The resulting deformation is shown below in Figure 8.1.

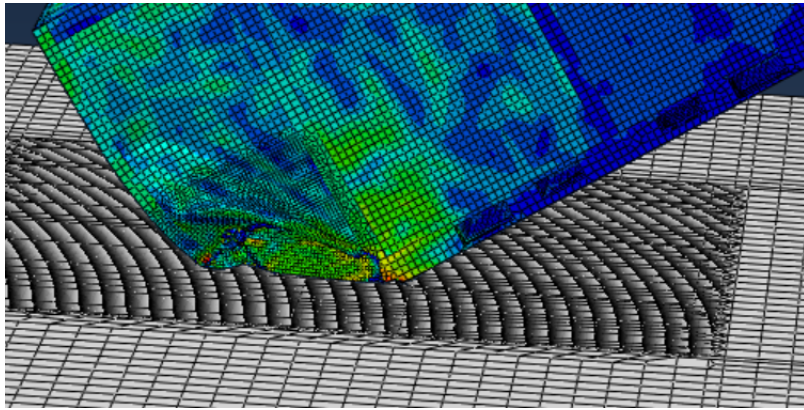


Figure 8.1: Resulting deformation with fine mesh in impact zone [51].

Increasing the part with finer mesh was investigated, but it was found to be most accurate to model the entire container with the finer mesh, despite the larger CPU time.

The mesh refinement for the panel was done by using a rigid container, and the mesh refinement for the container was done with a rigid panel. The reason was to obtain the correct mesh size for the container alone and the panel alone. Then the most appropriate mesh sizes were obtained, in relation to low CPU time together with sufficient enough accuracy. The deck and container was done with three and four different mesh sizes, respectively and is shown in Table 8.1 and 8.2. The choice of mesh sizes was taken from the requirements by *DNV-RP-C208* as described in Section 7.5.2. The smallest thickness in the impact zone for the container is 5mm and for the panel is 10mm. Due to the very large CPU time, also using the supercomputer, the lowest mesh size used for the container was five times the thickness, meaning 25mm.

Table 8.1: Mesh sizes for rigid deck.

Analysis	Mesh size container [mm]
First	100
Second	50
Third	25
Fourth	150

Table 8.2: Mesh sizes for rigid container.

Analysis	Mesh size impact zone panel [mm]
First	100
Second	50
Third	25

The mesh size of the panel outside the impact zone was 200mm for both rigid container and rigid deck due to saving CPU time. For the rigid container, the mesh size of the container was also left constant at 50mm and for the rigid deck, the mesh size of the panel in the impact zone was left constant at 50mm.

8.1.1 Rigid deck

The container was first performed with mesh sizes 100mm, 50mm and 25mm. Due to the odd result from the 25mm fine mesh shown in Figure 8.2, a mesh size of 150mm was also performed to control the pattern of the internal energy.

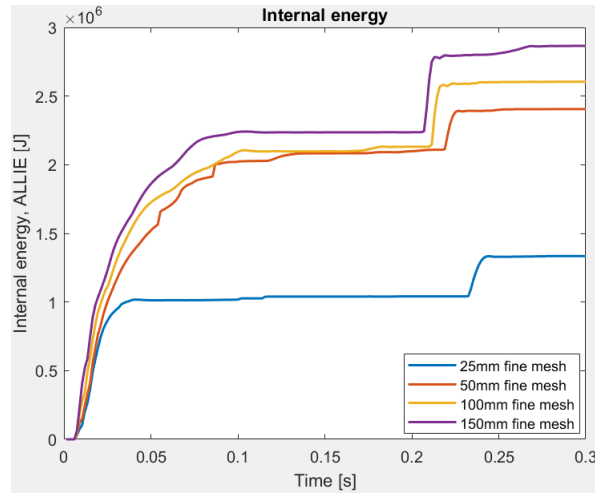


Figure 8.2: Internal energy for the analyses with rigid deck [51].

Furthermore, the difference in the final deformation of the container for the 25mm compared to the coarser meshes was large. The final deformation was taken right before the container bounced off the panel. The difference in deformation with 25mm and 50mm is shown in Figure 8.3. The difference between 50mm, 100mm and 150mm was not that noticeable. In addition, the 25mm fine mesh container bounce up of the panel much earlier than the others, not being able to absorb as much of the kinetic energy. It may indicate that the container became too stiff, which is interesting since it was assumed to be softer.

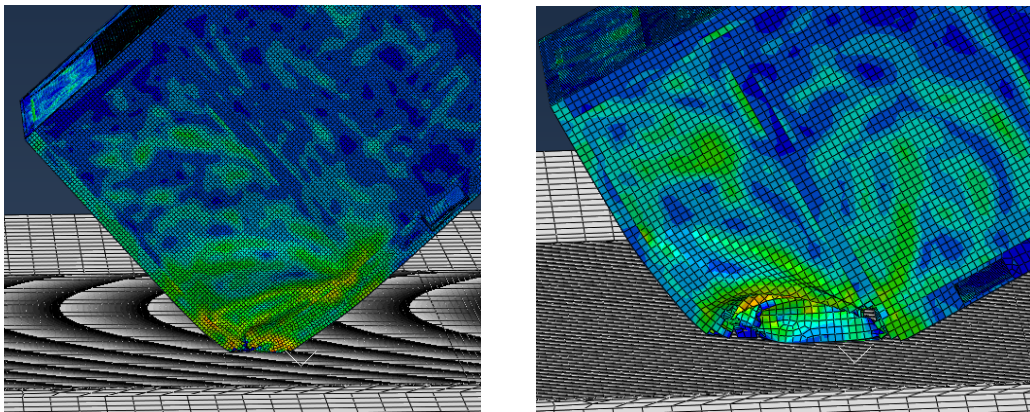


Figure 8.3: Final deformation for 25mm fine mesh to the left and 50mm fine mesh to the right [51].

Due to the odd result for the 25mm fine mesh, the mesh sensitivity was also done with a quasi-static model for 100mm, 50mm and 25mm fine mesh. The reason was to neglect uncertainties that may be the reason for the results for 25mm fine mesh. The internal energies found by the quasi-static analyses are plotted below.

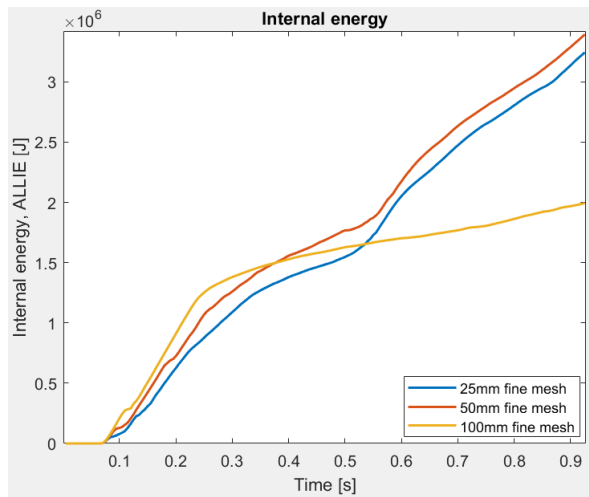


Figure 8.4: Internal energy from quasi-static analyses [51].

The result shows a minor difference between 25mm and 50mm fine mesh. Due to limited time and the fact that most of the analyses are going to be dynamic, the mesh size was chosen to be 50mm. This is not optimal with the requirements given in *DNV-RP-C208*. On the other hand, taking all into account it was found to be more accurate to take 50mm which followed the pattern from the 100mm and 150mm mesh sizes. Especially since the quasi-static model also shows minor difference in the internal energy. In addition, it was unacceptable to try with a mesh size lower than 25mm due to too high CPU time. It would probably result in higher accuracy to run an analysis with a mesh size somewhere between 25mm and 50mm, but was neglected due to limited time and much time spent on the mesh refinement. The advantages of using a 50mm mesh size were found to be higher than the disadvantages. If the 25mm fine mesh were to be used, a closer look into the dynamic analysis was necessary.

8.1.2 Rigid container

The panel was performed with the element lengths 100mm, 50mm and 25mm. The results for the internal energy and displacement are plotted below.

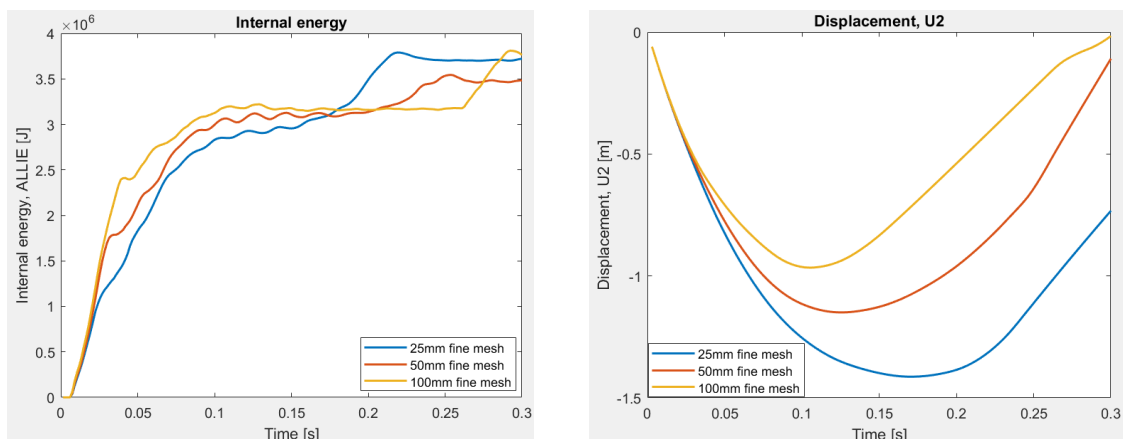


Figure 8.5: Internal energy and displacement for different mesh sizes [51].

The internal energy shows similar results for the different mesh sizes, but the displacement increases

for finer mesh and seems to not have converged. The container was placed around 0.14m above the panel for all the analyses for the mesh refinement. The force-time curve was also compared and is shown below.

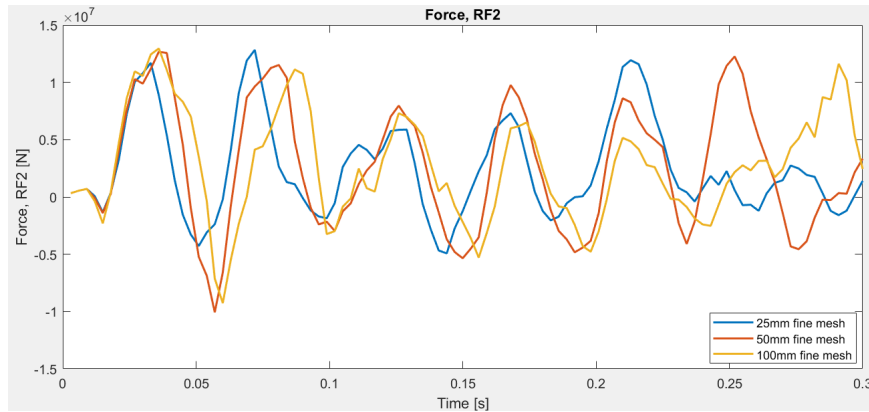


Figure 8.6: Force for different mesh sizes [51].

Despite some differences in the force-time curve, the curve was assumed sufficient and similar enough. Due to CPU time and the requirement from *DNV-RP-C208* of 50mm or lower, the mesh size was chosen to be 50mm. This was also since the mesh size of the container was chosen to be 50mm and using a 25mm mesh size on the panel would strict the requirements to the stable time step.

8.2 Point masses versus nonstructural mass

All the dynamic analyses from the mesh refinement were done with four equal point masses distributed around the container. Some impact scenarios were performed to validate the results. An analysis when the container falls with the whole front in the middle between girders was performed, which corresponds to impact scenario 4 presented later in Section 9.1. The analysis was first done with point masses, but resulted in odd results. The graphs of the energies showed that the kinetic energy never approaches zero. The distribution of the kinetic energies is plotted below.

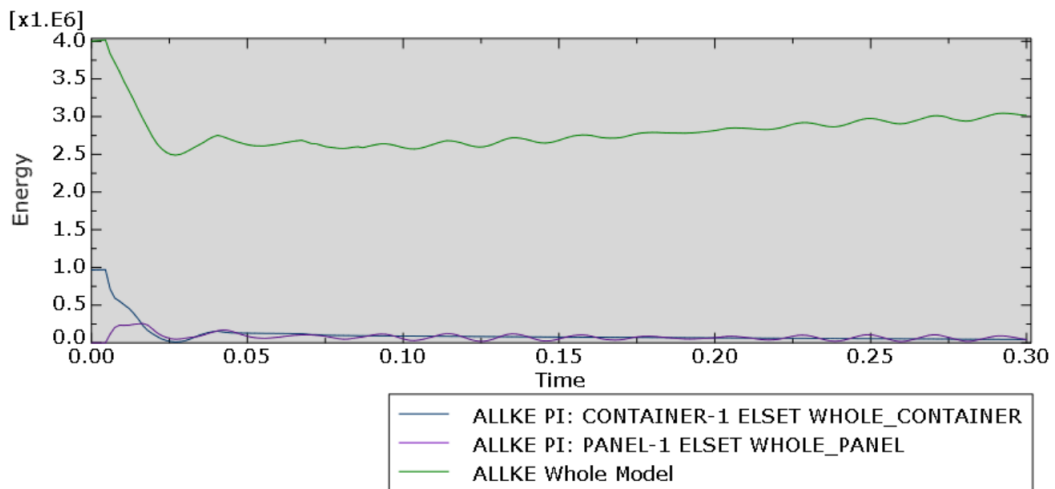


Figure 8.7: Distribution of kinetic energy for scenario 4 using point masses [51].

It was clearly something wrong in the kinetic energy for the container. The container itself weighed almost 5Te which corresponds to a kinetic energy of almost 1MJ, which is exactly the start kinetic energy for the container in this case. This gave an impression that the point masses resulted in unrealistic results. From deformation modes it may be that the point masses bounce out when the element obtain fracture due to element deletion. This may explain the high kinetic energy after impact. Further, the same scenario was performed by applying a nonstructural mass distributed over the whole container, which will be equivalent to increasing the density of the material. The nonstructural mass applied corresponds to the sum of the four point masses applied before, such that the total mass of the container was 20Te. The distribution of the kinetic energy using nonstructural mass is plotted below.

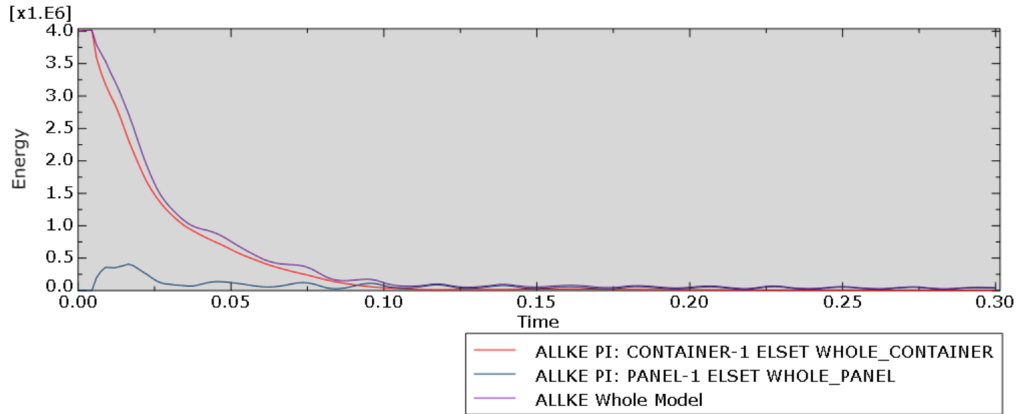


Figure 8.8: Distribution of kinetic energy for scenario 4 using nonstructural mass [51].

The kinetic energies using nonstructural mass gave a more realistic result and the start kinetic energy for the container corresponded to the weight with the nonstructural mass. To validate the results, another impact scenario was also compared using point masses or nonstructural mass. The container then fell with the bottom horizontal beam first, corresponding to impact scenario 1 presented later in Section 9.1. The results showed similar results. Based on the results, all the further analyses were performed with nonstructural mass instead of point masses.

Due to limited time, the mesh refinement was not done again. Since all were performed with the same impact scenario, the mesh refinement was considered sufficient. It is regardless important to note that the result from the mesh refinement may be unrealistic and may be the reason for the odd result using 25mm fine mesh on the container.

8.3 Discussion of computational time

Since the mesh refinement was done with either container or deck rigid, the actual computational time when both is deformable are compared. The reason was to see if it would be possible to increase the mesh size without getting unacceptable high CPU time. Another reason was to compare the CPU times for analyses using point masses and nonstructural mass. The CPU time for the different analyses is presented in Table 9.4. All the CPU times were for the container falling with the bottom horizontal beam first. Since the mesh refinement was done with point masses, the CPU time was also compared with point masses.

Table 8.3: CPU time for the different analysis [51].

Type of analysis	CPU time 50mm mesh size [s]	CPU time 25mm mesh size [s]
Rigid container point mass	2786	14169
Rigid deck point mass	11382	22686
Both deformable point mass	15962	-
Rigid container nonstructural mass	3362	-
Rigid deck nonstructural mass	5163	-
Both deformable nonstructural mass	9392	-

The effect on the CPU time by using nonstructural mass is also clearly seen. As described in Section 7.5.3, the stable time increment is determined by the dilatational wave speed which again is dependent on the density of the material. Using nonstructural mass will give similar results as increasing the density in the material parameters. When increasing the density, the dilatational wave speed decreases and hence the stable time increment increases. Table 9.4 shows a significant difference in the CPU time between using point masses and a nonstructural mass. To bring an additional mass to the system, it is in general easier to use nonstructural mass than several point masses [39].

It is clearly seen that the rigid deck analysis was more time consuming than the rigid container analysis. This was assumed since the container is more complex and has more elements than the fine mesh area of the panel. On the other hand, decreasing the mesh size of the impact zone of the panel for the rigid container analysis had a larger difference in the CPU time.

The analysis with both deformable with point masses used almost six times the CPU time for the one with the rigid container, using the same mesh size. This gives an impression that using 25mm mesh in the impact zone of the panel would cause an unacceptable high CPU time. Almost six times the CPU time for the rigid container corresponds to a CPU time of around 22 hours if using the same relationship of increase. Considering the high amount of analysis planned, it was reasonable to keep the mesh size at 50mm for the impact zone of the panel.

The analysis with both deformable with point masses had a CPU time almost one and a half larger than the one with a rigid deck, which will not increase the CPU time as much as for the rigid container analysis. On the other hand, due to the odd result of the 25mm mesh size of the container and that the damage of the panel is in general most critical, the mesh size of 50mm was kept. Furthermore, higher memory needed to perform analysis with finer mesh is also an important parameter.

Since further analyses are to be performed using nonstructural mass and not point mass, it was reasonable to compare the CPU time also with the nonstructural mass. The analysis with both deformable using nonstructural mass had a CPU time almost three times higher than the one using a rigid container and almost two times higher than the one using the rigid deck. This is different than the relationships for the point masses. Due to limited time, the 25mm fine mesh was not performed with nonstructural mass. Further, the 25mm fine mesh was assumed very time consuming based on the results from the point masses. Using 50mm fine mesh with both deformable using nonstructural mass resulted in almost 3 hours, but due to the much higher CPU time for 25 mm fine mesh using point mass, it was assumed a much higher CPU time also using nonstructural mass. The high increase in CPU time for 25mm fine mesh corresponds to the fact that it is the finest mesh size that controls the CPU time. It would have been manageable with the CPU time for some analyses, however it was assumed difficult due to the large number of analyses planned.

9 Analysis and Results

Different impact angles and locations of impact were investigated, in addition to the effect of changing the geometry of the panel. Due to the many uncertainties with including strain rate effects for the dynamic model based on theory from Section 6.2, the strain rate effects were neglected in all the numerical analyses.

Since most of the finite element analyses were performed with both container and deck deformable, the effect of neglecting a deformable container was performed with a rigid container against a deformable panel. In addition, some quasi-static analysis was performed to compare with the dynamic analyses and to easier obtain force-deformation curves. Further, to ensure an accurate estimate using the finite element analyses, sensitivity studies is an important part of the modelling procedure. The effects of changing BC, velocity, mesh and friction coefficient was analysed.

9.1 Impact scenarios

A comparison of different impact scenarios were performed. All analyses was performed dynamic with an initial velocity of 20 m/s to get conservative results. Using that $v = \sqrt{2gh}$, 20m/s result in a height around 20 meters, which is a conservative drop height. From the discussion of using point masses in Section 8.2 below, all further analyses were performed applying nonstructural mass such that the total weight of the container was 20Te.

The different impact scenarios was simplified into scenario 1, 2, 3, 4, 5, 6 and 7 by Table 9.1. Falling on the whole bottom or whole top first was neglected since it was assumed as the least critical scenario. In general, the impact scenarios were chosen to obtain the most critical results. Therefore are bottom edge impacting on or close to a girder has been neglected due to limited time. Impacting on or close to the stiffeners was assumed worse.

Table 9.1: Impact scenarios.

Impact zone on container	Scenario	Impact location
Bottom horizontal beam	1	In the middle between girders
Bottom horizontal beam	2	On longitudinal stiffener
Bottom horizontal beam	3	Skewed, in the middle between girders
Whole front/back	4	In the middle between girders
Whole front/back	5	Skewed, in the middle between girders
Bottom edge	6	On stiffener, in the middle between girders
Bottom edge	7	On the plate between stiffeners, in the middle between girders

All the analyses were done with a location where the container was as far away from the BCs as possible, such that the solution will be as independent of the BCs of the panel as possible. This was to get better and more realistic results.

The curves are most interesting during impact with the panel, and not when the container is started to bounce off and fall on other places on the panel. The damage to the panel is done during the first impact.

Since the analysis was done explicit, it is important to ensure that the energy is conserved during the analysis. The external work (ALLWK), internal energy (ALLIE), artificial strain energy (ALLAE), friction dissipation energy (ALLFD), kinetic energy (ALLKE), plastic dissipation energy (ALLPD), strain energy (ALLSE) and the total energy of the output set is attached in Appendix E. The total

strain energy ALLIE given from Abaqus contains both the elastic and plastic energy and is the sum of: the recoverable strain energy, the energy dissipated by rate-independent and rate-dependent plastic deformation, the energy dissipated by viscoelasticity, the artificial strain energy, the energy dissipated by damage, the energy dissipated by distortion control and the fluid cavity energy [43]. The artificial strain energy is the energy to control hourglass deformation [40]. The internal energy may be used to see the effect of the dissipated strain energy.

The hourglassing is not considered a problem when the artificial strain energy is low compared to the internal energy, preferably below 5% of the total internal energy. The artificial energy would often become lower for a more refine mesh [40].

9.1.1 Results

An illustration of all the different impact scenarios is given in Figure 9.1, where the different colours correspond to different sections and hence different material properties. Impact scenario 1 is shown with the mesh size which is equal for all the other scenarios. The yellow area on the panel illustrates the impact zone with the finer mesh.

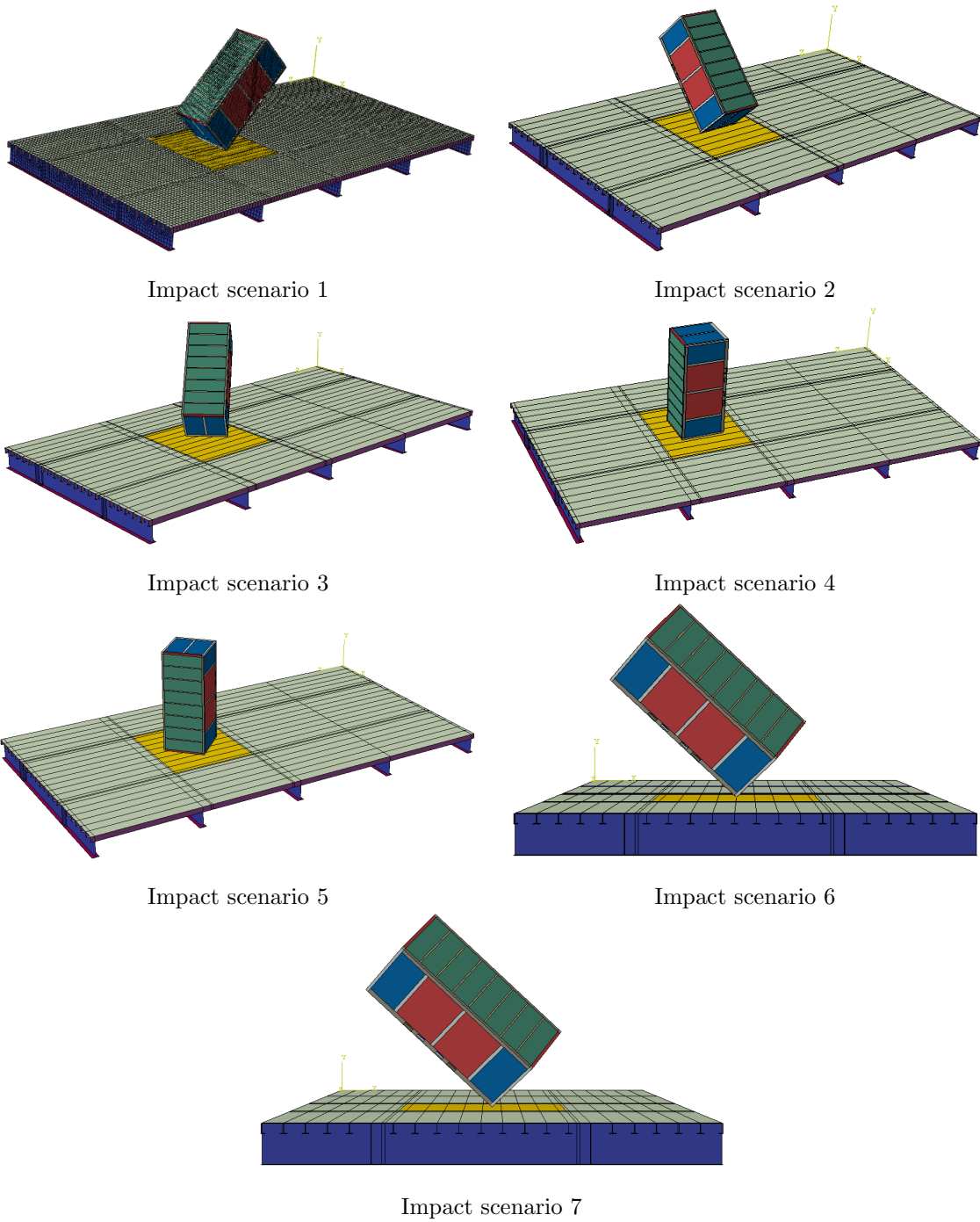


Figure 9.1: Illustration of the different impact scenarios [51].

The resulting deformation of the container and panel is given in Figure 9.2 and 9.3 below. Figure 9.3 shows the resulting damage in the panel seen from the plate side. The resulting damage in the panel seen from the stiffener side is attached in Appendix D.

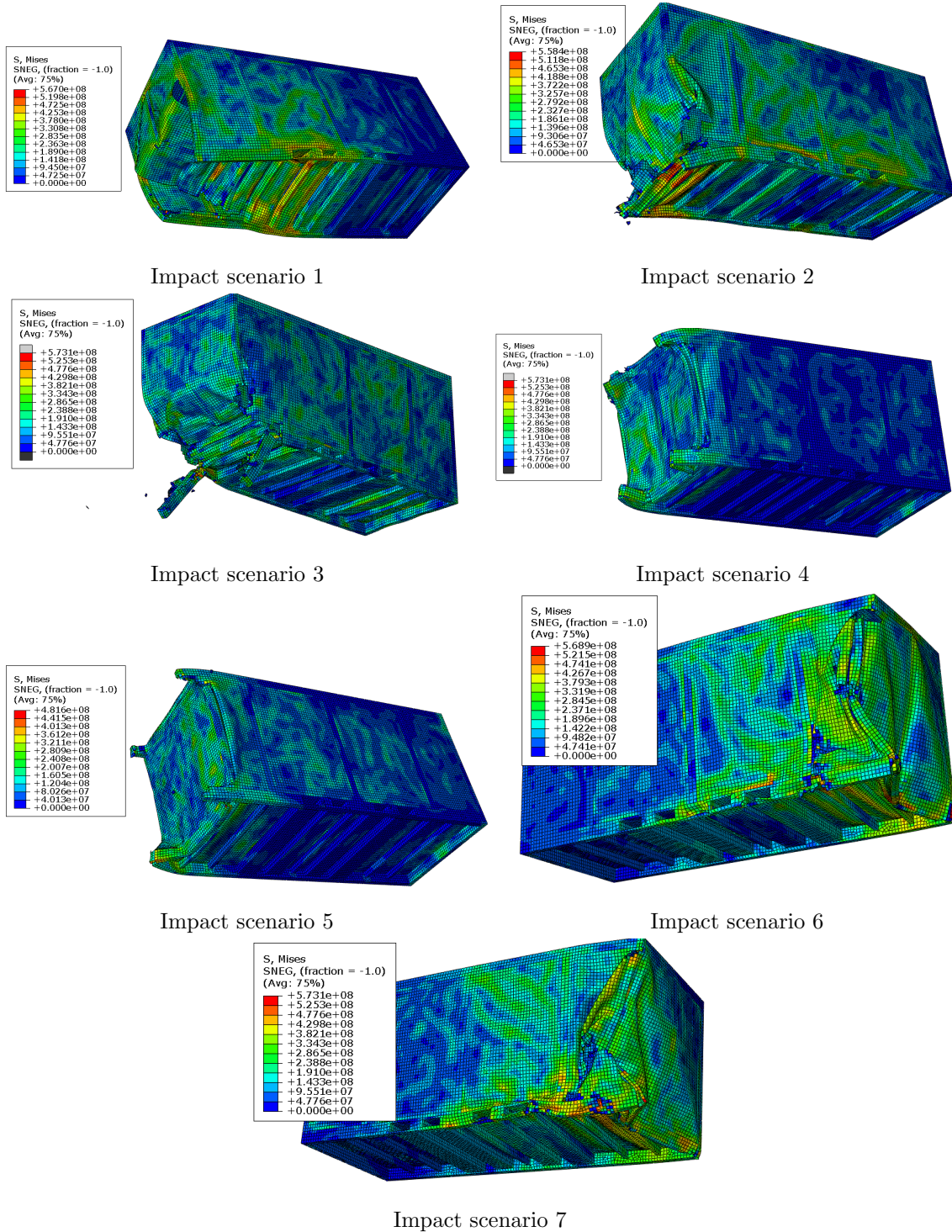


Figure 9.2: Deformed shape of the container at last increment [51].

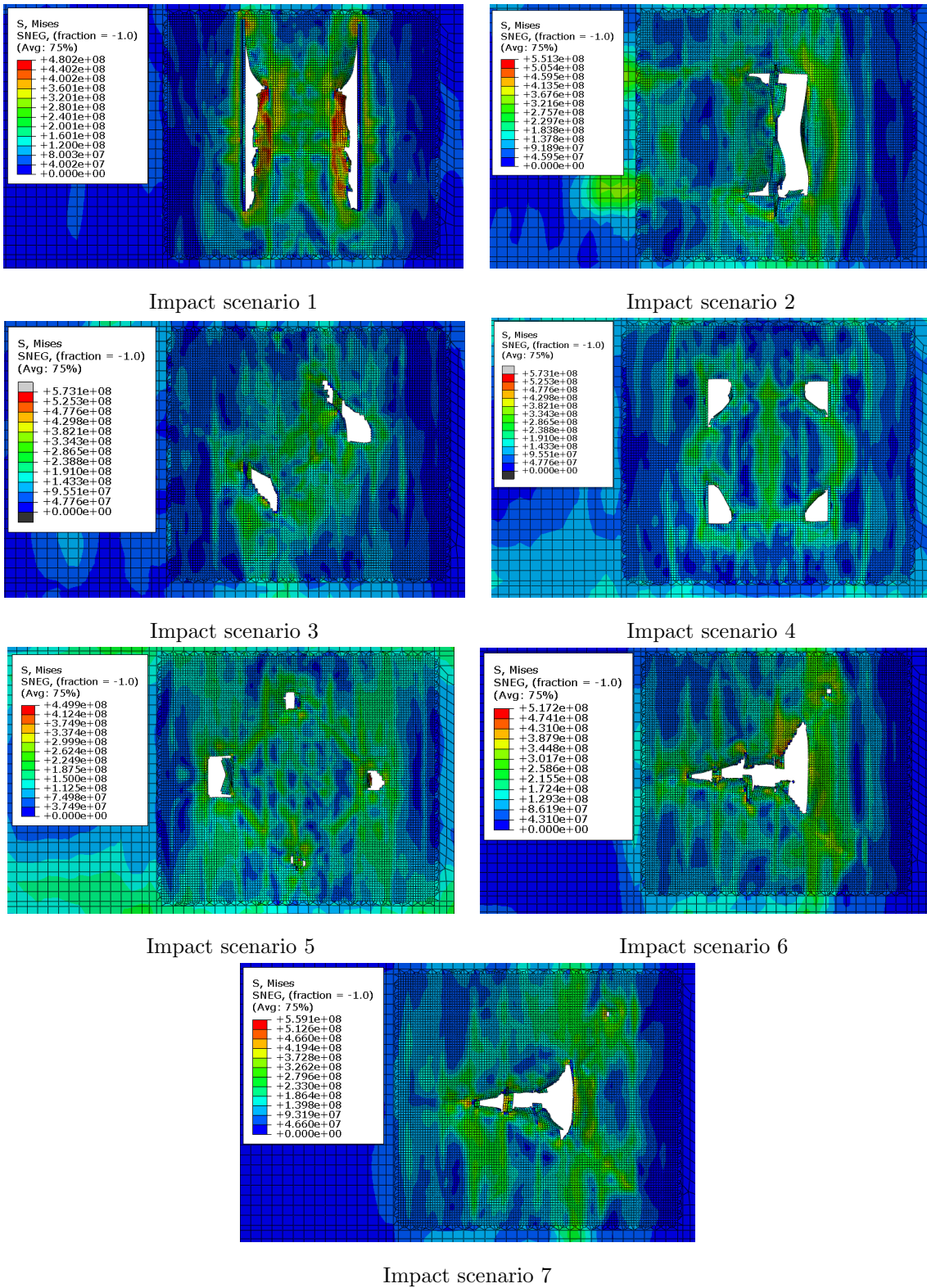


Figure 9.3: Deformed shape of the panel from above at last increment [51].

The distribution of energies has been the main result of the dynamic analysis. It is desirable that the container absorb as much as possible of the kinetic energy, resulting in less damage of the panel. The distribution of the different energies is attached in Appendix E.

The amount of energy absorption in the two parts will depend on the stiffness relationship between them as described in Section 3.2.2. From the results of the different impact scenarios it was concluded that the impact angle and impact location on the panel has a large impact on the damage of the container and panel. The reason is how much the container is able to absorb and how the panel is able to resist further penetration. The distribution of plastic dissipation energy, ALLPD is presented for all the scenarios in the table below. The total graphs for the distribution of the plastic dissipation energy for the different impact scenarios are attached in Appendix F.

Table 9.2: Distribution of plastic dissipation energy [51].

Impact scenario	ALLPD for container	ALLPD for panel
Scenario 1	59.9%	40.1%
Scenario 2	48.1%	51.9%
Scenario 3	62.3%	37.7%
Scenario 4	40.6%	59.4%
Scenario 5	31.6%	68.4%
Scenario 6	48.2%	51.8%
Scenario 7	56.4%	43.6%

The plastic dissipation energy was considered as the amount of damage in the model, hence the percentage above gives the damage of the container and damage of the panel. The energies were found as a percentage of the total plastic dissipation energy. The total plastic dissipation energy was different for the different impact scenarios since the contribution from the other energies will be different. An example is the amount to frictional dissipation energy.

The impact angle for scenarios 1, 2 and 3, for scenarios 4 and 5, and also for scenarios 6 and 7 was the same, but the impact location on the panel was different. The result shows a large difference for the scenarios, meaning that the impact location was quite as critical as the impact angle.

The different impact scenarios showed that the deformation of the container was highly affected by the impact angle. When falling with the bottom edge first as for impact scenarios 6 and 7, the deformation of the container was not significantly affected by the impact location. The same applies for impact scenarios 4 and 5. On the other hand, for the container falling with the whole bottom beam first, the impact location was found to be more important. For almost all the scenarios, the bottom side rails were shown to be quite strong, except for impact scenario 3 when falling skewed on the panel with the bottom beam first. For both impact scenarios 1 and 3, the bottom was deformed folding backwards as it penetrated the deck. For impact scenario 2, the bottom was stronger and deformed less. For both impact scenarios 4 and 5, the container was compressed from the bottom by the panel, except for the edges that penetrated the panel. For impact scenario 6 and 7, the bottom side rails were quite strong and the vertical end beam and plate were deformed backwards.

Furthermore, the damage of the panel also seemed to be dependent on the impact location as for the damage of the container. For impact scenarios 1,2 and 3, the panel obtained very different damage. This was assumed and shows the same relation as for the damage of the container.

The container was able to absorb the most amount of the kinetic energy when falling skewed with the bottom horizontal beam distributed over several stiffeners with a 45 impact angle, in other words the impact scenario 3. As seen by Figure 9.2 for impact scenario 3, the container got significant damage. The bottom plate and support transversal beams were folded backwards as the container penetrated the panel. The longitudinal bottom rails also obtained fracture. Corresponding to most energy absorption in the container for the impact scenario 3, the panel was less damaged. Figure 9.3 show little damage for impact scenario 3.

The container was able to absorb the smallest amount of the kinetic energy when falling skewed with the whole front first, in other words the impact scenario 5. The panel will then be able to absorb more of the energy with less damage since the impacting area of the container is larger. The kinetic energy from the container will be distributed over a larger area on the panel, meaning each stiffener have to resist a smaller energy. From Figure 9.3 for impact scenario 5, it is seen that the stresses are higher and distributed over a larger area than for the other scenarios. Corresponding to this, the container obtained minor damage compared to impact scenario 3. The same follows for impact scenario 4. The energy absorption in the container for impact scenario 4 was somewhat higher. Falling skewed on the panel was advantageous since the container will affect one more stiffener, hence distributing the energy over a larger area.

9.1.2 Final indentation of deck

The deformation of the container through the deck may be compared. A critical scenario would be if the container hits equipment below deck which may lead to fire or explosion. It is therefore critical to know how far the container penetrates the deck, in other words the ability the panel had to resist the impact in the different scenarios. The indentation (depth of deformation) of the deck was taken as the displacement at the node penetrated longest through the deck.

Table 9.3: Final indentation of deck [51].

Impact scenario	Indentation [mm]
Scenario 1	1353
Scenario 2	839
Scenario 3	914
Scenario 4	710
Scenario 5	775
Scenario 6	1117
Scenario 7	729

The indentation of deck is significant for all the impact scenarios. It would be interesting to know how far below deck the equipment is placed to know if the container will hit the equipment, but this was difficult to obtain. Impact scenario 1 and 6 is clearly the worst in relation to the indentation of deck. Comparing the results with the distribution of plastic dissipation energy in Table 9.2 gives interesting results. As described before, it is desirable that most of the energy is absorbed by the container. The indentation of deck was largest for impact scenario 1, while Table 9.2 gives that the container absorbed as much as 59.9% of the total plastic dissipation energy. Hence, the high amount of absorbed energy in the container was not reflected in the indentation of deck. On the other hand, the indentation of deck may be compared with the damage of the panel given in Figure 9.3, which quite corresponds well.

Something to note is the large difference in the indentation of deck for impact scenarios 6 and 7. The container penetrated through deck a lot longer when falling at the stiffener than on the plate between two stiffeners. The reason was that when the container fell on the plate, the stiffeners at both sides corresponded to the resistance of the panel and the container was deformed by the stiffeners and prevented from penetrating further. This may be seen at an early increment from Figure 9.4 for impact scenario 7. To what extent the stiffener will be able to prevent further penetration of deck by deforming the container will be highly dependent on the stiffener spacing.

Comparing impact scenario 1 with impact scenarios 2 and 3, there was also a large difference in the indentation of deck. The reason was the bottom side rails on the container. When falling with

the bottom side rails in the middle between two stiffeners, the panel was not able to resist the penetration of the bottom side rails. While falling with the bottom side rails skewed on the panel, the stiffeners are able to resist some of the further penetration of the bottom side rails. This may be seen at an early increment from Figure 9.4 for the different impact scenarios.

The acceptance criterion from *DNV-RP-C204* presented in Section 3.2.1 states that the load bearing function of the structure should be intact after impact. In other words, the container shall not hit equipment below deck which may lead to an unacceptable escalation of the extent of damage. Examples are fire or explosion. Since the distance to important equipment below deck was difficult to obtain, this will be difficult to compare. The whole container did not fall through the panel, but for some of the scenarios the final indentation could be critical. It is further important to remember that the analyses were performed as a worst case scenario with large impact mass and high impact velocity.

9.1.3 Deformation mechanisms of panel

The different deformation mechanisms in the panel are plotted below. The figures were taken where the deformation was easiest seen before large penetration of deck and hence element deletion. In other words, the deformations are from different times after impact and cannot directly be compared to each other. The colours represent the Von Mises stress, which is different for each impact scenario. The maximum Von Mises stresses shown in red color in Figure 9.4 is in the range of 530-570MPa.

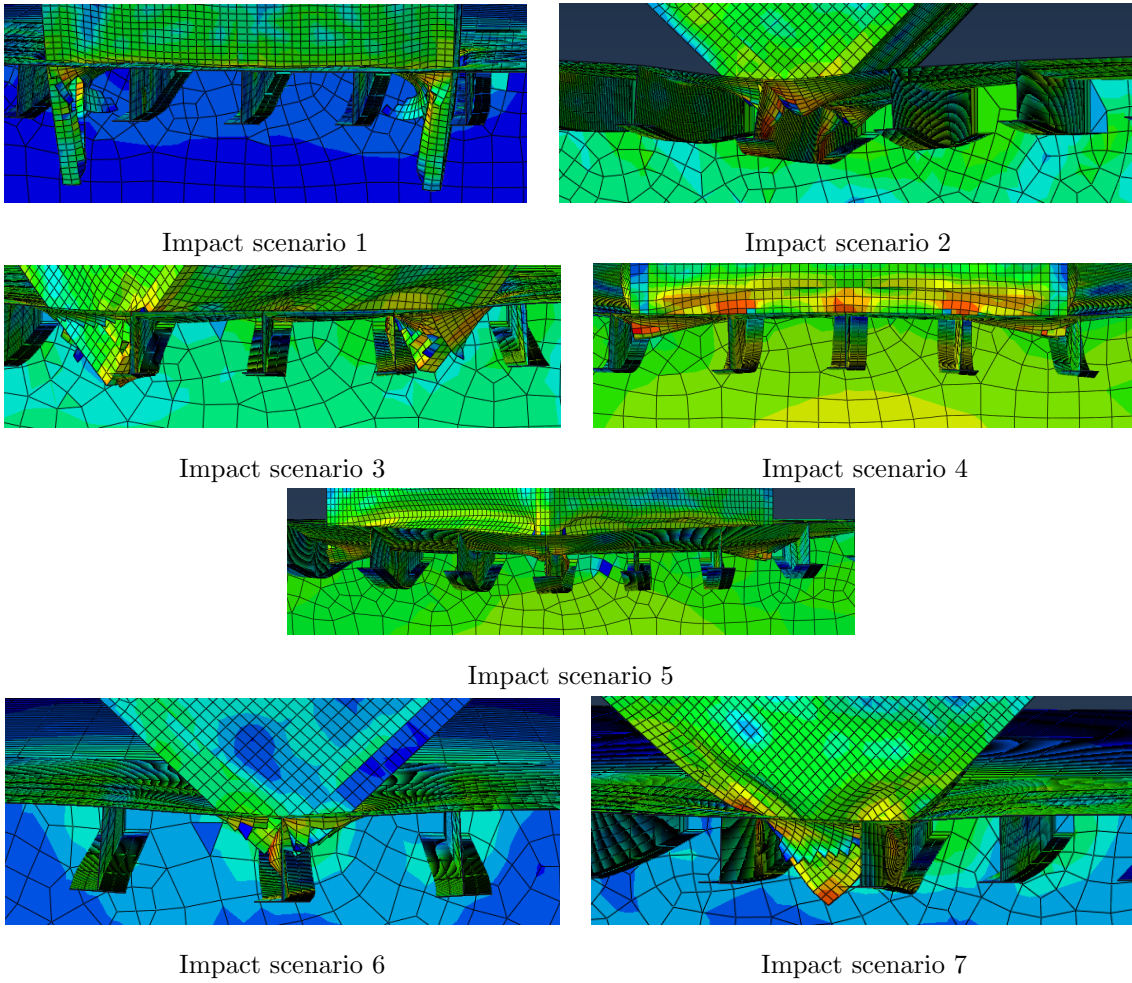


Figure 9.4: Deformation mechanism plotted from Abaqus [51].

To be able to easier compare the deformation mechanism with the theory presented in Section 5, a dynamic analysis without fracture criteria was performed for impact scenario 6. The reason was the high amount of element deletion in the analyses with fracture and therefore difficult to predict the deformation modes in the panel. The model in Abaqus will probably be a place between simply supported and clamped. The colours represent the displacement in the y-direction.

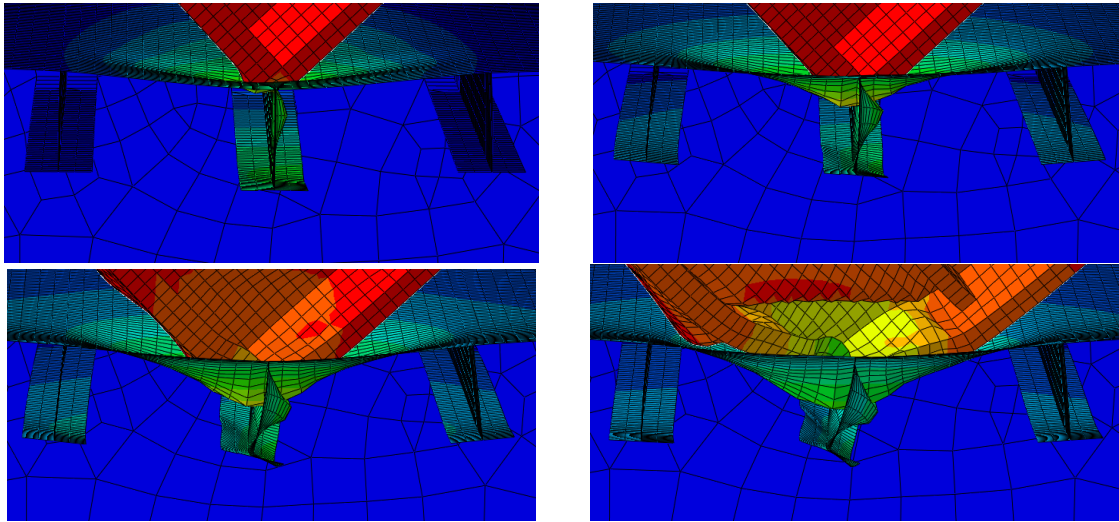


Figure 9.5: Deformation modes at time: 0.009s, 0.015s, 0.024s and 0.036s without fracture criteria[51].

The deformation at maximum displacement in the panel is shown below.

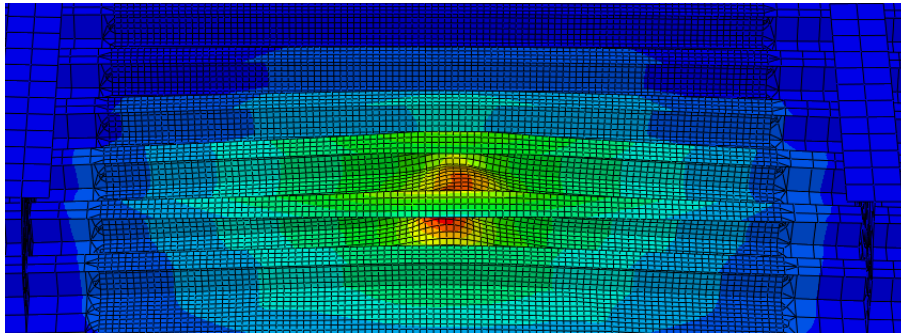


Figure 9.6: Deformation at maximum displacement without fracture criteria [51].

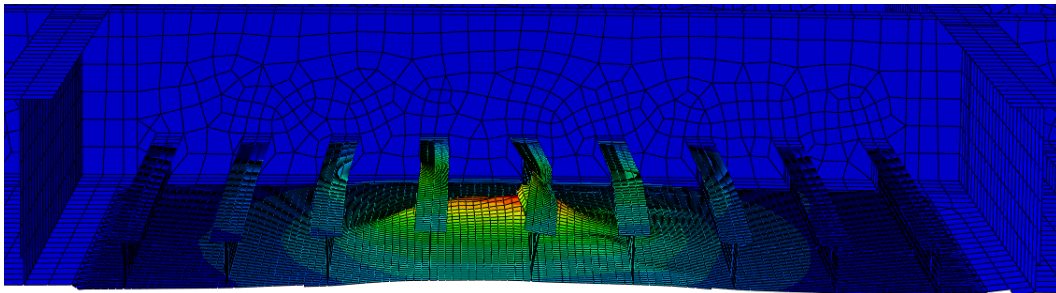


Figure 9.7: Deformation at maximum displacement without fracture criteria [51].

Shown from Figure 9.5, 9.6 and 9.7, there was tripping failure of the stiffener. In addition, the stiffener web buckled. Concluded by the figures, the deformation mechanism in Abaqus corresponds well to the theory. The figures from the analyses with fracture criteria also showed tripping failure and buckling of the stiffener web.

The existing resources of the deformation mechanism for containers are quite limited, such that the results from the finite element analyses are difficult to compare with existing theory. Further,

the container will also deform different dependent on if the walls are corrugated or not. The deformation of the container is discussed in Section 9.1.1.

9.1.4 Note on eccentric impact

All the impact scenarios are eccentric impacts except for scenarios 4 and 5. When the container is falling with an impact angle of 45 degrees on the panel, an effective mass is found using Equation 19,

$$m_{eff} = \left(\frac{\cos^2 45}{m_o} + \frac{\cos^2 45}{m_o} + \frac{\left(\frac{l}{r}\right)^2}{m_o} \right)^{-1}$$

where l/r is the radii of gyration. Using that $\cos^2 45 = \frac{1}{2} \cdot \sqrt{2}$ and that $l/r = 1$, the equation is further simplified.

$$m_{eff} = \left(\frac{1}{2m_o} + \frac{1}{2m_o} + \frac{1}{m_o} \right)^{-1} = \left(\frac{2}{m_o} \right)^{-1} = 0.5m_o$$

This means that half of the kinetic energy is transformed into energy due to rotation and the demand for energy dissipation is halved. Figure 3.3 may also be used to find the strain energy dissipation factor. Using that $x = l/r = 1$ is the radii of gyration and m_i is assumed infinite, the strain energy dissipation factor is found to be 0.5, which is the same as calculated above.

Comparing the calculations with the results from the finite element analysis seemed to be difficult. It was difficult to predict the exact time the container starts to rotate and the energy absorption will not only be because of the rotation when the container starts to rotate since the container will still impact through the deck. The spatial displacement in the y-direction and the rotational in y- and z-direction for impact scenario 1 is shown in Figure 9.8.

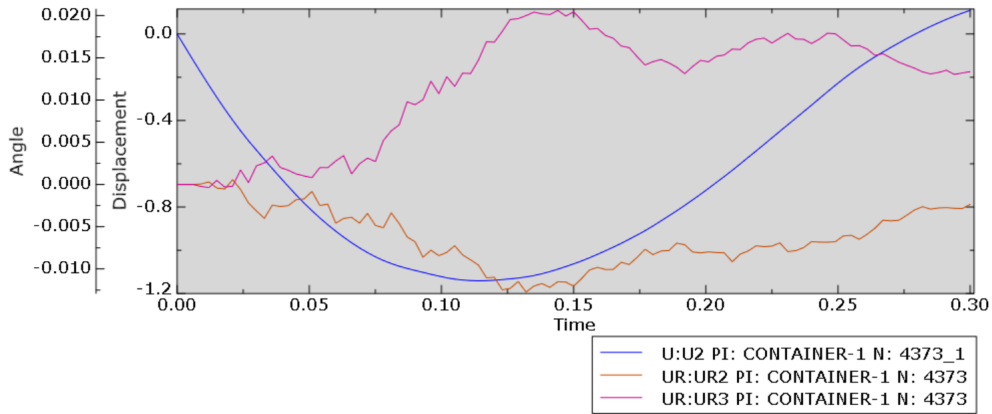


Figure 9.8: Spatial displacement in y-direction and rotational displacement in y- and z-direction [51].

As shown, the rotational displacement increased gradually, but the total energy absorption due to rotation is difficult to obtain. From the Figure in Appendix E for impact scenario 1, the kinetic energy was halved at around 0.09 seconds. From Figure 9.8, this was also where the rotational displacements significantly increased. From spatial displacement in the y-direction, the container started to fall down with the back end around 0.11 seconds. The calculation of half the kinetic

energy transformed into energy due to rotation was assumed sufficient, due to the fact that some of the energy before the back end starts to fall down is absorbed due to rotation. Ideally, further analyses and calculations should be performed to ensure the assumptions made, but the calculations give us an overview of the reality.

9.1.5 Note on energy balance

It is important to do an energy balance check to ensure that the results give an accurate estimate of the structural response. The energy balance from Abaqus is given by Equation 53 below [43].

$$ALLKE + ALLIE + ALLVD + ALLFD - ALLWK = E_{TOTAL} = constant \quad (53)$$

where

$$ALLIE = ALLSE + ALLPD + ALLCD + ALLAE + ALLDMD \quad (54)$$

ALLKE is the kinetic energy, ALLIE is the internal energy, ALLVD is the viscous dissipation energy, ALLFD is the frictional dissipation energy, ALLWK is the external work, ALLSE is the strain energy, ALLPD is the plastic dissipation energy, ALLCD is the creep dissipation energy, ALLAE is the artificial strain energy, ALLDMD is the damage dissipation energy and E_{TOTAL} is the total energy [43]. ALLCD was zero in the analysis.

The different energies are presented below and are the values at the last increment in the analyses. The energy balance was checked for impact scenario 7.

Table 9.4: Energies from Abaqus [51].

Type of energy	Value [MJ]
ALLAE	0.2481060
ALLDMD	0.0110436
ALLFD	0.4809810
ALLIE	3.6940100
ALLKE	0.1466730
ALLPD	3.3455700
ALLSE	0.0892826
ALLVD	0.0318644
ALLWK	0.3433420
E_{TOTAL}	4.0004300

The value of ALLIE directly from Abaqus was equal to the sum of ALLSE, ALLPD, ALLCD, ALLAE and ALLDMD as Equation 54 states. The total energy given from Abaqus seemed accurate due to an impact mass of 20Te and an initial velocity of 20m/s, resulting in a initial kinetic energy of 4MJ. Using Equation 53 the total energy is found as:

$$E_{TOTAL} = 0.1466730 + 3.694010 + 0.0318644 + 0.4809810 - 0.3433420 = 4.0101864$$

Due to the small difference between the computed total energy and the total energy directly from Abaqus, the analysis was assumed to give an accurate estimate of the structural response. The total energy should in general remain constant during the analysis, with an error of less than 1%

[37]. The total energy in impact scenario 7 almost remained constant with minor changes, therefore assumed to be sufficient.

In addition, the artificial strain energy should be compared to the internal energy to ensure that the hourglassing is not a problem. The artificial strain energy was 6.7% of the internal energy, which was somewhat high. This was considered sufficient enough due to time pressure, but should preferably be below 5%.

9.2 Rigid vs deformable container

Analysis of a rigid container was also performed to see the effect of neglecting a deformable container. The analysis was done for impact scenario 1.

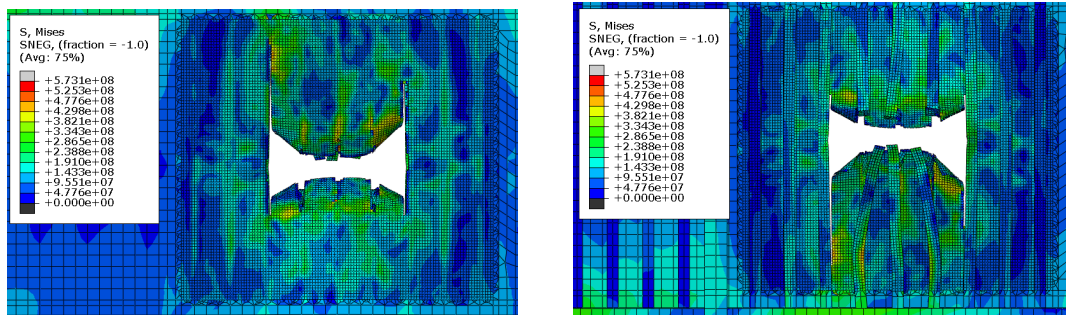


Figure 9.9: Deformed shape of the panel from above to the left and from under to the right [51].

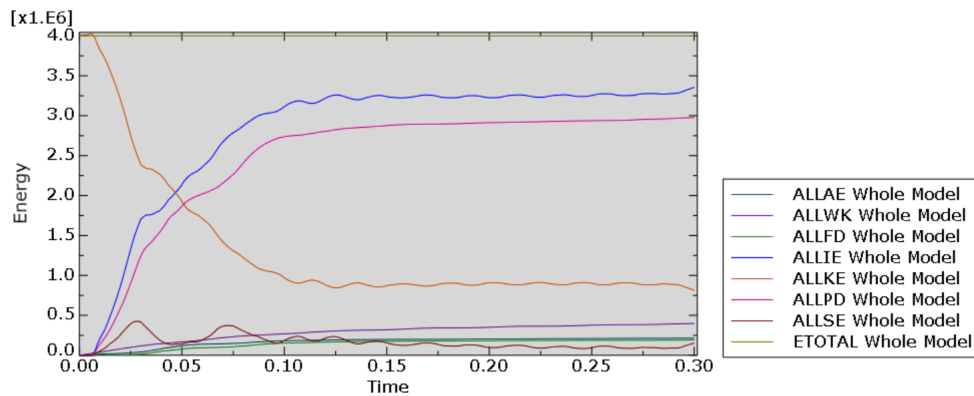


Figure 9.10: Different energies for impact scenario 1 with rigid container [51].

When neglecting the energy the container will be able to absorb, the panel will need to absorb all the energy, resulting in more damage. The effect of neglecting deformable container will hence be obtained too conservative and hence unrealistic results. The panel will be able to resist more of the dropped object than seen in an analysis with the rigid container, hence resulting in less damage of the panel. Comparing Figure 9.9 with the damage for the panel for impact scenario 1 in Figure 9.3, the panel got significantly more damage using rigid container. When neglecting the deformation of the bottom of the container between the bottom side rails, the whole impact area of the container penetrated the deck and cut through all the stiffeners. Also comparing Figure 9.10 with the energies from impact scenario 1 in Appendix E, the total energy absorption was lower when using a rigid container and a large amount of the kinetic energy was not absorbed.

9.3 Geometry study of the panel

Together with the modelling, a script was developed such that it was easy to change the geometry of the deck structure. For every command done in Abaqus, a code line will be made. Then the specific values were changed with a variable, such that changing a variable in the script will easily change the geometry of the panel by using the run script option in Abaqus. This was by far more efficient than remodelling the whole deck structure for every change in geometry. The variables used were the stiffener size, girder size, stiffener spacing and girder spacing. The change in thickness of the stiffener, girder and plate was easily done in Abaqus directly in the material properties and was therefore not included as a variable in the script. The script is not attached due to confidential information about the container. The results of changing the mentioned variables are described in the sections below. The initial values of the variables are given from Table 7.2.

All the variables have been investigated for three chosen scenarios, presented in Table 9.5 below. The scenarios were chosen based on probability and to give a sufficient overview of the impact scenarios. Scenario 7 was chosen instead of scenario 6, since it is a higher probability that the container falls on the plate than directly on a stiffener. The same reason was for scenarios 1, 2 and 4, which seemed to be a less likely impact scenario. It is more likely that the container will fall skewed with an angle on the panel.

Table 9.5: Impact scenarios for geometry study of the panel.

Impact zone	Scenario	Impact location
Bottom horizontal beam	3	Skewed, in the middle between girders
Whole front/back	5	Skewed, in the middle between girders
Bottom edge	7	On the plate between stiffeners, in the middle between girders

The main goal of the geometry study was to change the geometry of the panel to see what had the most effect on the structural resistance of the panel. All analysis has therefore been performed dynamic with both the container and panel deformable. To be able to compare the different geometry changes, it was changed with an equal relationship. In the end, what's important for a producer is the construction cost, meaning the cost of steel. Each change in stiffener size, girder size, plate thickness, stiffener spacing and girder spacing was done such that the total weight of the panel was increased the same amount for each change.

9.3.1 Change in stiffener size

The test value for the stiffener web height made the foundation for the other test values of the panel. The stiffener web height was chosen to increase to 400mm over the whole panel, which increased the total weight of the panel from 75526.3kg to 79833.4kg resulting in an increase of around 4307kg in total. The other variables were hence chosen such that the total weight of the panel increased with the same weight.

Table 9.6: Values for change in stiffener size.

Variable	Original value [mm]	Test value [mm]
Stiffener web height, $h_{w,s}$	300.00	400.00
Stiffener flange width, $b_{f,s}$	200.00	268.12
Stiffener web thickness, $t_{w,s}$	11.00	14.67
Stiffener flange thickness, $t_{f,s}$	17.00	22.79

The results from the different analyses are presented in the table below. As before, the plastic dissipation energy was used as a measure of damage. The plastic dissipation energy for the container is given in Table 9.7 below.

Table 9.7: Plastic dissipation energy with changed stiffener size [51].

Variable	Scenario	Original ALLPD container	Test ALLPD container	% difference
$h_{w,s}$	3	62.3%	63.8%	+1.5%
$h_{w,s}$	5	31.6%	37.9%	+6.3%
$h_{w,s}$	7	56.4%	60.5%	+4.1%
$b_{f,s}$	3	62.3%	62.2%	-0.1%
$b_{f,s}$	5	31.6%	32.5%	+0.9%
$b_{f,s}$	7	56.4%	61.8%	+5.4%
$t_{w,s}$	3	62.3%	65.5%	+3.2%
$t_{w,s}$	5	31.6%	35.6%	+4.0%
$t_{w,s}$	7	56.4%	65.1%	+8.7%
$t_{f,s}$	3	62.3%	61.4%	-0.9%
$t_{f,s}$	5	31.6%	32.5%	+0.9%
$t_{f,s}$	7	56.4%	62.4%	+6.0%

The effect of increasing the different variables was hence very dependent on the impact scenario. The advantage of increasing the stiffener web height was significant for impact scenario 5. For both impact scenarios 3 and 7, changing the stiffener web thickness will be the most advantageous change in stiffener size. On the other hand, changing all the variables had a small or negotiable effect for impact scenario 3, and resulted in a decrease in the plastic dissipation energy for two of the analyses. The highest % increase was for impact scenario 7 when increasing stiffener web thickness.

9.3.2 Change in girder size

The original and test values of the girder size are given in Table 9.8.

Table 9.8: Values for change in girder size.

Variable	Original value [mm]	Test value [mm]
Girder web height, $h_{w,g}$	1200.00	1512.42
Girder flange width, $b_{f,g}$	400.00	654.39
Girder web thickness, $t_{w,g}$	15.00	18.90
Girder flange thickness, $t_{f,g}$	20.00	32.13

The plastic dissipation energy for the container from the different analyses is presented in the table below.

Table 9.9: Plastic dissipation energy with changed girder size [51].

Variable	Scenario	Original ALLPD container	Test ALLPD container	% difference
$h_{w,g}$	3	62.3%	61.7%	-0.6%
$h_{w,g}$	5	31.6%	36.1%	+4.5%
$h_{w,g}$	7	56.4%	62.0%	+5.6%
$b_{f,g}$	3	62.3%	62.0%	-0.3%
$b_{f,g}$	5	31.6%	34.5%	+2.9%
$b_{f,g}$	7	56.4%	64.3%	+7.9%
$t_{w,g}$	3	62.3%	62.5%	+0.2%
$t_{w,g}$	5	31.6%	33.1%	+1.5%
$t_{w,g}$	7	56.4%	63.9%	+7.5%
$t_{f,g}$	3	62.3%	62.0%	-0.3%
$t_{f,g}$	5	31.6%	34.2%	+2.6%
$t_{f,g}$	7	56.4%	64.2%	+7.8%

The results from the change in girder size showed a somewhat similar pattern to the change in stiffener size. All the changes in girder size gave negligible effect for impact scenario 3. Impact scenario 7 had the largest effect for all the different changes and the highest % increase was for increased girder flange width. Increasing the girder web thickness and girder flange thickness gave almost the same results as changing the girder flange width. For impact scenario 5, the most advantageously was increasing the girder web height. This was the same as for changing the stiffener size.

9.3.3 Change in plate thickness

The original and test values of the plate thickness are given in Table 9.10.

Table 9.10: Values for change in plate thickness.

Variable	Original value [mm]	Test value [mm]
Plate thickness, t	10.00	11.64

The plastic dissipation energy for the container from the different analyses is presented in the table below.

Table 9.11: Plastic dissipation energy with changed plate thickness [51].

Variable	Scenario	Original ALLPD container	Test ALLPD container	% difference
t	3	62.3%	60.3%	-2.0%
t	5	31.6%	31.0%	-0.6%
t	7	56.4%	68.3%	+11.9%

The effect of increasing the plate thickness was major for impact scenario 7, which was as assumed. Falling directly on the plate with one edge first will be very dependent on the strength of the plate and hence increasing the damage in the container when the panel becomes stronger. For impact scenarios 3 and 5, the plastic dissipation energy actually decreased, so changing the plate thickness had no positive effect on the damage of the container.

9.3.4 Change in stiffener or girder spacing

The effect of changing stiffener or girder spacing is more difficult to compare with the cost of steel, since it will increase or decrease the total area of the panel. The stiffener and girder spacing was decreased, given a new mass and length of the panel. Then the mass was found per meter and multiplied by the actual length of the panel. This was assumed sufficient since the impact zone was a small part of the total area of the panel. Decreasing the stiffener or girder spacing resulted in a smaller total area of the panel since there are now more stiffeners and girders per length. When decreasing the longitudinal stiffener spacing, the longitudinal girder spacing was also decreased, since the number of stiffeners between the girders was unchanged. The script could probably be improved to take this into account, but was neglected due to limited time and the fact that the results were assumed approximately the same. An improved script would make the procedure of finding correct test values easier. On the other hand, if the container impacts closer to the edges, an improved script must be made. The change in girder spacing was only performed by changing the transverse girder spacing. The original and test values of the stiffener and girder spacing are given in Table 9.12.

Table 9.12: Values for change in stiffener and girder spacing.

Variable	Original value [mm]	Test value [mm]
Stiffener spacing, l_s	640.00	570.75
Transverse girder spacing, l_g	6135.00	4624.00

The plastic dissipation energy for the container from the different analyses is presented in the table below.

Table 9.13: Plastic dissipation energy with changed stiffener or girder spacing [51].

Variable	Scenario	Original ALLPD container	Test ALLPD container	% difference
l_s	3	62.3%	60.1%	-2.2%
l_s	5	31.6%	25.2%	-6.4%
l_s	7	56.4%	67.5%	+11.1%
l_g	3	62.3%	62.5%	+0.2%
l_g	5	31.6%	41.5%	+9.9%
l_g	7	56.4%	59.7%	+3.3%

Changing the stiffener spacing shows a significantly less amount of energy absorbed by the container, especially for the impact scenario 5, then falling skewed with the whole front first. The reason may be that with a decreased stiffener spacing the kinetic energy from the container will be distributed over more stiffeners, and the panel will probably absorb more energy compared with before and hence less damage for the container. It is also important to remember that decreasing the stiffener spacing also decreased the longitudinal girder spacing. When falling with the whole front first for impact scenario 5, the decreased longitudinal girder spacing may contribute positively to the strength of the panel since the impact zone of the container was closer to the girders.

Impact scenario 7 - edge on the plate first, had opposite effect with decreasing the stiffener spacing. This proves that the stiffeners deform the container and prevent the container from further penetrating of deck, as discussed in Section 9.1.2. A decreased stiffener spacing results in a lower indentation before deformation of the container and hence more energy absorbed by the container. For impact scenario 7 with normal stiffener spacing the container penetrates through the stiffeners as shown in Figure 9.3, but when decreasing the stiffener spacing none of the stiffeners was penetrated.

9.3.5 Comparison

An overview of the impact scenario with the highest increase in the plastic dissipation energy of the container for every change in geometry is given below.

Table 9.14: Plastic dissipation energy for container for the impact scenario with the highest increase.

Variable	Scenario	Original ALLPD container	Test ALLPD container	% difference
$h_{w,s}$	5	31.6%	37.9%	+6.3%
$b_{f,s}$	7	56.4%	61.8%	+5.4%
$t_{w,s}$	7	56.4%	65.1%	+8.7%
$t_{f,s}$	7	56.4%	62.4%	+6.0%
$h_{w,g}$	7	56.4%	62.0%	+5.6%
$b_{f,g}$	7	56.4%	64.3%	+7.9%
$t_{w,g}$	7	56.4%	63.9%	+7.5%
$t_{f,g}$	7	56.4%	64.2%	+7.8%
t	7	56.4%	68.3%	+11.9%
l_s	7	56.4%	67.5%	+11.1%
l_g	5	31.6%	41.5%	+9.9%

From the results, it was in general seen that the effect of increasing the strength has the largest effect for impact scenario 7. For every different geometry change except for changing the stiffener web height and transverse girder spacing, the % difference was largest for impact scenario 7.

For some of the analyses it had no positive effect on increasing the strength of the panel. For the change in girder and stiffener size, the difference was so small that it was assumed negligible. On the other hand, changing the stiffener spacing led to a significantly lower amount of energy absorbed by the container. This was especially for the impact scenario 5.

Further, it will be difficult to predict how the container will fall, hence a middle way of all the results is probably most advantageous in relation to the strength of the panel. The average increase in the energy absorption in the container for the three impact scenarios is presented in the table below.

Table 9.15: Average increase in ALLPD container for the different geometry changes.

Variable	Average increase in ALLPD container
$h_{w,s}$	4.0%
$b_{f,s}$	2.1%
$t_{w,s}$	5.3%
$t_{f,s}$	2.0%
$h_{w,g}$	3.2%
$b_{f,g}$	3.5%
$t_{w,g}$	3.1%
$t_{f,g}$	3.4%
t	3.1%
l_s	0.8%
l_g	4.5%

From Table 9.15, the change in the stiffener size was found to be most advantageous if assuming the container will fall as a combination of the three impact scenarios.

9.4 Quasi-static analyses

Force-deformation curves were found by quasi-static analyses which neglect the inertia effects. Quasi-static analyses with rigid deck, rigid container and both container and deck deformable were presented in the following sections.

9.4.1 Quasi-static with rigid dekk

The analyses were performed with a rigid deck to see the amount of energy the container will be able to absorb for the different impact scenarios. Since the deck was rigid, the impact location on the deck was irrelevant. Hence the quasi-static analysis was done with the bottom horizontal beam first, the whole front first and the bottom edge first.

Due to more data points in the history output than the field output, it was assumed more accurate to derive the energy given from the history output than plotting the force from the field output. The data points from the field output were fewer due to the high memory needed. The data points from the history output are not memory dependent. The external work was derived since it includes both the internal energy and frictional dissipation energy. The force-deformation curves from the field output were compared to the derived energy-deformation curves to ensure that deriving the energy gave correct force-deformation curves. The force-deformation and energy-deformation curve is plotted below.

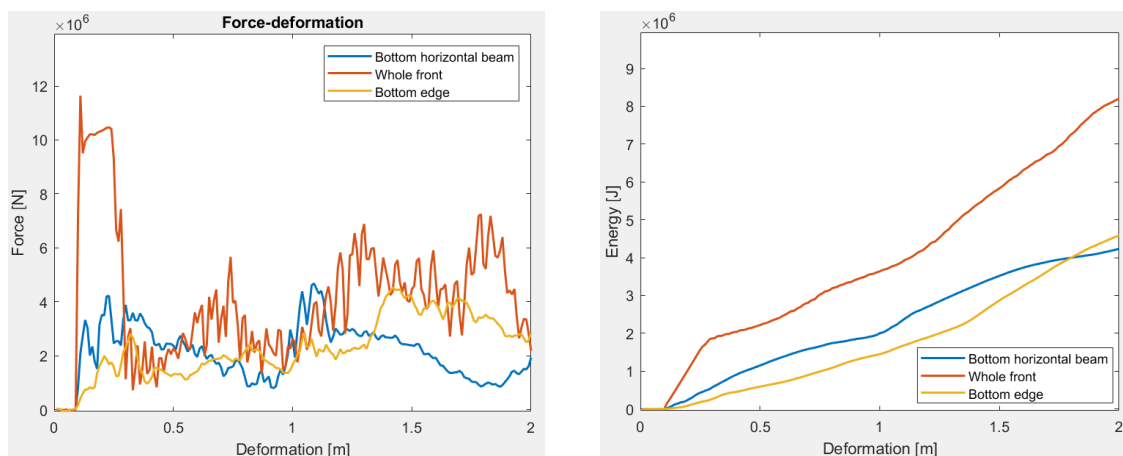


Figure 9.11: Force-deformation and energy-deformation curve for quasi-static analyses with rigid deck [51].

Figure 3.1 shows the distribution of dissipated strain energy by independent force-deformation curves when the container is rigid or the deck is rigid. Since containers are approximately equal with a small difference, but the deck could be very different, it seemed to be relevant to use a rigid deck. In this way, the force-deformation curve for the container may be used in combination with force-deformation curves for different decks and may be used to estimate the amount of strain energy the container is able to absorb in different cases.

Since the container had constant velocity forcing into the deck, the final indentation and damage may be found for different impact velocities. Different impact velocities results in different energies and hence the final deformation may easily be found from the energy-deformation curve from Figure 9.11.

The deformation of the container for the different cases is shown below.

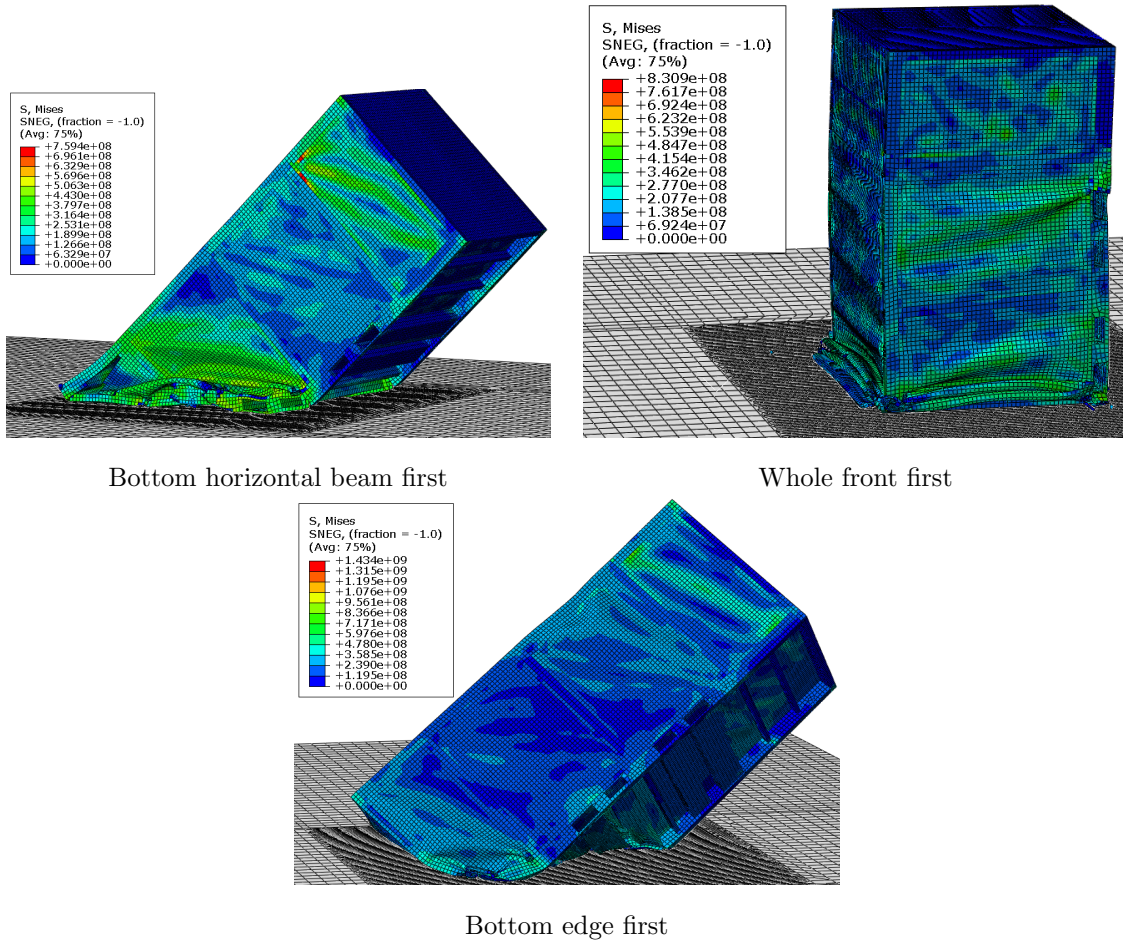


Figure 9.12: Deformation of container with rigid deck [51].

Compared with the deformation of the container for the dynamic analyses in Figure 9.2, the deformation from the quasi-static analyses shows similarities, keeping in mind that the dynamic analyses were performed with a deformable deck.

9.4.2 Force-deformation curves

A quasi-static analysis with a rigid container was performed. Due to limited time, only the impact scenario 7 was performed. The effect of using a rigid container was also performed with a dynamic analysis, but was performed quasi-static to compare the force-deformation curves. Force-deformation curves were plotted from Abaqus based on Figure 3.1. The force-deformation curve for the container was found using a rigid deck and the force-deformation curve for the deck was found using a rigid container. The resulting force-deformation curve is plotted in Figure 9.13 below.

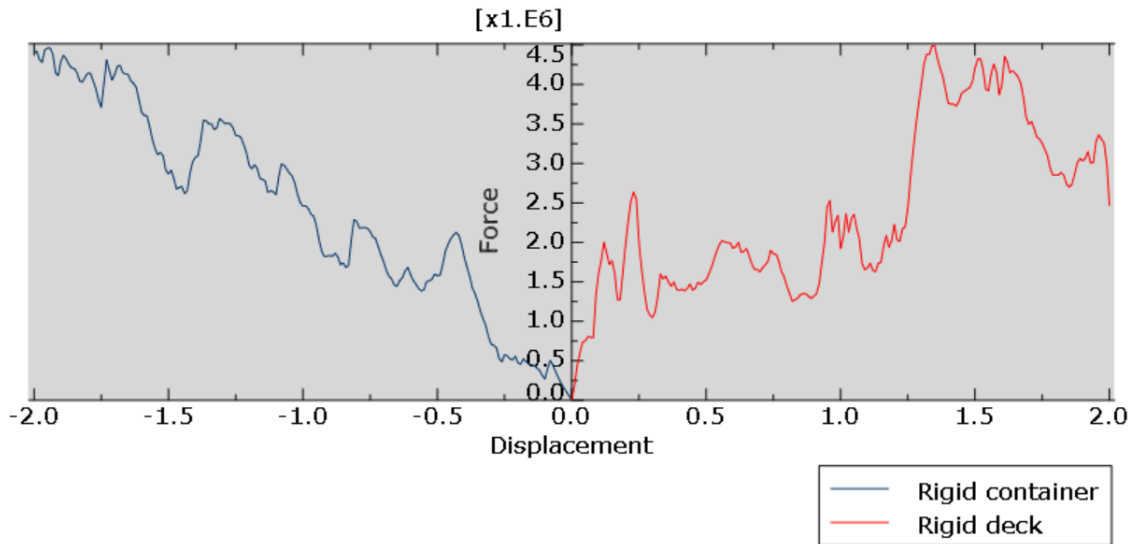


Figure 9.13: Force-deformation curve using rigid container and rigid deck [51].

As described in Section 3.2.2, the force-deformation curves made independent of each other may be used to find the total dissipated strain energy. The total dissipated strain energy with both container and deck deformable will not be equal to the total strain energy dissipation found by this method. When the curves are found independently of each other, it will not account for the interaction effect between them. In an analysis with both deformable, the stronger object will probably experience less damage than the softer one. When the softer structure deforms, the impact force will be distributed over a larger contact area and the resistance of the stronger structure will increase. The energy dissipation correction factor in Equation 3 is used to account for the effect. This may be discussed since the resistance of the softer structure probably also will increase.

9.4.3 Quasi-static with both deformable

A quasi-static analysis with both deformable was performed to be able to compare with results from the dynamic analysis with both deformable. Another purpose was to see if the the force-deformation curves in Figure 9.13 could give reasonable results when comparing with the dissipated strain energy from an analysis with both deformable.

The deformable analysis will now take into account the interaction effect between the container and the panel, where the stronger structure will probably be less damaged than the softer one. The distribution of the dissipated strain energy from the quasi-static analyses for both container and deck deformable is shown below.

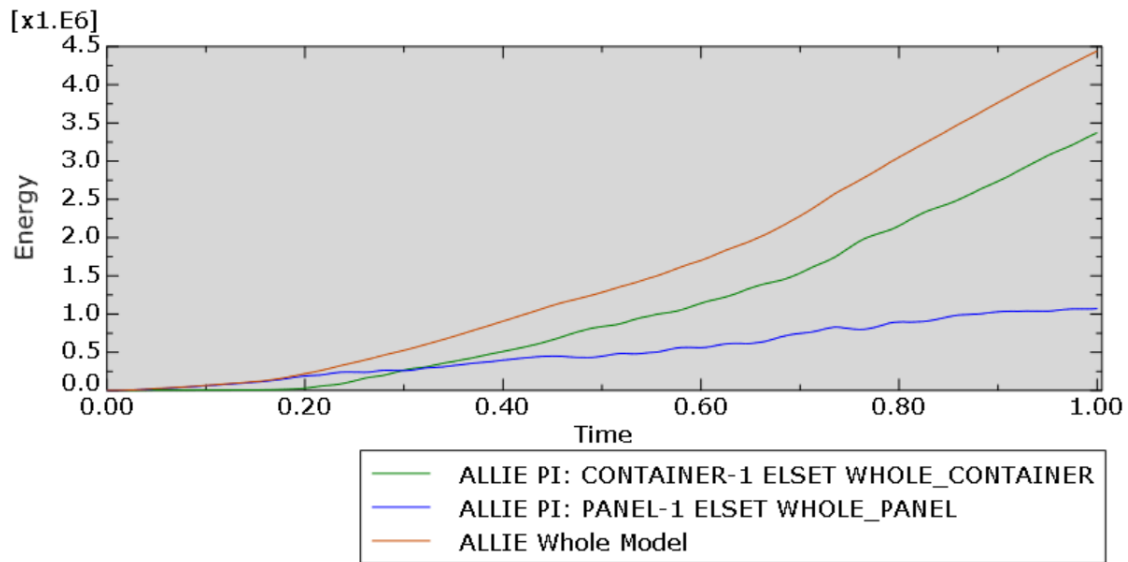


Figure 9.14: Distribution of internal energy from quasi-static analysis [51].

Figure 9.14 shows that most of the energy was absorbed by the container. Compared with the force-deformation curve in Figure 9.13, the panel will absorb most of the energy from the start. For example, using that the force is 2.5MN will roughly correspond to around 0.32MJ absorbed by the container and 1.25MJ absorbed by the panel. Using a force of 3MN gives a much higher energy absorbed by the container, which now is higher than the energy absorbed by the deck. This is because of the peak in the force-deformation curve for the rigid deck at 0.25m. The same can be seen in Figure 9.14 after 0.3s and 0.28MJ absorbed by the container. Most of the energy was absorbed by the container as seen by the end of the analysis. The total energy absorbed by the panel shown in Figure 9.14 is lower than the one found with the force-deformation curve in 9.13. The reason may be the interaction effect. As assumed, the panel will absorb less energy than predicted since it is found to be stronger.

For comparing the quasi-static and dynamic analyses with both deformable, the different % of plastic dissipation energy is given below.

Table 9.16: Plastic dissipation energies for quasi-static and dynamic analysis - Impact scenario 7 [51].

Analysis	Impact velocity	ALLPD container	ALLPD panel
Quasi-static	2m/s constant	77.1%	22.9%
Dynamic	20m/s	56.4%	43.6%

The results show a significant difference in the energy absorption between the two different methods. In the quasi-static analysis all dynamic effects are neglected and the container is forced down in the y-direction, neglecting all deformation due to motion in other directions.

The container is able to absorb more of the energy in the quasi-static analysis. In the dynamic analysis, the container was falling down resulting in a larger contact area and hence more energy absorption in the panel. Since the container is forced down with a constant velocity of 2 m/s, the initial kinetic energy for the quasi-static energy is only 1/100 compared to the initial kinetic energy for the dynamic analysis.

9.5 Sensitivity study

To ensure that the analyses were performed as accurately as possible, a sensitivity study is important. The different analyses were performed for impact scenario 7 - bottom edge on the plate between two stiffeners. The effect of changing BC was also performed for impact scenario 4 - whole front first.

9.5.1 Boundary condition

The panel was modelled with fixed BCs as described in Section 7.6. The effect of using pinned BCs, where the panel was fixed for all translational degrees but not for the rotational degrees, was investigated. A pinned BC was applied to both impact scenarios 4 and 7, and compared to the ones with fixed BC. The results are presented in the table and figures below.

Table 9.17: Plastic dissipation energy for container with changed BC [51].

Impact scenario	Total ALLPD, fixed BC [MJ]	Total ALLPD, pinned BC [MJ]
4	3.65494	3.65953
7	3.34557	3.41048

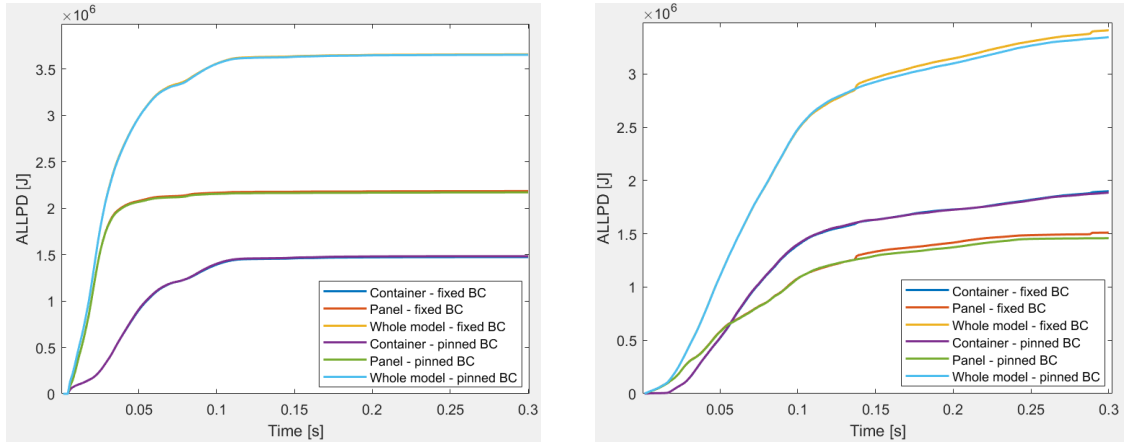


Figure 9.15: ALLPD for fixed and pinned BC for impact scenario 4 to the left and 7 to the right [51].

The effect of choosing between pinned or fixed BCs had negligible or no effect on the plastic energy absorption for both scenarios. For impact scenario 7, there was a slight increase in the energy absorption by the panel for the fixed BC, but the difference is negligible. The assumption of using fixed BCs was hence assumed to give sufficient results.

9.5.2 Friction

In Abaqus, a friction coefficient was included by the penalty friction formulation in the interaction properties as described by Section 7.5.4. For all the analyses a friction coefficient of 0.2 was used. To see the effect of friction, a parametric study was conducted using the friction coefficients 0, 0.2 and 0.4. It was assumed conservative to neglect the friction, but will result in an unreal response. The difference in energy dissipation due to friction and plastic dissipation energy of container is given in Table 9.18.

Table 9.18: Energy dissipation due to friction, ALLFD [51].

Friction coefficient [-]	Frictional dissipation energy [MJ]	% ALLPD container
0.0	-	66.7%
0.2	0.480981	56.4%
0.4	0.692876	54.8%

The graphs for the total different frictional dissipation energy and total dissipated energy for the model are given in Figure 9.16.

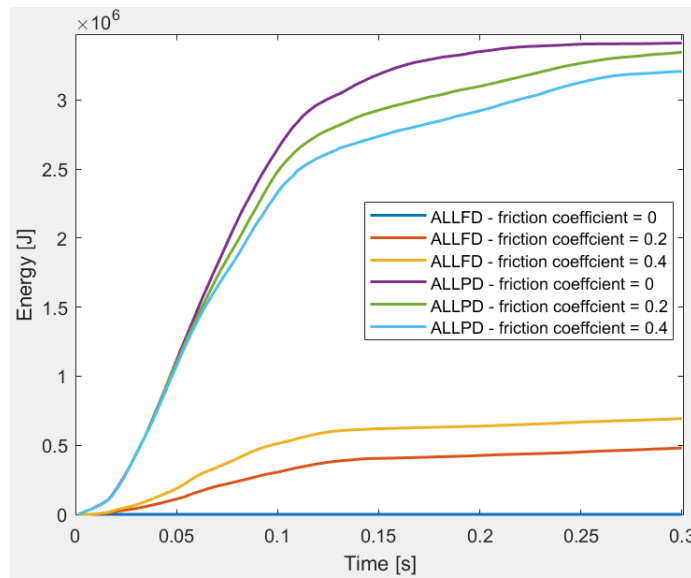


Figure 9.16: ALLFD and ALLPD for different friction coefficients [51].

The amount of energy dissipated due to friction increased with an increased friction coefficient. When the friction coefficient was set to zero there will be no frictional dissipation energy. It will be conservative to neglect friction since no energy dissipated due to friction will increase the energy to be dissipated by the container and the panel. This is seen by Figure 9.16 where the plastic dissipation energy decreased for increased friction coefficient. Hence a frictional coefficient of 0.2 was assumed realistic, and more on the conservative side than increasing the coefficient further.

9.5.3 Mass of container

The effect of changing the mass of the container was performed and the different analyses are summed up in the table below. Changing the mass will hence change the kinetic energy. The impact velocity of 20 m/s remained unchanged.

Table 9.19: Values for change in impact mass [51].

Mass of container [Te]	% ALLPD container	% ALLPD of kinetic energy
20	56.4%	83.6%
15	58.0%	83.9%
10	63.1%	78.4%
5	57.8%	72.2%

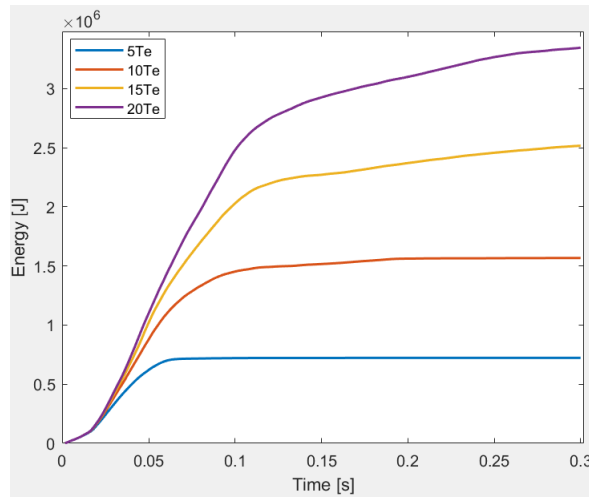


Figure 9.17: Total plastic dissipation energy for different impact mass [51].

The % of the total plastic dissipation compared with the initial kinetic energy was somewhat affected by the impact mass. It was an increase in the total energy absorption due to increasing impact mass. The total ALLPD of kinetic energy seemed to converge towards a higher impact mass. The amount the container was able to absorb was quite unaffected by the impact mass. The result from impact mass 10Te was somewhat different from the others, but was disregarded due to the other results. The differences were anyhow so small, that it was assumed negligible.

9.5.4 Impact Velocity

Due to simplicity, the container was placed right above the panel with an initial velocity. Meaning changing the initial velocity will change the drop height of the container and hence change the kinetic energy. All previous analyses were done with an initial velocity of 20 m/s. The effect of impact velocity was investigated while the mass of the container of 20Te remained unchanged.

Table 9.20: Values for change in impact velocity.

Impact velocity [m/s]	Corresponding drop height [m]	Kinetic energy [MJ]
20	20.4	4.00
15	11.5	2.25
10	5.1	1.00
5	1.3	0.25

Table 9.21: Values for change in impact velocity [51].

Impact velocity [m/s]	% ALLPD container	% ALLPD of kinetic energy
20	56.4%	83.6%
15	60.8%	83.5%
10	62.4%	81.8%
5	25.0%	85.7%

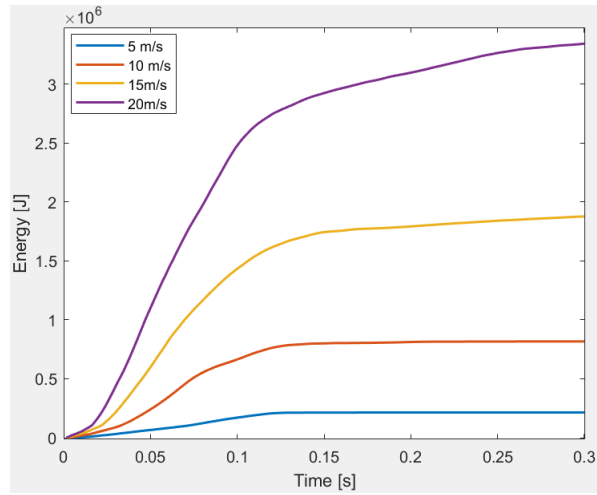


Figure 9.18: Total plastic dissipation energy for different impact velocities [51].

The % ALLPD of kinetic energy in the model was assumed to be unaffected by the change in impact velocity, due to the small differences in ALLPD. Since the kinetic energy is not increased with the same amount as for the impact mass, Figure 9.18 shows an increase of the difference in ALLPD from one to another. The increase in impact mass gives that the energy absorption was increased the same for the different masses. This corresponds to $E_{kin} = 1/2mv^2$.

Further, the amount of ALLPD for the container seemed to be very affected when the velocity of the container gets low. The initial kinetic energy is then only 0.25MJ and the panel absorbed a large amount of the energy. The low amount of energy absorbed by the container for the 5m/s impact velocity corresponds well to the force-deformation curve in Figure 9.13. When the impact energy is very low, the panel will absorb most of the energy. As discussed, this will change when the impact energy becomes higher. An impact velocity of 20m/s was assumed sufficient to represent the structural response. Hence choosing 5m/s corresponding to a drop height of 1.3m will give a wrong representation of the energy absorption, since the drop height is mostly much higher.

10 Structural response using hand calculations

A comparison with hand calculations is important to quality check the results from the numerical model. The response of the deck may be assessed using hand calculations based on plastic theory. The stiffener is assumed clamped between the two transverse girders with a stiffener span of $L = 6.135m$. Due to simplicity, the container is assumed to fall right between the two girders, meaning the hinge positions are known. Then the container may be simplified as a point mass, as shown in Figure 4.3. The cross-sectional values of the stiffener and important parameters are presented again in Table 10.1 due to get an overview.

Table 10.1: Cross-sectional values and other parameters used for hand calculations.

Part	Symbol	Value
Stiffener spacing	s	640mm
Transverse girder spacing/Stiffener span	L	6135mm
Stiffener web height	$h_{w,s}$	300mm
Stiffener flange width	$b_{f,s}$	200mm
Plate thickness	t	10mm
Stiffener web thickness	$t_{w,s}$	11mm
Stiffener flange thickness	$t_{f,s}$	17mm
Elastic modulus	E	210000Mpa
Mass of container	m	20000kg
Yield stress	f_y	346.9MPa
Velocity of container	v	20m/s
Resulting drop height of container	h	20.39m
Gravity	g	9.81m/s ²
Length of impact zone of container	d	2428mm

The yield stress is chosen from Table 7.3. The panel is only S355 steel, but the thickness is both above and below 16mm. Therefore the lowest yield stress σ_{yield} between the two different S355 steels are used to be conservative.

10.1 Plastic theory using yield hinges

Neglecting friction and other parameters, all the energy is preserved, meaning the kinetic energy must be equal to the absorbed energy. The kinetic energy is given by Equation 1 and the absorbed energy of the stiffener(s) is given by Equation 22. The resulting relationships assuming clamped beam are given below.

$$E_{kin} = 4\theta M_p = 4 \tan^{-1} \left(\frac{2w}{L} \right) M_p \quad (55)$$

where M_p is the plastic moment capacity and θ is expressed by geometry as shown in Figure 4.3. Further, using that $E_{kin} = \frac{1}{2}mv^2$ the resulting deformation may be found by Equation 56.

$$w = \frac{\tan \left(\frac{E_{kin}}{4M_p} \right) \cdot L}{2} \quad (56)$$

The calculation is chosen for impact scenario 4 - falling with the whole front first across several stiffeners. The calculations may be compared to the results from Abaqus. Impact scenario 4 is

chosen since it falls at the middle of the stiffener span for all the stiffeners and falls with an impact angle of 90 degrees relative to the panel. The comparison with hand calculations will hence be easier than using some of the other impact scenarios, such that the energy dissipated by rotation of the container may be neglected.

Since the analysis is done with a deformable container and the plastic theory with point masses doesn't take that into account, the mass of the container is reduced such that the kinetic energy absorbed by the container is neglected. As given by Table 9.2, 40.59% of the energy is absorbed by the container, which reduces the total kinetic energy to 2.38MJ and a mass of 11882kg which is used in the hand calculations. Since the container is falling across several stiffeners, the kinetic energy is divided by the total number of stiffeners affected. This number is found by dividing the total length of the impact zone of the container, d , which is the width of the container by the stiffener spacing. This gives $n = d/s = 2428/640 = 3.79$ and rounding up affects four stiffeners. The kinetic energy for one stiffener is then $2.38\text{MJ}/4 = 0.594\text{MJ}$.

The plastic moment capacity is found as the plastic section modulus multiplied by the yield stress. As described in Section 4 the plastic neutral axis is the axis that divides the stiffener into two equal parts. The plastic section modulus is a calculation based on the plastic neutral axis. To find the plastic neutral axis the effective plate width must be calculated as described in Appendix G.1. Using the effective plate width may be discussed, since this is the width corresponding to buckling of stiffened panels. It could have been more accurate to use the reduced plate flange since this corresponds to a stiffener in bending. It will anyhow most likely lead to small differences. The exact calculation of the plastic moment capacity using plastic section modulus, plastic neutral axis and effective plate width is attached in Appendix G. The total deformation using plastic theory is then given by the equation below.

$$w = \frac{\tan\left(\frac{5.94 \cdot 10^5 \text{Nm}}{4 \cdot 5.39 \cdot 10^5 \text{Nm}}\right) \cdot 6.135 \text{m}}{2} = 867.87 \text{mm}$$

10.2 Including membrane effects

Using plastic theory with work considerations using yield hinges may give conservative and unrealistic results since the membrane effects are neglected. When including for the membrane effects the stiffener should be able to absorb more energy at lower deformation than before, which gives us a better capacity of the panel given that the stiffeners will be able to develop membrane stresses before the fracture criterion is reached.

The calculation for total deformation is found using the formulas from *DNV-RP-C204* presented in Section 3.2.3. The curve for $R(w)$, collapse resistance as a function of deformation can be integrated to give the total energy. Then the deformation is found by assuming this area under the curve is equal to the kinetic energy that needs to be absorbed by the stiffener. The calculations are summed below and are assumed so generally that the calculations are not attached.

Table 10.2: Important parameters used for membrane effects.

Part	Symbol	Value	dimension
Plate area	A_p	3931.51	mm ²
Stiffener web area	A_w	3300.00	mm ²
Stiffener flange area	A_f	3400.00	mm ²
Stiffener area	A_s	6700.00	mm ²
Total area, stiffener and whole plate flange	A	13100.00	mm ²
Plastic section modulus	W_p	$1.55 \cdot 10^6$	mm ³
Factor separating clamped and pinned	c_1	2	-

The resulting calculations using the equations presented in Section 3.2.3 are given below.

$$w_c = \frac{1.2W_p}{A} = \frac{1.2 \cdot 1.55 \cdot 10^6}{13100} = 142.33mm$$

$$R_0 = \frac{8c_1f_yW_p}{L} = \frac{8 \cdot 2 \cdot 346.9 \cdot 1.55 \cdot 10^6}{6135} = 1.41 \cdot 10^6 N$$

$$n^* = \frac{A_p - A_s}{A_p + A_s} = \frac{3931.51 - 6700}{3931.51 + 6700} = -0.26$$

$$a_2 = \frac{1}{2} \left(\frac{A_p}{A_s} + 1 \right) \left(\frac{A_f}{A_w} + 1 \right) = \frac{1}{2} \left(\frac{3931.51}{6700} + 1 \right) \left(\frac{3400}{3300} + 1 \right) = 1.61$$

$$a_1 = \frac{0.9}{a_2} \left(1 + \frac{2A_f}{A_w} \right) = \frac{0.9}{1.61} \left(1 + \frac{2 \cdot 3400}{3300} \right) = 1.71$$

The equivalent elastic, axial stiffness k is found using Equation 8. K_{node} is the axial stiffness of the node with the considered member removed, where it is assumed infinite for a noncontinuous plate field and assumed EA/L for a continuous plate field. Assuming a continuous plate field, k and c are found by the equations below. Abaqus probably corresponds to a place between noncontinuous and continuous plate, but the impact zone on the panel is quite far away from the applied fixed BCs. Abaqus is hence assumed to be more approximate to a continuous plate field. In addition, using a continuous plate field will result in a larger total deformation, and the assumption of using a continuous plate field is therefore conservative.

$$k = \left(\frac{1}{\frac{EA}{L}} + \frac{L}{2EA} \right)^{-1} = \left(\frac{1}{\frac{210000 \cdot 13100}{6135}} + \frac{6135}{2 \cdot 210000 \cdot 13100} \right)^{-1} = 2.99 \cdot 10^5 N/mm$$

$$c = \frac{4c_1kw_c^2}{f_yAL} = \frac{4 \cdot 2 \cdot 2.99 \cdot 10^5 \cdot 142.33^2}{346.9 \cdot 13100 \cdot 6135} = 1.74$$

$\bar{w}^* = \bar{w}$ that gives $n_1(\bar{w}) = n^*$ where $\bar{w} = w/c_1w_c$. Since the deformation w is the unknown and the one to be found, the rest of the calculations is used with excel using deformation from 0mm to 1000mm with a step of 0.1mm, resulting in a column with 10000 values. Using the formula for \bar{w} for each deformation, resulting in also 10000 values and so on. Then n_1 and n_2 was found for each \bar{w} .

The formulas used from *DNV-RP-C204* assume that the plastic neutral axis is in the plate flange, which is often the case. In other words, the plate area A_p is assumed larger than the stiffener area A_s . Further, this is not the case for this panel. It can be discussed whether the stiffener spacing probably is somewhat low compared to what's most common or the stiffener is larger than normal. When $A_p < A_s$, n^* will be negative and the formulas is invalid. To be able to use the formulas a change has to be made. The excel sheet was used to see the effect on the total deformation with changing different values. The effective plate width and plate thickness were changed such that the plate area was just a little larger than the stiffener area, resulting in a total deformation of 363.8mm. Changing only A_p in the formulas for a_2 and n^* and not calculating the plastic neutral axis again, resulted in a total deformation of 368.4mm. Lastly, only the factor n^* was set to 0.0001 to be close to zero, resulting in a total deformation of 370.1mm. The conclusion is that the different changes will result in very small differences, and changing n^* is chosen to be the most conservative and will not influence the formulas where the area of the plate is used. The calculation to find the total deformation is further shown.

\bar{w}^* is found such that $n_1(\bar{w}^*) = n^* = 0.0001$, resulting in $\bar{w}^* = 0.01$. The transition factor, C_t is hence found by the equation below.

$$C_t = (1 - a_2 \cdot c \cdot \bar{w}^*)e^{a_2 \cdot c \cdot \bar{w}^*} = (1 - 1.61 \cdot 5.21 \cdot 0.01)e^{1.61 \cdot 5.21 \cdot 0.01} = 1.00$$

As described above, \bar{w} , n_1 , n_2 , r_1 , r_2 and R/R_0 is found for each deformation w , resulting in a column of 10000 elements for each of the variables. The resulting resistance R is then found by multiplying every R/R_0 with the constant value for R_0 . The curve for the resistance R against deformation w is integrated and the total deformation is found where the area under the resistance-deformation curve is equal to the kinetic energy that must be absorbed by one of the stiffeners. As described with using the plastic theory, one of the stiffeners must absorb a kinetic energy of $5.94 \cdot 10^5 \text{Nm}$. The resulted deformation is hence 370.1mm when including the membrane effects.

10.3 Tensile fracture in yield hinges

The deformation to rupture due to tensile fracture in yield hinges was found using the equations presented in Section 3.2.5. The non-dimensional plastic stiffness H and the critical strain ε_{cr} is taken from Table 3.2 using that the steel grade is S355. The yield strain is taken as the yield stress divided by the elastic modulus. The calculation of the elastic section modulus is attached in Appendix G.

The plastic zone length factor and displacement factor, respectively c_{lp} and c_w is found below,

$$c_{lp} = \frac{\left(\frac{\varepsilon_{cr}}{\varepsilon_y} - 1\right) \frac{W}{W_p} H}{\left(\frac{\varepsilon_{cr}}{\varepsilon_y} - 1\right) \frac{W}{W_p} H + 1} = \frac{\left(\frac{0.15}{0.0017} - 1\right) \cdot \frac{1.33 \cdot 10^6}{1.55 \cdot 10^6} \cdot 0.0034}{\left(\frac{0.15}{0.0017} - 1\right) \cdot \frac{1.33 \cdot 10^6}{1.55 \cdot 10^6} \cdot 0.0034 + 1} = 0.21$$

$$c_w = \frac{1}{c_1} \left[c_{lp} \left(1 - \frac{1}{3} c_{lp}\right) + 4 \left(1 - \frac{W}{W_p}\right) \frac{\varepsilon_y}{\varepsilon_{cr}} \right] \left(\frac{kl}{d_c}\right)^2$$

$$= \frac{1}{2} \left[0.21 \left(1 - \frac{1}{3} 0.21\right) + 4 \left(1 - \frac{1.33 \cdot 10^6}{1.55 \cdot 10^6}\right) \frac{0.0017}{0.15} \right] \left(\frac{3067.5}{600}\right)^2 = 2.61$$

where kl is half the stiffener span since the container is assumed to fall in the middle of the girders. The characteristic dimension d_c given from Section 3.2.4 is taken from two times the stiffener web

height. The axial flexibility factor is given by Equation 7.

$$c_f = \left(\frac{\sqrt{c}}{1 + \sqrt{c}} \right)^2 = \left(\frac{\sqrt{1.74}}{1 + \sqrt{1.74}} \right)^2 = 0.32$$

The deformation before rupture is found below.

$$w = d_c \cdot \frac{c_1}{2c_f} \left(\sqrt{1 + \frac{4c_w c_f \varepsilon_{cr}}{c_1}} - 1 \right) = 600 \cdot \frac{2}{2 \cdot 0.32} \left(\sqrt{1 + \frac{4 \cdot 2.61 \cdot 0.32 \cdot 0.15}{2}} - 1 \right)$$

$$= 221.31 \text{ mm}$$

10.4 Comparison with result from nonlinear finite element analysis

The analysis for impact scenario 4 from Abaqus was compared with the results from the hand calculations. The deformation was taken from the top of the stiffener web in the middle of the two transverse girders as shown in the figures below. The chosen stiffener was the stiffener in the middle of the impact zone, assuming this was the stiffener with the largest deformation.

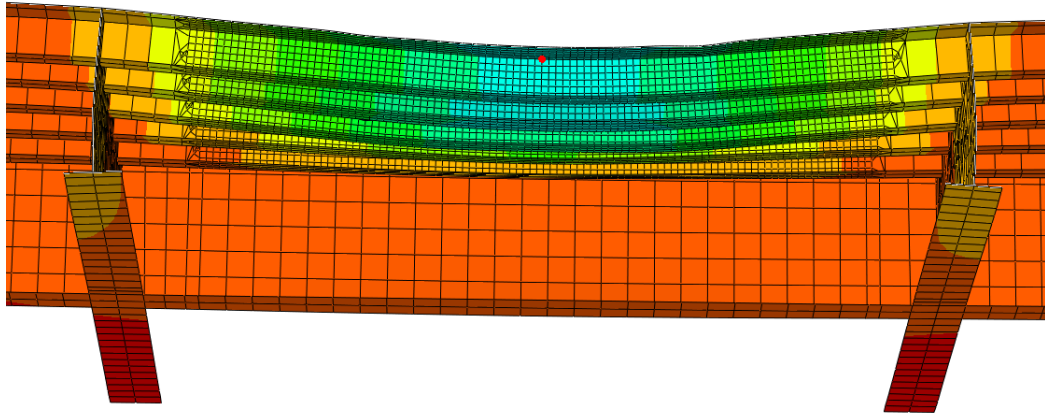


Figure 10.1: Deformation point on top of stiffener web [51].

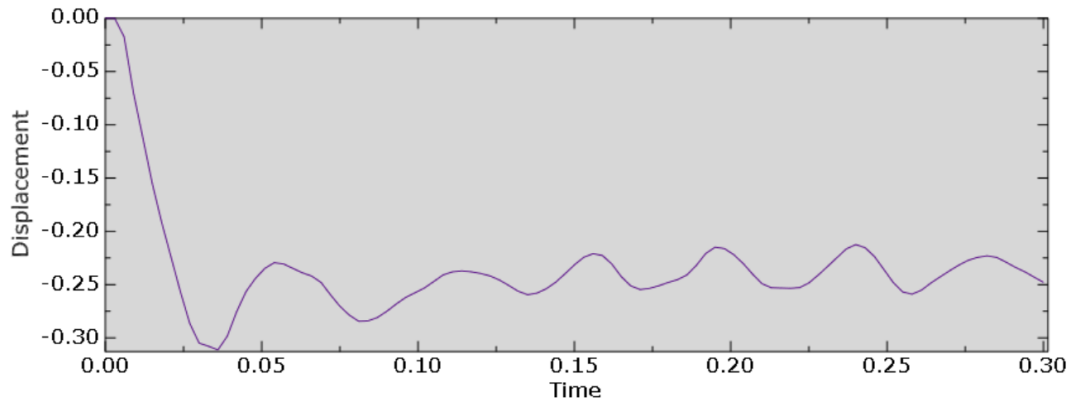


Figure 10.2: Deformation of stiffener for impact scenario 4[51].

From the graph above, the maximum displacement of the stiffener was found to be 311.23mm after 0.036 seconds, before the container starts to bounce. The total deformation in the middle of the stiffener span from Abaqus and hand calculations is summed up in Table 10.3.

Table 10.3: Total deformation in the middle of the stiffener span.

Type	Total deformation [mm]
Nonlinear finite element analysis	311.23
Plastic theory using yield hinges	867.87
Including membrane effects	370.10

The results are quite interesting. As assumed the plastic theory using yield hinges will result in very conservative results. The membrane effects are shown to have a very significant effect. Using plastic theory without membrane effects will hence significantly underestimate the strength of the panel. The calculation including membrane effects is of course much more time consuming. On the other hand, only using the plastic theory with yield hinges will result in a very unreal response of the stiffener.

The result from using the formulas from *DNV-RP-C204* corresponds quite well with the result from the finite element analysis in Abaqus. It is as assumed that the deformation using hand calculations will be somewhat higher, since it will of course not be able to include all the effects that the finite element analysis will and hence Abaqus will give a lower deformation. Among other things, the hand calculation will not take into account energy dissipated to friction. The formulas will be somewhat conservative, but the difference is small and the result matches well.

The deformation to rupture due to tensile fracture in yield hinges was found to be 221.31mm. As seen by the equations, the deformation is independent of the impact scenario. Deformation to rupture was more complex to compare with results from the nonlinear finite element analysis in Abaqus due to the assumption of where rupture is. Rupture was here assumed when all the elements in the stiffener were gone due to element deletion, preferably at the expected place corresponding to hinge location. This will correspond to fracture in yield hinges. Since the deformation was independent of the impact scenario, impact scenario 6 - falling with one edge on stiffener first, was compared due to simplicity.

The deformation at the middle node in the stiffener flange, where the hinge location is assumed is plotted below.

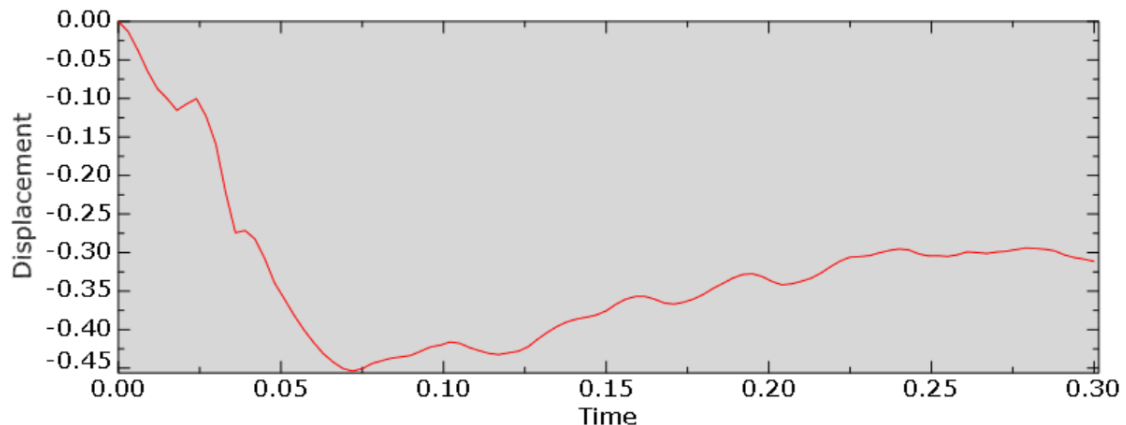


Figure 10.3: Deformation of stiffener for impact scenario 6 [51].

Compared with the deformation at every increment in Abaqus, the deformation to rupture will be between 0.030s and 0.033s. The deformation at the two times is shown below.

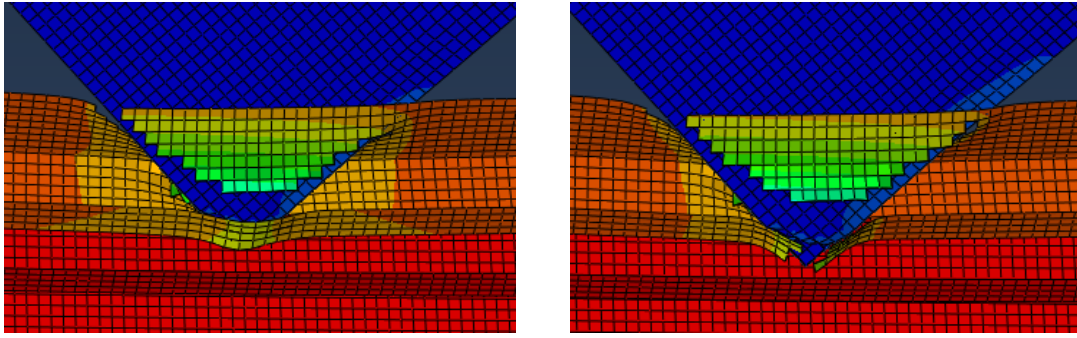


Figure 10.4: Deformation to rupture of stiffener from Abaqus[51].

The deformation for the two times compared with deformation calculated from *DNV-RP-C204* is shown in Table 10.4 below.

Table 10.4: Total deformations.

Type	Total deformation [mm]
Using <i>DNV-RP-C204</i>	221.31
Using Abaqus at t=0.03s	159.53
Using Abaqus at t=0.033s	222.16

The deformation at t=0.033s corresponds very well with the deformation to rupture using the formulas in *DNV-RP-C204* and is hence assumed sufficient. It may be assumed that the deformation to rupture is right before t=0.033s in Abaqus.

11 Conclusion

The structural response of a stiffened panel due to impact from dropped objects has been assessed by using the non-linear finite element software Abaqus/Explicit. Most of the analyses have been performed dynamic where both the container and deck are deformable. The emphasis has been on the distribution of energy absorption between the container and the stiffened panel. Different impact scenarios were performed and showed large differences dependent on the impact angle and impact location on the panel. The final indentation of deck was established where the worst case was falling with the bottom horizontal beam first with 45 degrees. Using a rigid container and neglecting the amount of energy the container is able to absorb have been found to be very conservative. On the other hand, the dynamic analyses with both deck and container deformable are quite complex resulting in difficulties to obtain all desirable results.

A parametric study of the panel by changing the stiffener size, girder size, plate thickness, stiffener spacing and girder spacing have been conducted, where the emphasis has been to increase the amount of energy absorbed by the container. The change in stiffener size, girders size, plate thickness, stiffener spacing and girder spacing was in general most advantageous for the container falling with the bottom edge first between two stiffeners. In other words, the increase of the energy absorbed by the container was in general largest for the container falling with the bottom edge first. How the container would fall is difficult to predict and a choice based on probability must be made. The impact scenario will most likely be a combination of all the scenarios. Comparing the average increase in the energy absorption in the container between the three impact scenarios, the change in the stiffener web thickness was found to be most advantageous. Meaning the largest average increase in energy absorption by the container was for increased stiffener web thickness.

The results from the finite element analyses showed that both the final indentation of deck and the impact area of the container are important to study. Higher energy absorption in the container will not directly give lower damage in the panel. Container falling with whole front first gave the lowest amount of energy absorbed by the container, but also little damage of the panel since the large impact area on the container results in an energy distribution over a larger area. The final indentation of deck did not correspond to the energy absorbed by the container. It was found to be more dependent on how much the stiffeners were able to prevent further penetration of the strong bottom rails on the container. Initially, it was desirable to obtain most of the damage in the container and hence most energy absorbed by the container. Further, the most desirable is to obtain a high plastic dissipation before the container penetrates the deck, independent on where the energy is absorbed. Hence, the amount of plastic dissipation energy before penetrating the deck could be a useful measure of total damage for further analyses.

At the beginning of the master's thesis, the most critical scenario was assumed fall with one edge between two stiffeners. The energy is then dissipated over a small area in the panel and the edge of the container is sharp. The non-linear finite element analyses showed different results. Container falling with one edge on the stiffener were found to be worse since the stiffeners were able to penetrate further indentation of the container when falling between them. When falling directly on the stiffener, the container cuts through the stiffener.

The deformation of the stiffeners has been compared with relevant theory and tripping of the stiffeners was shown. Hand calculations using plastic theory with yield hinges significantly underestimated the strength of the panel. The effect of membrane effects was found to be large and corresponded well with the results from the finite element analysis. Further, the deformation to rupture using formulas from *DNV-RP-C208* also corresponded well to the results from Abaqus.

12 Further work and improvements

Throughout the process, several tasks have been neglected or assumptions have been made due to limited time. There is on the other hand room for improvements. Below are some further work presented.

- The unnatural result from the mesh size sensitivity for the rigid deck with 25mm fine mesh should be looked more into. It would have been desirable to use a finer mesh, but was disregarded due to the odd result.
- For some of the analyses, the artificial strain energy is somewhat too high. The results are still assumed sufficient enough, but it should be lower to obtain more accurate results. The artificial strain energy should be lower for a finer mesh, and may also be better if the reason for the odd 25mm fine mesh was found.
- The given assignment tasks included impact simulations of other dropped objects if the time permits. Due to many unforeseen challenges, this task was skipped. Other dropped objects could for example be a swivel in a lifting frame.
- For the hand calculations, the resistance curve for plates and corresponding total deformation could also be calculated based on Equation 28, which is also equivalent to Equation 5. Only the resistance when assuming falling directly on stiffeners was discussed. Further, the deformation to rupture due to tensile fracture in yield hinges was performed, but the calculation for local buckling could also be included.
- The formulas for the force-deformation curve from *DNV-RP-C204* assumes that $h_{ws}/t_{ws} < 20$ and that $A_p > A_s$ which is not the case in the calculations and some assumptions has been made. The effects of still using the formulas should be performed. In addition, the effective plate width was used for calculation of the plastic moment. It may be more accurate to use the reduced plate flange corresponding to stiffeners in bending. The effect of using effective plate width for the hand calculations should be performed.
- For this master's thesis, the effect of strain rate has only been discussed and not included in the nonlinear finite element analysis, due to the complicated model. The effect of strain rate could be made for further work.
- To validate the results from the nonlinear finite element analysis more than using hand calculations, several drop tests could be performed.
- The impact scenarios are chosen based on the assumed worst case scenario. Further work could be assessing the structural response also when falling on a girder and with the whole bottom of the container first. In addition, the energy absorption relationship could be established based on lower impact masses.
- The effect of using different fracture criteria could be performed. For example looking into the different results by using the Johnson-Cook and Cockcroft-Latham criterion.
- It could be interesting to see the effect on the structural resistance by changing the material in the panel, either another steel type or another material.
- It could be informative to perform analysis with emphasis on different equipment inside the container and allowing the equipment to move inside the container. This will be an advanced analysis, but hence more realistic.

-
- Since the critical equipment around laydown areas should be protected for dropped objects, it could be interesting to see the effect of impact protection. To see if the impact protection is strong enough to resist the container from penetrating the deck.

Bibliography

- [1] Dassault Systemes Simulia 6.14. *24.2.3 Damage evolution and element removal for ductile metals*. URL: <http://130.149.89.49:2080/v6.14/books/usb/default.htm>. (accessed: 15.04.2022).
- [2] Dassault Systemes Simulia 6.5. *11.6.2 Damage initiation*. URL: <https://classes.engineering.wustl.edu/2009/spring/mase5513/abaqus/docs/v6.5/books/usb/default.htm?startat=pt04ch11s06abm38.html#usb-mat-cdamageinit>. (accessed: 15.04.2022).
- [3] Dassault Systemes Simulia 6.5. *Damage evolution*. URL: <https://classes.engineering.wustl.edu/2009/spring/mase5513/abaqus/docs/v6.5/books/key/default.htm?startat=ch04abk02.html#usb-kws-mdamageevolution>. (accessed: 15.04.2022).
- [4] Jørgen Amdahl. *Buckling and Ultimate Strength of Marine Structures, Chapter 1: Elastic-Plastic Analyses of Beams, Frames and Plates*. Lecture notes from TMR4205 Buckling and Ultimate Strength of Marine Structures. 2005.
- [5] Jørgen Amdahl. *Buckling and Ultimate Strength of Marine Structures, Chapter 3: Buckling of stiffened plates*. Lecture notes from TMR4205 Buckling and Ultimate Strength of Marine Structures. 2013.
- [6] Jørgen Amdahl. *Buckling and Ultimate Strength of Marine Structures, Chapter 7: Plastic Methods of Analysis*. Lecture notes from TMR4205 Buckling and Ultimate Strength of Marine Structures. 2010.
- [7] Jørgen Amdahl. *Energy absorption in ship-platform impacts*. Norwegian University of Science and Technology, Trondheim, 1983. Chap. 4.8.3.
- [8] Jørgen Amdahl. *Response of structures exposed to explosion*. NTNU, Department of Marine Technology. 2005.
- [9] Jørgen Amdahl and Zhaolong Yu. *Design against ship collisions with the new DNV-RP-C204*. unpublished. Personal communication. May. 3, 2022.
- [10] Andreas Bergstad. *Assessment of Hull Response due to Impact from falling object*. Master's thesis. Norwegian University of Science and Technology, Trondheim. NTNU Open. 2014.
- [11] Bernt Johan Leira - Professor at Department of Marine Tecnology. *Personal communication*. unpublished. Sept. 29, 2021.
- [12] Jørgen Amdahl - Professor at Department of Marine Tecnology. *Personal communication*. unpublished. Oct. 28, 2021.
- [13] Jørgen Lima Hansen. *Analysis and Design of Ship Collision Barriers on a Submerged Floating Tunnel subjected to Large Ship Collisions*. Master's thesis. Norwegian University of Science and Technology, Trondheim. NTNU Open. 2015.
- [14] Odd Sture Hopperstad and Tore Børvik. *Modelling of plasticity and failure with explicit finite element methods*. Lecture notes from TKT4128 Støtmekanikk. 2021. Chap. 3, 5 and 6.
- [15] Sintef Materials and Chemistry. *Structural impact on offshore structures*. 2006. URL: https://www.sintef.no/globalassets/upload/materialer_kjemi/anvendt-mekanikk-og-korrosjon/faktaark/structural-impact-web.pdf. (accessed: 10.03.2022).
- [16] MathWorks. *MATLAB R2019a*. URL: <https://www.mathworks.com/products/matlab.html>. (accessed: 13.01.2022).
- [17] Torgeir Moan. *Accidental limit state criteria and accidental loads*. Lecture notes from TMR4195 Havkonstruksjoner. 2000. Chap. 2 and 6.
- [18] Torgeir Moan. *Chapter 12: Nonlinear analysis*. Lecture notes from TMR4305 Statisk og dynamisk analyse av marine konstruksjoner. Chap. 12.1.1, 12.6.3 and 12.7.3.

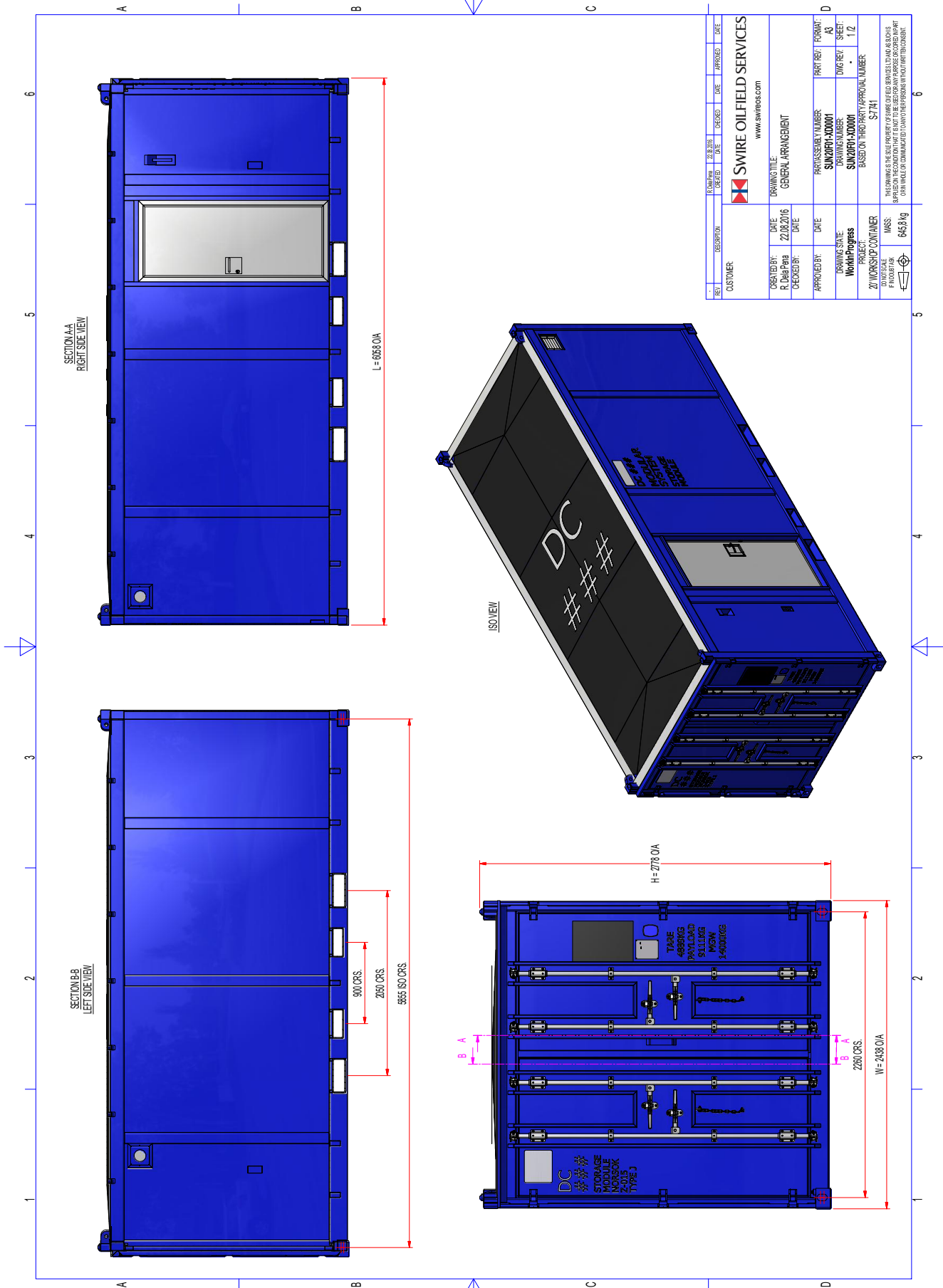
-
- [19] Woongshik Nam, Odd Sture Hopperstad and Jørgen Amdahl. *Modelling of the ductile-brittle fracture transition in steel structures with large shell elements: A numerical study*. Norwegian University of Science and Technology, Trondheim. NTNU Open. 2018.
- [20] Ingve Nilsen. *Dropped object protection analyses*. Master's thesis. University of Stavanger. UiS Brage. 2014.
- [21] Nowatec. *Dropped Objects*. URL: https://nowatec.no/?page_id=113. (accessed: 13.04.2022).
- [22] OEG Offshore. *DNV 2.7-1 Offshore Container Fleet*. URL: <https://www.oegoffshore.com/uploads/files/OEGOffshoreContainerWallChartNORWAY2021.pdf>. (accessed: 13.01.2022).
- [23] Ozgur Ozguc. *The assessment of impact damage caused by dropped objects on floating offshore structures*. 2020. URL: <https://journals.sagepub.com/doi/pdf/10.1177/1475090220972586>. (accessed: 10.03.2022).
- [24] Pei Pei, Zhongcai Pei and Zhiyong Tang. *Numerical and Theoretical Analysis of the Inertia Effects and Interfacial Friction in SHPB Test Systems*. 2020. URL: <https://www.ncbi.nlm.nih.gov/pmc/articles/PMC7663437/>. (accessed: 13.04.2022).
- [25] Petroleumtilsynet. *Ptil gransker hendelse med fallende gjenstand på West Bollsta*. 2020. URL: <https://www.ptil.no/tilsyn/viktige-meldinger/2020/ptil-gransker-hendelse-med-fallende-gjenstand-pa-west-bollsta/>. (accessed: 23.02.2022).
- [26] Petroleumtilsynet. *Statoil - Gullfaks B - Gransking av hendelse med fallende Eagle rørhåndteringskran*. 2017. URL: <https://www.ptil.no/tilsyn/granskingsrapporter/2017/statoil-gullfaks-b-gransking-av-kranhendelse/>. (accessed: 23.02.2022).
- [27] Petroleumtilsynet. *Statoil - Heidrun - Gransking av hendelse med fallende gjenstand*. 2016. URL: <https://www.ptil.no/tilsyn/granskingsrapporter/2016/statoil---heidrun---gransking-av-hendelse-med-fallende-gjenstand/>. (accessed: 23.02.2022).
- [28] *Proceedings of the 20th International Ship and Offshore Structures Congress*. Committee v.1 Accidental limit states. Chap. 1.2.4.2, pp. 168. Belgium and Amsterdam: IOS Press BV, 2018.
- [29] Tjark Tilman Schwebe. *Dynamic Collapse of the Hull Girders in a Container Ship in Waves*. Master's thesis. Norwegian University of Science and Technology, Trondheim. NTNU Open. 2016.
- [30] Elisabeth Seglem. *Statfjord A-ulykken som ikke kunne skje*. 2012. URL: <https://www.aftenbladet.no/aenergi/i/Kly16/statfjord-a-ulykken-som-ikke-kunne-skje>. (accessed: 23.02.2022).
- [31] Swire Energy Services. *Offshore containers Overview*. URL: <https://swirees.com/offshore-containers/offshore-containers>. (accessed: 13.01.2022).
- [32] Swire Energy Services. *Rigging loft Overview*. URL: <https://swirees.com/offshore-containers/rigging-lofts-and-lifting-frames>. (accessed: 16.02.2022).
- [33] Dassault Systemes Simulia. *About general contact in Abaqus/Explicit*. URL: <https://abaqus-docs.mit.edu/2017/English/SIMACAEITNRefMap/simaitn-c-contactgeneral.htm>. (accessed: 15.04.2022).
- [34] Dassault Systemes Simulia. *About mechanical contact properties*. URL: <https://abaqus-docs.mit.edu/2017/English/SIMACAEITNRefMap/simaitn-c-contactmechanical.htm>. (accessed: 28.05.2022).
- [35] Dassault Systemes Simulia. *Defining a symmetry/antisymmetry/encastre boundary condition*. URL: <https://abaqus-docs.mit.edu/2017/English/SIMACAECAERefMap/simacae-t-lbibcEDITORSSYMMETRY.htm>. (accessed: 06.05.2022).
- [36] Dassault Systemes Simulia. *Defining rigid body constraints*. URL: <https://abaqus-docs.mit.edu/2017/English/SIMACAECAERefMap/simacae-t-itnhelptopicrigid.htm>. (accessed: 29.05.2022).

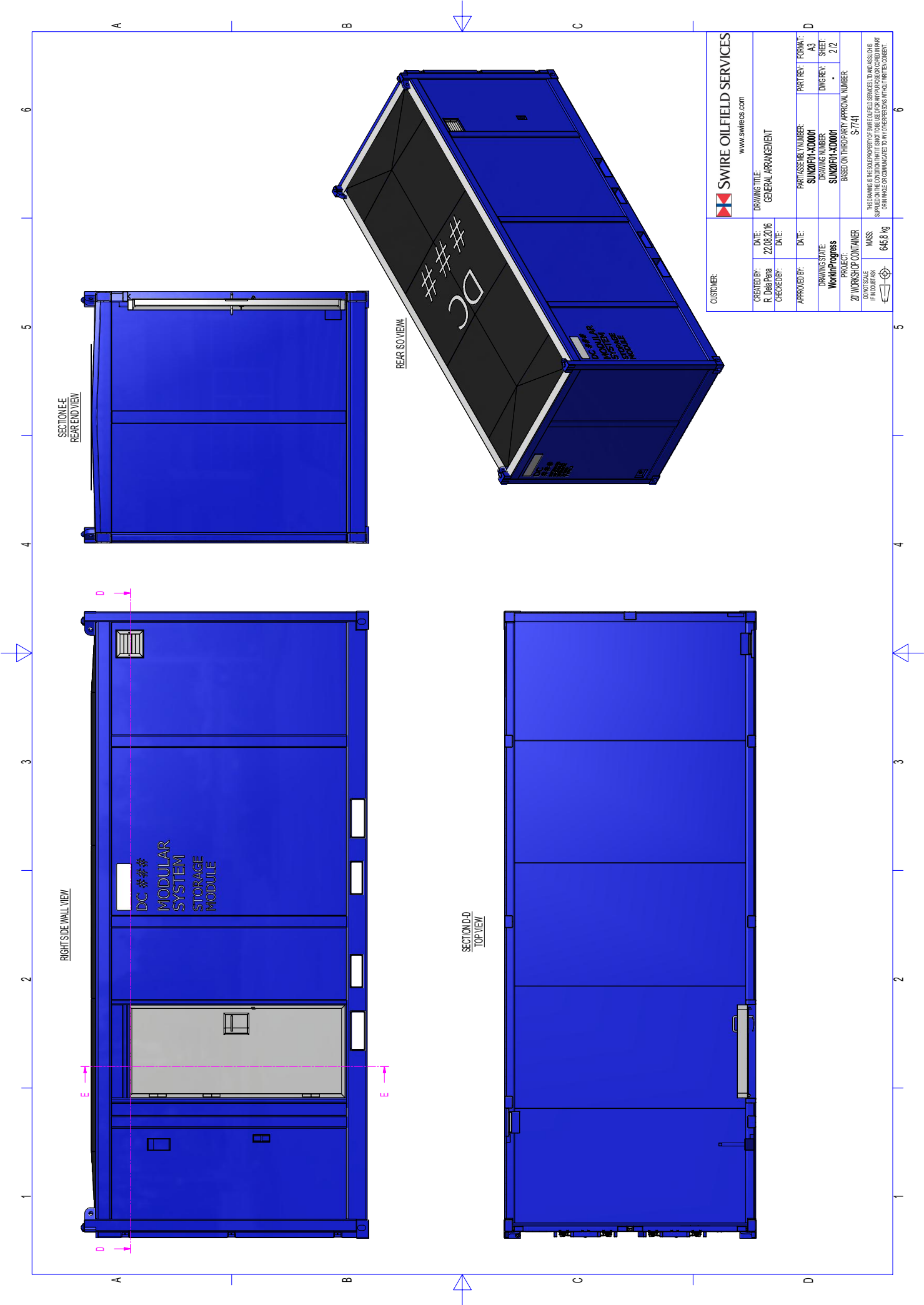
-
- [37] Dassault Systemes Simulia. *Energy balance*. URL: <https://classes.engineering.wustl.edu/2009/spring/mase5513/abaqus/docs/v6.6/books/gsx/default.htm?startat=ch03s07.html>. (accessed: 19.05.2022).
- [38] Dassault Systemes Simulia. *Explicit dynamic analysis*. URL: <https://abaqus-docs.mit.edu/2017/English/SIMACAEANLRefMap/simaanl-c-expdynamic.htm>. (accessed: 06.05.2022).
- [39] Dassault Systemes Simulia. *Nonstructural mass definition*. URL: <https://abaqus-docs.mit.edu/2017/English/SIMACAEMODRefMap/simamod-c-nonstructuralmass.htm>. (accessed: 08.05.2022).
- [40] Dassault Systemes Simulia. *Postprocessing*. URL: <https://abaqus-docs.mit.edu/2017/English/SIMACAEGSARefMap/simagsa-c-matblastpostprocessing.htm>. (accessed: 02.05.2022).
- [41] Dassault Systemes Simulia. *Rigid body definition*. URL: <https://abaqus-docs.mit.edu/2017/English/SIMACAEMODRefMap/simamod-c-rigidoverview.htm>. (accessed: 29.05.2022).
- [42] Dassault Systemes Simulia. *Three-dimensional conventional shell element library*. URL: <https://abaqus-docs.mit.edu/2017/English/SIMACAEELMRefMap/simaelm-r-shellgeneral.htm>. (accessed: 28.05.2022).
- [43] Dassault Systemes Simulia. *Total energy output*. URL: <https://abaqus-docs.mit.edu/2017/English/SIMACAEOUTRefMap/simaout-c-exp-totalenergyoutput.htm>. (accessed: 02.05.2022).
- [44] Dassault Systemes Simulia. *Understanding constraints*. URL: <https://abaqus-docs.mit.edu/2017/English/SIMACAECAERefMap/simacae-c-itnconstraint.htm>. (accessed: 21.05.2022).
- [45] Dassault Systemes Simulia. *Material damage and failure*. URL: <https://imechanica.org/files/19-damage-failure.pdf>. (accessed: 15.04.2022).
- [46] Anne Kathrine Vaagsnes Singelstad. *Non-linear analysis of a space frame subjected to loading from dropped objects*. Master's thesis. University of Stavanger. UiS Brage. 2009.
- [47] Dave Talloen - Sevan SSP. *Personal communication*. unpublished. Sept. 16, 2021.
- [48] Erling Fredriksen - Sevan SSP. *Personal communication*. unpublished. Sept. 14, 2021.
- [49] Torstein Alexander Pettersen - Sevan SSP. *Personal communication*. unpublished. Sept. 14, 2021.
- [50] Martin Storheim. *Structural Response in Ship-Platform and Ship-Ice Collisions*. Doctoral thesis. Norwegian University of Science and Technology, Trondheim. NTNU Open. 2016.
- [51] Dassault Systemes. *Dassault Systemes SIMULIA Abaqus CAE 2019*. URL: <https://www.3ds.com/products-services/simulia/products/abaqus/abaquscae/>. (accessed: 13.01.2022).
- [52] Rikard Tørnqvist. *Design of Crashworthy Ship Structures*. Doctoral thesis. Technical University of Denmark, Department of Mechanical Engineering. 2003.
- [53] Shengwen Tu et al. *Stress-strain curves of metallic materials and post-necking strain hardening characterization: A review*. 2019. URL: <https://sintef.brage.unit.no/sintef-xmlui/bitstream/handle/11250/2720965/Tu.pdf?sequence=4>. (accessed: 07.06.2022).
- [54] Det Norske Veritas. *DNV-OS-A101 Safety principles and arrangements*. Offshore standards. 2021.
- [55] Det Norske Veritas. *DNV-OS-C101 Design of offshore steel structures, general - LRFD method*. Offshore standards. 2021.
- [56] Det Norske Veritas. *DNV-RP-C201 Buckling Strength of Plated Structures*. Recommended Practice. 2010.
- [57] Det Norske Veritas. *DNV-RP-C204 Structural design against accidental loads*. Recommended Practice. 2021.

-
- [58] Det Norske Veritas. *DNV-RP-C208 Determination of structural capacity by non-linear element analysis methods*. Recommended Practice. 2021.
- [59] Cargostore Worldwide. *20ft Closed Top CCU*. URL: <https://cargostore.com/20ft-dnv-closed-top/>. (accessed: 19.01.2022).
- [60] Zhaolong Yu, Jørgen Amdahl and Yanyan Sha. *Large inelastic deformation resistance of stiffened panels subjected to lateral loading*. Marine Structures 59 pp. 342-365. ScienceDirect. Norwegian University of Science and Technology, 2018.

Appendix

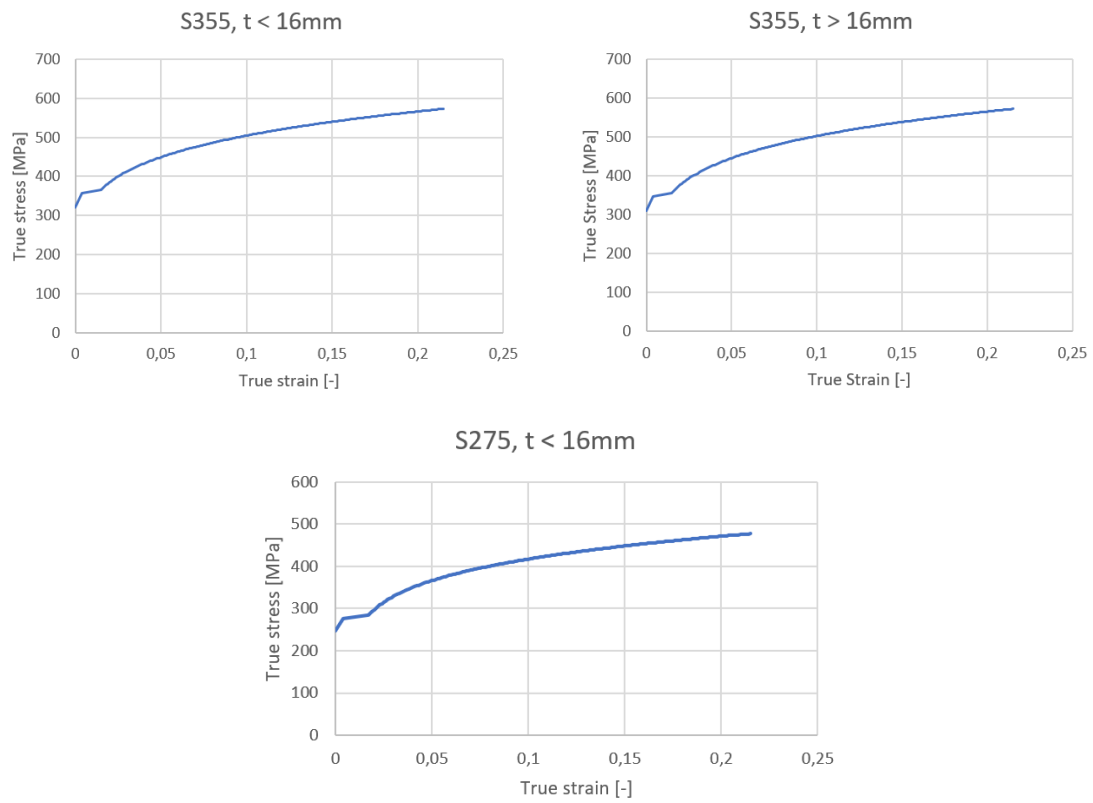
A General arrangement 20ft container





CUSTOMER:	SWIRE OILFIELD SERVICES www.swires.com	
	CREATED BY: R. Dea Pera	DATE: 22.08.2016
CHECKED BY:	DATE:	DRAWING TITLE: GENERAL ARRANGEMENT
APPROVED BY:	DATE:	PART/ASSEMBLY NUMBER: SUN20F0-AD001
DRAWING STATE: WorkInProgress	PROJECT: 20 WORKSHOP CONTAINER	PART REV.: A3
PROJECT: S-7741	DO NOT SCALE FINISH ASK	DWG REV.: 2/2
MASS: 6458 kg	BASED ON THIRD PARTY APPROVAL NUMBER: S-7741	
<small> THIS DRAWING IS THE PROPERTY OF SWIRE OILFIELD SERVICES LTD. NO PARTS THEREOF ARE TO BE REPRODUCED OR TRANSMITTED IN ANY FORM OR BY ANY MEANS WITHOUT THE WRITTEN CONSENT OF SWIRE OILFIELD SERVICES LTD. </small>		

B True stress- true strain graphs



True stress - true strain curves [58].

C True stress - True strain values

True stress and true strain values from *DNV-RP-C208* [58].

S355, t 16mm		S355, t 16mm		S275, t 16mm	
True strain	True stress	True strain	True stress	True strain	True stress
0	311	0	320	0	248
0.004	346.9	0.004	357	0.004	276.5
0.015	355.9	0.015	366.1	0.017	283.9
0.016	360.600	0.016	370.199	0.018	288.885
0.017	365.011	0.017	374.081	0.019	293.471
0.018	369.169	0.018	377.771	0.020	297.723
0.019	373.105	0.019	381.289	0.021	301.691
0.020	376.842	0.020	384.650	0.022	305.412
0.021	380.402	0.021	387.870	0.023	308.919
0.022	383.802	0.022	390.962	0.024	312.236
0.023	387.056	0.023	393.935	0.025	315.386
0.024	390.181	0.024	396.799	0.026	318.385
0.025	393.183	0.025	399.563	0.027	321.248
0.026	396.075	0.026	402.235	0.028	323.988
0.027	398.864	0.027	404.820	0.029	326.617
0.028	401.558	0.028	407.324	0.030	329.143
0.029	404.165	0.029	409.754	0.031	331.576
0.030	406.689	0.030	412.113	0.032	333.922
0.031	409.138	0.031	414.407	0.033	336.189
0.032	411.515	0.032	416.638	0.034	338.381
0.033	413.825	0.033	418.812	0.035	340.503
0.034	416.071	0.034	420.928	0.036	342.562
0.035	418.259	0.035	422.994	0.037	344.560
0.036	420.390	0.036	425.010	0.038	346.501
0.037	422.469	0.037	426.979	0.039	348.390
0.038	424.497	0.038	428.903	0.040	350.228
0.039	426.478	0.039	430.785	0.041	352.019
0.040	428.414	0.040	432.627	0.042	353.765
0.041	430.306	0.041	434.430	0.043	355.469
0.042	432.158	0.042	436.196	0.044	357.133
0.043	433.971	0.043	437.927	0.045	358.759
0.044	435.746	0.044	439.624	0.046	360.349
0.045	437.486	0.045	441.289	0.047	361.904
0.046	439.192	0.046	442.923	0.048	363.427
0.047	440.865	0.047	444.527	0.049	364.918
0.048	442.507	0.048	446.103	0.050	366.379
0.049	444.119	0.049	447.651	0.051	367.811
0.050	445.702	0.050	449.173	0.052	369.216
0.051	447.257	0.051	450.669	0.053	370.595
0.052	448.785	0.052	452.141	0.054	371.948
0.053	450.288	0.053	453.589	0.055	373.277
0.054	451.766	0.054	455.014	0.056	374.582
0.055	453.220	0.055	456.417	0.057	375.865
0.056	454.651	0.056	457.799	0.058	377.127

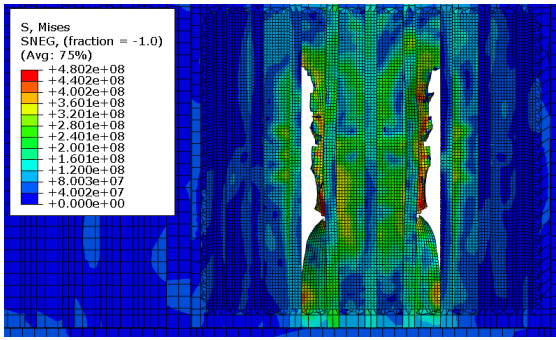
S355, t 16mm		S355, t 16mm		S275, t 16mm	
True strain	True stress	True strain	True stress	True strain	True stress
0.057	456.060	0.057	459.160	0.059	378.367
0.058	457.447	0.058	460.502	0.060	379.588
0.059	458.813	0.059	461.823	0.061	380.789
0.060	460.160	0.060	463.126	0.062	381.971
0.061	461.486	0.061	464.411	0.063	383.136
0.062	462.794	0.062	465.679	0.064	384.282
0.063	464.084	0.063	466.929	0.065	385.412
0.064	465.355	0.064	468.163	0.066	386.526
0.065	466.610	0.065	469.380	0.067	387.623
0.066	467.848	0.066	470.582	0.068	388.705
0.067	469.069	0.067	471.769	0.069	389.772
0.068	470.275	0.068	472.940	0.070	390.825
0.069	471.466	0.069	474.098	0.071	391.864
0.070	472.641	0.070	475.241	0.072	392.889
0.071	473.802	0.071	476.371	0.073	393.901
0.072	474.949	0.072	477.487	0.074	394.899
0.073	476.082	0.073	478.591	0.075	395.886
0.074	477.202	0.074	479.681	0.076	396.860
0.075	478.309	0.075	480.760	0.077	397.822
0.076	479.403	0.076	481.826	0.078	398.773
0.077	480.485	0.077	482.881	0.079	399.712
0.078	481.554	0.078	483.924	0.080	400.641
0.079	482.612	0.079	484.957	0.081	401.559
0.080	483.658	0.080	485.978	0.082	402.466
0.081	484.693	0.081	486.988	0.083	403.363
0.082	485.717	0.082	487.988	0.084	404.251
0.083	486.730	0.083	488.978	0.085	405.128
0.084	487.733	0.084	489.958	0.086	405.996
0.085	488.725	0.085	490.928	0.087	406.855
0.086	489.708	0.086	491.889	0.088	407.705
0.087	490.681	0.087	492.840	0.089	408.546
0.088	491.644	0.088	493.783	0.090	409.379
0.089	492.597	0.089	494.716	0.091	410.203
0.090	493.542	0.090	495.640	0.092	411.019
0.091	494.477	0.091	496.556	0.093	411.827
0.092	495.404	0.092	497.464	0.094	412.627
0.093	496.322	0.093	498.363	0.095	413.419
0.094	497.232	0.094	499.254	0.096	414.203
0.095	498.133	0.095	500.137	0.097	414.981
0.096	499.026	0.096	501.013	0.098	415.751
0.097	499.912	0.097	501.881	0.099	416.514
0.098	500.789	0.098	502.741	0.100	417.270
0.099	501.659	0.099	503.594	0.101	418.019
0.100	502.521	0.100	504.440	0.102	418.761
0.101	503.376	0.101	505.279	0.103	419.497
0.102	504.224	0.102	506.111	0.104	420.226
0.103	505.064	0.103	506.936	0.105	420.950
0.104	505.898	0.104	507.754	0.106	421.667

S355, t 16mm		S355, t 16mm		S275, t 16mm	
True strain	True stress	True strain	True stress	True strain	True stress
0.105	506.725	0.105	508.566	0.107	422.378
0.106	507.545	0.106	509.371	0.108	423.082
0.107	508.358	0.107	510.170	0.109	423.782
0.108	509.165	0.108	510.962	0.110	424.475
0.109	509.966	0.109	511.749	0.111	425.163
0.110	510.760	0.110	512.530	0.112	425.845
0.111	511.548	0.111	513.304	0.113	426.521
0.112	512.330	0.112	514.073	0.114	427.193
0.113	513.106	0.113	514.836	0.115	427.859
0.114	513.877	0.114	515.594	0.116	428.520
0.115	514.641	0.115	516.346	0.117	429.176
0.116	515.400	0.116	517.092	0.118	429.826
0.117	516.153	0.117	517.833	0.119	430.472
0.118	516.901	0.118	518.569	0.120	431.114
0.119	517.644	0.119	519.300	0.121	431.750
0.120	518.381	0.120	520.025	0.122	432.382
0.121	519.113	0.121	520.745	0.123	433.009
0.122	519.839	0.122	521.461	0.124	433.631
0.123	520.561	0.123	522.171	0.125	434.249
0.124	521.278	0.124	522.877	0.126	434.863
0.125	521.989	0.125	523.578	0.127	435.472
0.126	522.696	0.126	524.274	0.128	436.077
0.127	523.398	0.127	524.966	0.129	436.678
0.128	524.096	0.128	525.653	0.130	437.275
0.129	524.789	0.129	526.335	0.131	437.868
0.130	525.477	0.130	527.013	0.132	438.457
0.131	526.161	0.131	527.687	0.133	439.041
0.132	526.840	0.132	528.357	0.134	439.622
0.133	527.51	0.133	529.022	0.135	440.199
0.134	528.186	0.134	529.683	0.136	440.773
0.135	528.852	0.135	530.340	0.137	441.342
0.136	529.514	0.136	530.993	0.138	441.908
0.137	530.172	0.137	531.642	0.139	442.470
0.138	530.826	0.138	532.287	0.140	443.029
0.139	531.476	0.139	532.928	0.141	443.584
0.140	532.122	0.140	533.565	0.142	444.136
0.141	532.764	0.141	534.199	0.143	444.684
0.142	533.402	0.142	534.828	0.144	445.229
0.143	534.037	0.143	535.454	0.145	445.771
0.144	534.667	0.144	536.077	0.146	446.309
0.145	535.294	0.145	536.695	0.147	446.844
0.146	535.917	0.146	537.310	0.148	447.376
0.147	536.537	0.147	537.922	0.149	447.905
0.148	537.153	0.148	538.530	0.150	448.430
0.149	537.766	0.149	539.135	0.151	448.953
0.150	538.375	0.150	539.736	0.152	449.472
0.151	538.980	0.151	540.334	0.153	449.989
0.152	539.582	0.152	540.929	0.154	450.502

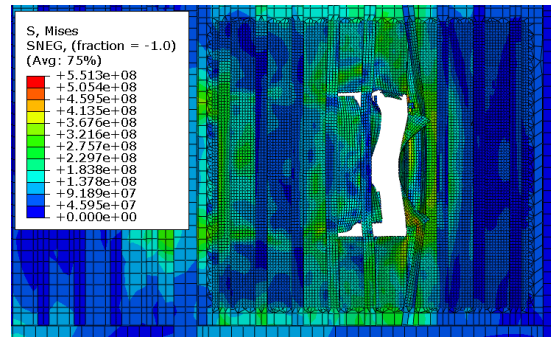
S355, t 16mm		S355, t 16mm		S275, t 16mm	
True strain	True stress	True strain	True stress	True strain	True stress
0.153	540.181	0.153	541.520	0.155	451.013
0.154	540.777	0.154	542.109	0.156	451.521
0.155	541.369	0.155	542.694	0.157	452.026
0.156	541.958	0.156	543.275	0.158	452.528
0.157	542.544	0.157	543.854	0.159	453.027
0.158	543.126	0.158	544.430	0.160	453.523
0.159	543.706	0.159	545.002	0.161	454.017
0.160	544.282	0.160	545.572	0.162	454.508
0.161	544.856	0.161	546.139	0.163	454.997
0.162	545.426	0.162	546.702	0.164	455.483
0.163	545.994	0.163	547.263	0.165	455.966
0.164	546.558	0.164	547.821	0.166	456.446
0.165	547.119	0.165	548.376	0.167	456.925
0.166	547.678	0.166	548.928	0.168	457.400
0.167	548.234	0.167	549.478	0.169	457.873
0.168	548.787	0.168	550.024	0.170	458.344
0.169	549.337	0.169	550.568	0.171	458.813
0.170	549.884	0.170	551.110	0.172	459.278
0.171	550.429	0.171	551.648	0.173	459.742
0.172	550.971	0.172	552.185	0.174	460.203
0.173	551.511	0.173	552.718	0.175	460.662
0.174	552.047	0.174	553.249	0.176	461.119
0.175	552.581	0.175	553.777	0.177	461.573
0.176	553.113	0.176	554.303	0.178	462.025
0.177	553.641	0.177	554.826	0.179	462.475
0.178	554.168	0.178	555.347	0.180	462.923
0.179	554.692	0.179	555.865	0.181	463.369
0.180	555.214	0.180	556.381	0.182	463.812
0.181	555.733	0.181	556.895	0.183	464.253
0.182	556.249	0.182	557.406	0.184	464.693
0.183	556.764	0.183	557.915	0.185	465.130
0.184	557.275	0.184	558.422	0.186	465.565
0.185	557.785	0.185	558.92	0.187	465.998
0.186	558.292	0.186	559.428	0.188	466.429
0.187	558.797	0.187	559.927	0.189	466.858
0.188	559.299	0.188	560.425	0.190	467.285
0.189	559.800	0.189	560.920	0.191	467.710
0.190	560.298	0.190	561.414	0.192	468.133
0.191	560.794	0.191	561.904	0.193	468.555
0.192	561.287	0.192	562.393	0.194	468.974
0.193	561.779	0.193	562.880	0.195	469.391
0.194	562.268	0.194	563.364	0.196	469.807
0.195	562.755	0.195	563.847	0.197	470.221
0.196	563.240	0.196	564.327	0.198	470.633
0.197	563.723	0.197	564.806	0.199	471.043
0.198	564.204	0.198	565.282	0.200	471.452
0.199	564.683	0.199	565.756	0.201	471.858
0.200	565.160	0.200	566.229	0.202	472.263

S355, t 16mm		S355, t 16mm		S275, t 16mm	
True strain	True stress	True strain	True stress	True strain	True stress
0.201	565.635	0.201	566.699	0.203	472.666
0.202	566.108	0.202	567.167	0.204	473.068
0.203	566.579	0.203	567.634	0.205	473.467
0.204	567.048	0.204	568.098	0.206	473.865
0.205	567.515	0.205	568.561	0.207	474.262
0.206	567.980	0.206	569.022	0.208	474.656
0.207	568.443	0.207	569.481	0.209	475.049
0.208	568.904	0.208	569.938	0.210	475.441
0.209	569.363	0.209	570.393	0.211	475.831
0.210	569.821	0.210	570.846	0.212	476.219
0.211	570.277	0.211	571.298	0.213	476.606
0.212	570.730	0.212	571.748	0.214	476.991
0.213	571.182	0.213	572.196	0.215	477.374
0.214	571.633	0.214	572.642	-	-
0.215	572.081	0.215	573.087	-	-

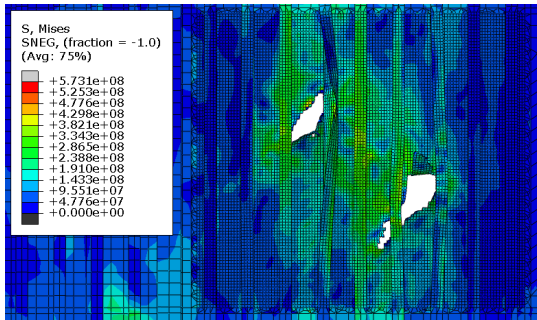
D Final damage of panel shown from stiffener side



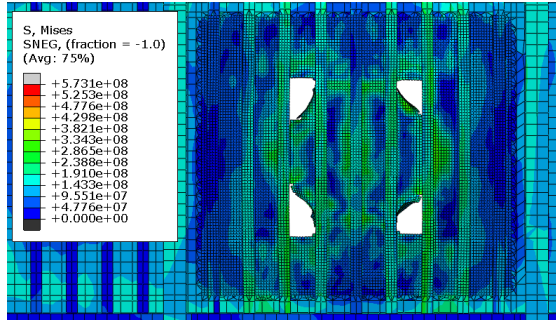
Impact scenario 1



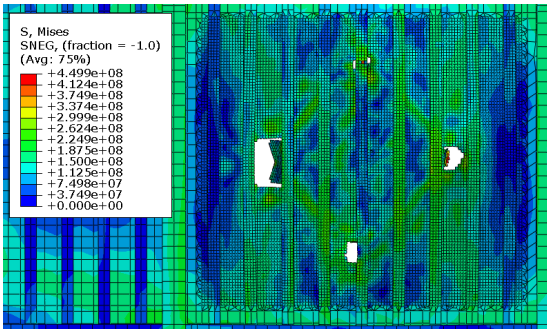
Impact scenario 2



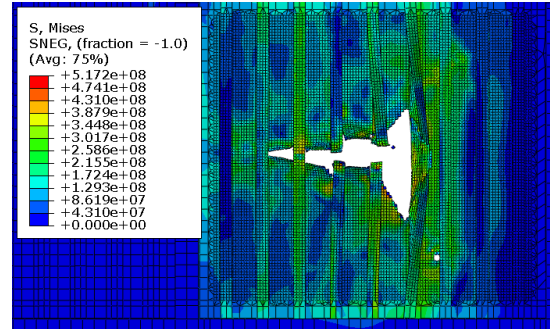
Impact scenario 3



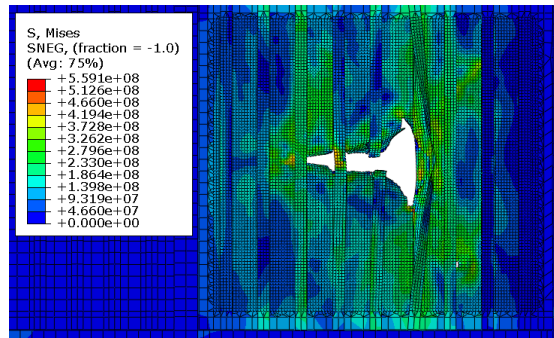
Impact scenario 4



Impact scenario 5

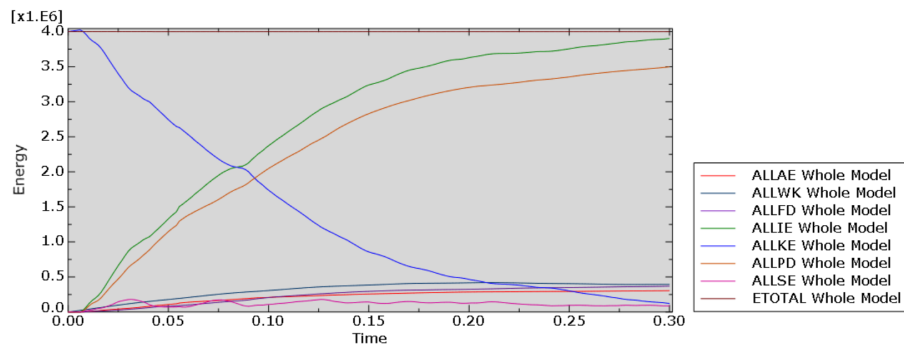


Impact scenario 6

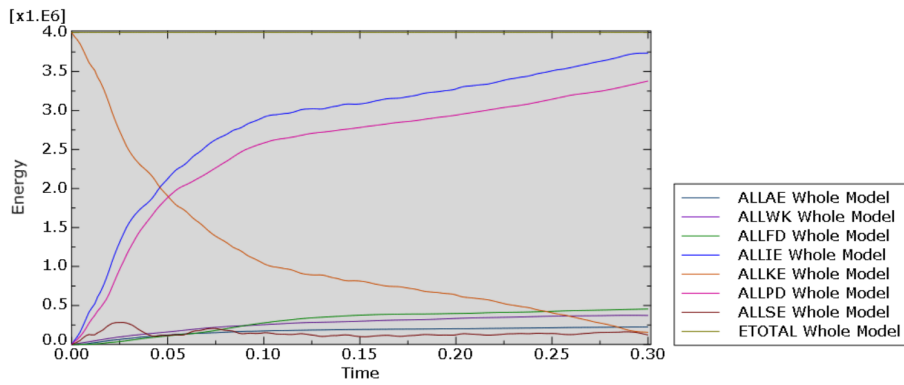


Impact scenario 7

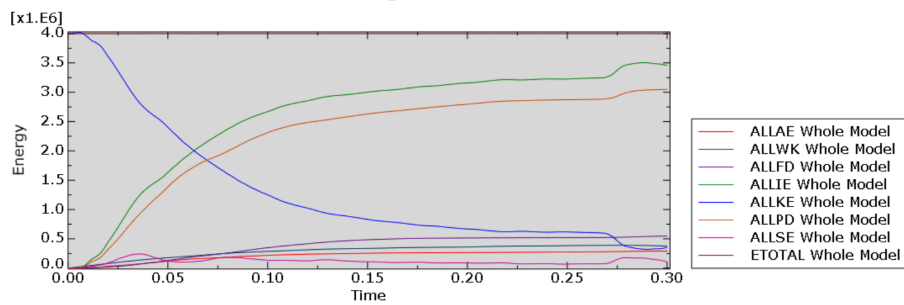
E Energies for impact scenario 1-7



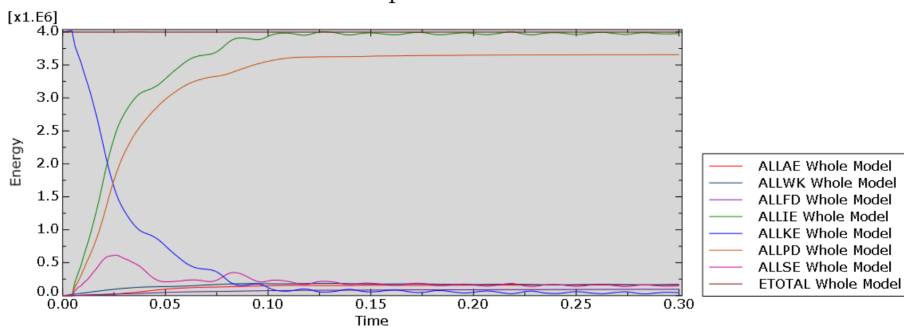
Impact scenario 1



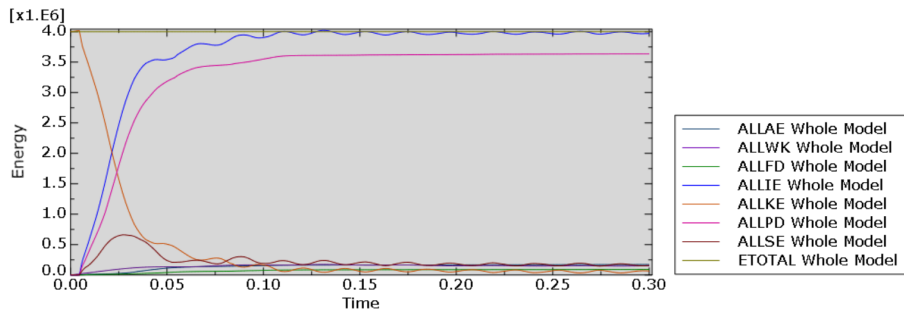
Impact scenario 2



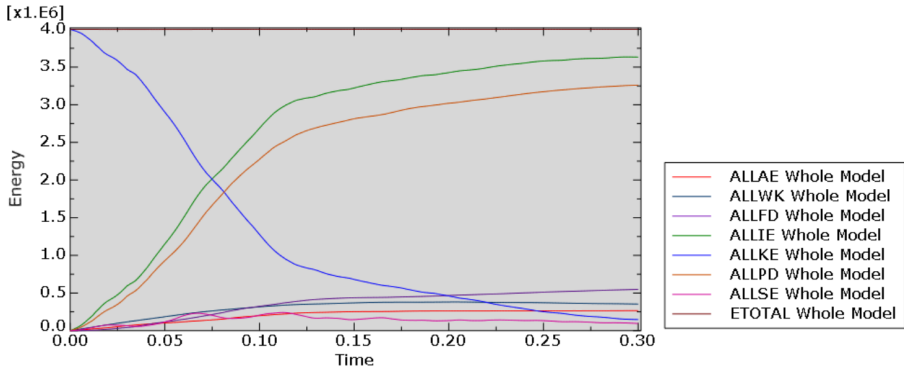
Impact scenario 3



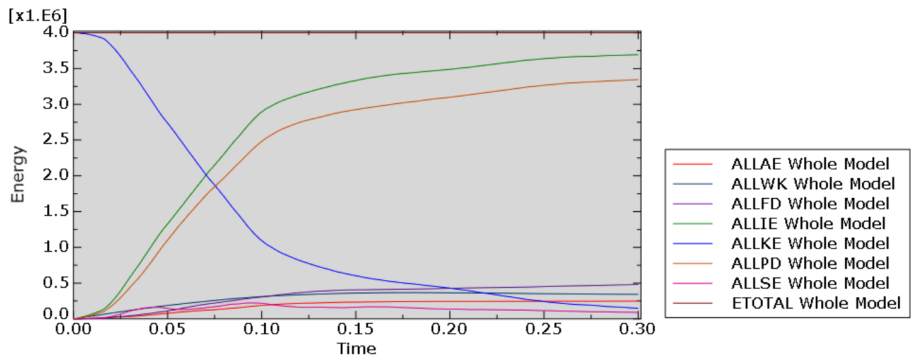
Impact scenario 4



Impact scenario 5

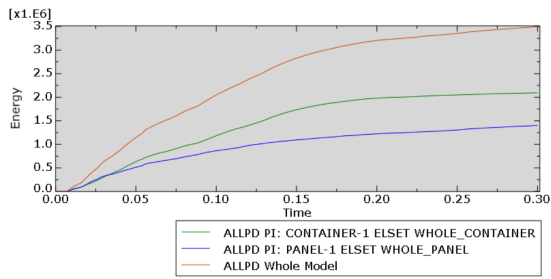


Impact scenario 6

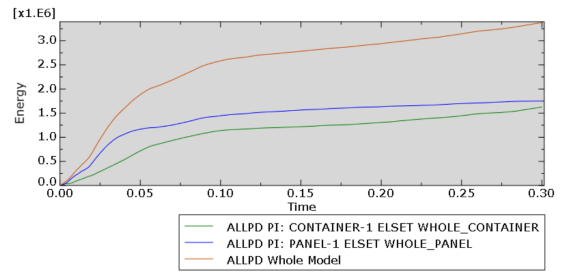


Impact scenario 7

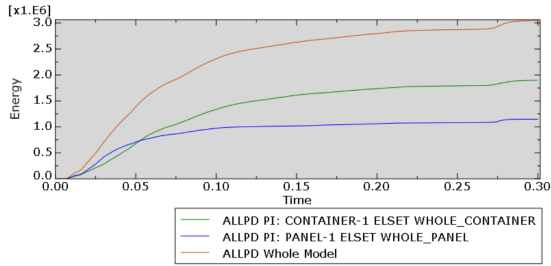
F Distribution of plastic dissipation energy for impact scenario 1-7



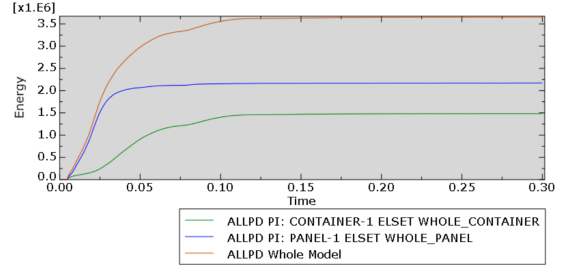
Impact scenario 1



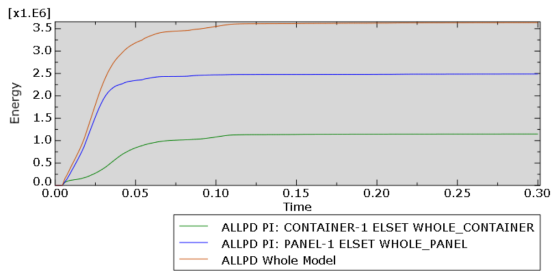
Impact scenario 2



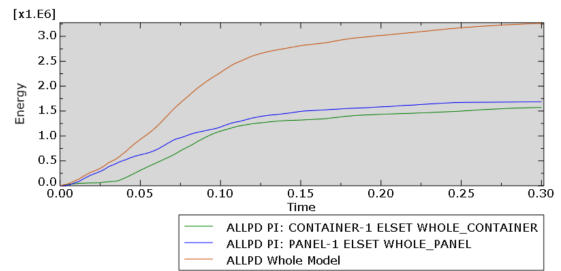
Impact scenario 3



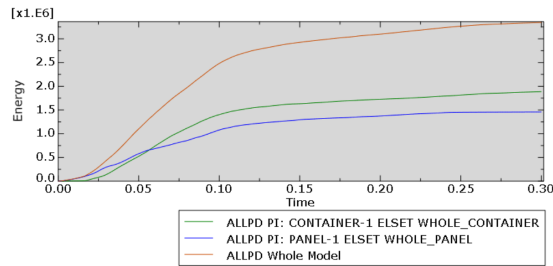
Impact scenario 4



Impact scenario 5



Impact scenario 6



Impact scenario 7

G Hand calculations

G.1 Effective plate width

The procedure of calculating the effective plate width s_e is attached below, taken from equations expressed in *DNV-RP-C201* [56]. C_{xs} is the reduction factor due to stresses in the longitudinal direction and C_{ys} is the reduction factor for compression stresses in the transverse direction. $C_{ys} = 1$ is assumed due to simplicity and C_{xs} is found by the reduced plate slenderness $\bar{\lambda}_p$.

$$C_{xs} = \begin{cases} \frac{\bar{\lambda}_p - 0.22}{\bar{\lambda}_p^2} & \text{if } \bar{\lambda}_p > 0.673 \\ 1.0 & \text{if } \bar{\lambda}_p \leq 0.673 \end{cases}$$

$$\bar{\lambda}_p = 0.525 \frac{s}{t} \sqrt{\frac{f_y}{E}} = 0.525 \frac{640}{10} \sqrt{\frac{346.9}{210000}} = 1.37$$

$$C_{xs} = \frac{\bar{\lambda}_p - 0.22}{\bar{\lambda}_p^2} = \frac{1.37 - 0.22}{1.37^2} = 0.61$$

$$s_e = C_{xs} \cdot C_{ys} \cdot s = 0.61 \cdot 1.00 \cdot 640 = 393.15 \text{ mm}$$

G.2 Plastic neutral axis

The plastic neutral axis is found as the distance from the bottom of the stiffener.

$$\begin{aligned} y_p &= \frac{(s_e \cdot t) + (s_e \cdot h_{w,s}) + (s_e \cdot t_{f,s}) - (b_{f,s} \cdot t_{f,s}) - (h_{w,s} \cdot t_{w,s}) + (s_e \cdot h_{w,s}) + (s_e \cdot t_{f,s})}{2 \cdot s_e} \\ &= \frac{(393.15 \cdot 10) + (393.15 \cdot 300) + (393.15 \cdot 17) - (200 \cdot 17) - (300 \cdot 11) + (393.15 \cdot 300) + (393.15 \cdot 17)}{2 \cdot 393.15} \\ &= 313.48 \text{ mm} \end{aligned}$$

G.3 Plastic section modulus

$$\begin{aligned} W_p &= (b_{f,s} \cdot t_{f,s} \cdot (y_p - \frac{t_{f,s}}{2})) + (h_{w,s} \cdot t_{w,s} \cdot (y_p - \frac{h_{w,s}}{2} - t_{f,s})) \\ &+ (s_e \cdot (h_{w,s} + t_{f,s} + t - y_p) \cdot (\frac{h_{w,s} + t_{f,s} + t - y_p}{2})) - (s_e \cdot (y_p - h_{w,s} - t_{f,s}) \cdot (\frac{y_p - h_{w,s} - t_{f,s}}{2})) \\ W_p &= (200 \cdot 17 \cdot (313.48 - \frac{17}{2})) + (300 \cdot 11 \cdot (313.48 - \frac{300}{2} - 17)) \\ &+ (393.15 \cdot (300 + 17 + 10 - 313.48) \cdot (\frac{300 + 17 + 10 - 313.48}{2})) \\ &- (393.15 \cdot (313.48 - 300 - 17) \cdot (\frac{313.48 - 300 - 17}{2})) = 1.55 \cdot 10^6 \text{ mm}^3 \end{aligned}$$

G.4 Plastic moment capacity

$$M_p = W_p \cdot f_y = 1.55 \cdot 10^6 \cdot 346.90 = 5.39 \cdot 10^8 \text{ Nmm}$$

G.5 Elastic neutral axis

$$\begin{aligned} y_b &= \frac{(s_e \cdot t \cdot (t_{f,s} + h_{w,s} + \frac{t}{2})) + (h_{w,s} \cdot t_{w,s} \cdot (\frac{h_{w,s}}{2} + t_{f,s})) + (b_{f,s} \cdot t_{f,s} \cdot (\frac{t_{f,s}}{2}))}{(h_{w,s} \cdot t_{w,s}) + (t_{f,s} \cdot b_{f,s}) + (s_e \cdot t)} \\ &= \frac{(393.15 \cdot 10 \cdot (17 + 300 + \frac{10}{2})) + (300 \cdot 11 \cdot (\frac{300}{2} + 17)) + (200 \cdot 17 \cdot (\frac{17}{2}))}{(300 \cdot 11) + (17 \cdot 200) + (393.15 \cdot 10)} \\ &= 173.63 \text{ mm} \end{aligned}$$

$$y_t = h_{w,s} + t_{f,s} + t - y_b = 300.00 + 17.00 + 10.00 - 173.63 = 153.37 \text{ mm}$$

G.6 Moment of inertia

$$\begin{aligned} I &= \frac{b_{f,s} \cdot t_{f,s}^3}{12} + (b_{f,s} \cdot t_{f,s} \cdot (y_b - \frac{t_{f,s}}{2})^2) + \frac{t_{w,s} \cdot h_{w,s}^3}{12} + (t_{w,s} \cdot h_{w,s} \cdot (y_b - \frac{h_{w,s}}{2} - t_{f,s})^2) \\ &+ \frac{s_e \cdot t^3}{12} + (s_e \cdot t \cdot (t_{f,s} + h_{w,s} + \frac{t}{2} - y_b)^2) \\ &= \frac{200 \cdot 17^3}{12} + (200 \cdot 17 \cdot (173.63 - \frac{17}{2})^2) + \frac{11 \cdot 300^3}{12} + (11 \cdot 300 \cdot (173.63 - \frac{300}{2} - 17)^2) + \frac{393.15 \cdot 10^3}{12} \\ &+ (393.15 \cdot 10 \cdot (17 + 300 + \frac{10}{2} - 173.63)^2) \\ &= 2.04 \cdot 10^8 \text{ mm}^4 \end{aligned}$$

G.7 Elastic section modulus

$$W_{yb} = \frac{I}{y_b} = \frac{2.04 \cdot 10^8}{173.63} = 1.18 \cdot 10^6 \text{ mm}^3$$

$$W_{yt} = \frac{I}{y_t} = \frac{2.04 \cdot 10^8}{153.37} = 1.33 \cdot 10^6 \text{ mm}^3$$

The elastic section modulus is the highest value of the elastic section modulus at bottom and the elastic section modulus at top, respectively W_{yb} and W_{yt} . Hence $W = W_{yt} = 1.33 \cdot 10^6 \text{ mm}^3$.

